PEOPLE'S DEMOCRATIC REPUBLIC OF ALGERIA
MINISTRY OF HIGHER EDUCATION AND SCIENTIFIC RESEARCH
YAHIA FARES UNIVERSITY OF MEDEA
FACULTY OF TECHNOLOGY



Master's degree dissertation

Field: Mechanical Engineering.

Specialty: Energetic

Numerical study of a cogeneration cycle in view: thermoelectric considerations

Presented by:
Mr Youcef amine REBAHI
Proposed and Directed by :
Prof. Younes Chiba
Dr. Abdelkrim Terfai

Academic year : 2024-2025

SUMMARY

إهداء 5

Acknowledgments 6

NOMENCLATURE 7

LIST OF FIGURES 9

TABLE LIST 11

ملخص 12

Abstract 12

Résumé 12

General Introduction 14

CHAPTER I : General Information on Cogeneration Systems 16

I-1 :General Introduction 16

I-2 : State of the art : 17

I-5-2 :Types of cogeneration technologies and their assessment: 29

I-5-3 :Cogeneration system powered by an internal combustion engine (reciprocating motion): 30

I-5-3-1: Reciprocating Engine Technology: 30

a. Engine System : 31

b. Thermal Power Generation: 32

c. Performance: 34

d. Engine Speed Classification: 35

e. Installation: 36

I-5-3-2 : Gas Turbine Cogeneration System with Heat Recovery: 37

Introduction: 37

I-5-3-2-1 :Gas turbine system technology: 38

I-5-3-2-2: Types of Gas Turbines: 39

a. Aeroderivative Gas Turbines: 39

b. Industrial gas turbines: 39

c. Performance Characteristics: 39

d. Heat Recovery: 40

I-5-3-3. Steam Turbine 41

Introduction 41

I-5-3-3-1 : Steam Turbine Cogeneration System Technology 43

I-5-3-3- 2:Cogeneration System Components: 43

a. Boilers : 44
b. Steam Turbine : 44
I-5-3-3-3 Performance Characteristics 45
CHAPTER II: Theoretical and Numerical study 49
II.1. Introduction 49
II-1 : System Description 49
II-2 : Principle of the absorption machine: 53
II-3 : Energy analysis : 56
II-4 Exergy analysis : 57
II-5 : Economic analysis: 58
II-6 : Performance criteria: 59
II-7 : SCO_2 cycle system : 59
II-8 : ARC system : 60
II-9 : ORC system: 61
II-10 : Cost functions of system components : 62
II-11 : MATLAB program explanation : 63
II-11-1 : MATLAB Program 63
CHAPTER III : Results and discussions 66
III -1 : Preliminary design result : 66
III -2 : Thermodynamic analysis results : 69
III -3 : Change the absorbent gas(NH3) : 76
CHAPTER IV : Comparison of results 84
IV-1 :First comparison : 85
IV-2 : second comparison : 86
IV-2-1 : Key Takeaways : 87
IV-3 : Third comparison : 88
IV- 4 : Fourth comparison: 89
IV-5-1 : General Shape and Behavior : 92
IV-5-2 : Pressure Dependence : 92
IV-5-3 : Specific Heat Capacity Range : 93
IV-5-4 : Temperature Range : 93
IV-6 : Sixth comparison: 93
IV-6-1 : Similarities Between the Two Charts: 94
IV-6-2 : Differences Between the Two Charts: 95
IV-6-3 : Summary: 95

general conclusion and Perspectives :..... 97
Bibliographical references :..... 99

إهداء

إلى من زرعوا فيّ الأمل، وغرسوا فيّ القيم، وهدوا دربي

إلى أمي وأبي (رباحي محمد، بخاري ح)، مصدر الحنان، وسند الحياة، وسبب نجاحي. دعواتكم كانت نورًا أضاء لي دربي، وصبركم كان قوةً سندتني في كل لحظة. مهما كتبتُ، لن أوفيكم حقكم.

إلى عائلتي الكريمة، التي أحاطتني بحبها ودعمها وتشجيعها، شكرًا لكم على ثقتكم، وكلماتكم الطيبة، وحضوركم الدائم

إلى كل أصدقائي و زملائي الأعزاء و الى كل من آمن بي وساندني ولو بكلمة

أهدي هذا العمل المتواضع إليكم جميعًا، امتنانًا وتقديرًا

Acknowledgments

I extend my sincere thanks and appreciation to the distinguished members of the examination committee, who honored me by accepting to discuss this modest scholarly work and dedicated their time and effort to evaluate and enrich it with their valuable comments and constructive criticism. Especially Prof. Younes Chiba and Dr. Abdelkrim Tarfai.

I have the utmost respect and appreciation for your diligence and attention, and for the knowledge and experience you have contributed to improving and refining this work. May God reward you abundantly and bless your knowledge and contributions.

NOMENCLATURE

Symbol	Designation	Unit
A	area	m^2
P	density	kg/m^3
DNI	direct normal irradiance	W/m^2
η	efficiency	(%)
E	exergy	kW
Z	investment cost	$
λ	heat conductivity coefficient	W/m^2K
t	heat storage time	h
Q	heat transfer rate	kW
n	life time	year
m	mass flow rate	kg/s
V	volume	m^3
W	power	MW
cp	specific heat	kJ/(kg·K)
h	specific enthalpy	kJ/kg
ARC	absorption refrigeration cycle	
Abs	absorber	
An	anode	
CRF	capital recovery factor	
CSP	concentrating solar power	
X	concentration	
Ca	cathode	
Con	condenser	
Ch	chemical	
D	destruction	
eva	evaporator	
NH_3	gas ammonia	
gen	generator	
hel	heliostat	
HTF	heat transfer fluid	
HTR	high-temperature regenerator	
Ir	interest rate	
LTR	low temperature regenerator	
MC	main compressor	
MCFC	molten carbonate fuel cell	
MSHE	molten salt heat exchanger	
net	net power	
OHE	ORC heat exchanger	
OP	ORC pump	
ORC	organic Rankine cycle	

OT	ORC turbine	
PC	pre-cooler	
ph	physical	
RC	repression compressor	
r	refrigerant	
rec	receiver	
ST	SCO_2 turbine	
SCO_2	supercritical carbon dioxide	
ss	strong solution	
sur	surface	
LCOE	The levelized cost of energy	
tow	tower	
val	valve	
ws	weak solution	

LIST OF FIGURES

Figure I.1: Installation of a cogeneration engine in Morbihan [35]……(13)

Figure I.2: Distribution of electricity production in Africa in 2015[41]……..(20)

Figure I.3: Cogeneration with modern engine technology[36]
……...…….(25)

Fig. I.4: Closed-loop heat recovery system[46]……....(27)

Fig. I.5. Internal combustion engine cogeneration unit[47]…….(28)

Fig. I.6 : Cogeneration installations Principle[38]…….(28)

Fig. I.7 : Fuel cell micro-tri-generation[49]……..(29)

Fig. I..8: Single-cycle gas turbine cogeneration systems (Brayton cycle) integrated into a waste heat steam boiler [54]……(30)

Fig. I.9. Centrale de cogénération à turbine à gaz[60]……...(34)

Fig I.10: Boiler/steam turbine system [59]…….(36)

Fig II.1:flow chart of SMCT system……(41)

Fig II.2: T-s diagram of SCO2 cycle, ORC, and ARC……(41)

Fig.II .3 : Flow Chart of MCFC-SCO2 Brayton Cycle System……...(43)

Fig.II .4 : the evaporator in the absorption machine[22]…… (44)

Fig.II .5 : the evaporator and the absorber in the absorption machine[22]……..... .(45)

Fig.II .6: the evaporator; the concentrator and the absorber in the absorption machine[22]
.(45)

Fig.II .7 : the simple absorption machine system[22]……(45)

Fig.II .8 : the absorption machine system with system supplements increase[22]… ..(46)

Fig III .1 : Exergy destruction of various components……. (59)

Fig. III .2 : Variation of the specific heat capacity of CO2 at constant pressure with temperature…….(60)

Fig. III . 3 : Effect of *T*salt,in on exergy destruction and molten salt flow in tower receiver..(61)

Fig. III . 4 : Effect of DNI on exergy destruction and molten salt flow in tower receiver…(62)

Fig. III . 5 : Variation of the specific heat capacity of CO2 with temperature at constant pressure…….(63)

Fig. III . 6 : Daily Solar DNI and Thermal Storage Tank Behavior……..(64)

Fig. III . 7: Exergy Destruction of System Components (NH3-based) ……(65)

Fig. III . 8: Corrected NH3 Specific Heat Capacity near Critical Point…….(66)

Fig. III . 9 : The effect of T_{salt,in} on the thermal energy destruction and flow of molten salt in the presence of NH3 ……(67)

Fig. III . 10 : Effect of DNI on energy destruction and flow of molten salt in the case of NH3……(68)

Fig. III . 11 : NH3 Specific Heat vs Temperature……..(69)

Fig. III . 12 : Daily behavior of solar thermal storage tank and energy consumption in NH3 condition……..(71)

Fig IV .1 : Exergy destruction of various components……(74)

Fig. IV . 2 : Exergy Destruction of System Components (NH3-based) ……(74)

Fig. IV . 3: Corrected NH3 Specific Heat Capacity near Critical Pointv……(75)

Fig. IV .4 : Variation of the specific heat capacity of CO2 at constant pressure with temperature……(75)

Fig. IV . 5 : The effect of T_{salt,in} on the thermal energy destruction and flow of molten salt in the presence of NH3 ……(77)

Fig. IV . 6 : Effect of *T*salt,in on exergy destruction and molten salt flow in tower receiver

……(77)

Fig. IV . 7: Effect of DNI on energy destruction and flow of molten salt in the case of NH3……(78)

Fig. IV. 8 : Effect of DNI on exergy destruction and molten salt flow in tower receiver ……(78)

Fig. IV . 9 : NH3 Specific Heat vs Temperature……(80)

Fig. IV . 10 : Variation of the specific heat capacity of CO2 with temperature at constant pressure……(80)

Fig. IV . 11 : Daily Solar DNI and Thermal Storage Tank Behavior……(82)

Fig. IV . 12 : Daily behavior of solar thermal storage tank and energy consumption in NH3 condition……(82)

TABLE LIST

Table I.1: Cogeneration potential (bagasse) for Eastern and Southern Africa……(27)

Table I.2. Advantages and disadvantages of cogeneration technology.……(29)

Table I .3:. The reciprocating motor attribute……(32)

Table I.4. Typical performance parameters of the cogeneration engine for spark-ignition engines……(35)

Table I.5. Types of reciprocating motors by speed (Values available in MW) ……(35)

Table I.6. Summary of gas turbine attributes……(38)

Table I. 7. Summary of performance characteristics of cogeneration systems using gas turbine cogeneration plants ……(40)

Table I. 8: Summary of steam turbine attributes described in detail in this chapter……(42)

Table I. 9: . Summary of performance characteristics of commercially available boosted steam turbines used in cogeneration applications from 500 kW to 15 MW ……(45)

Table I. 10: Performance Characteristics of Backpressure Steam Turbine……(46)

Table I. 11: Performance characteristics of a steam turbine of a natural gas boiler…(47)

Table II.1 Input parameters of SMCT system……(51)

Table II .2 : Reasons for choosing MATLAB for this project……(63)

Table III .1 : SMCT system simulation results……(67)

Table III .2 : Thermodynamic parameters of SMCT system at each state point……(68)

Table III .3 : Thermodynamic parameters of the SMCT system at each point in the NH3 state……(68)

Table III .4 : Economic cost for the SMCT system ……(69)

ملخص
تُقدّم هذه الدراسة تحليلاً حراريًا لدورة توليد مشترك تعتمد على آلة تبريد بالامتصاص، مرتبطة بنظام طاقة شمسية أسطواني-قطع مكافئ يهدف إلى تزويد التوربينات ببخارٍ محمص.
تم تطوير نموذج حسابي باستخدام برنامج ماتلاب لمحاكاة عمل الدورة المقترحة. وقد تم تقييم أداء النظام من خلال حساب الكفاءة العامة للدورة، بالإضافة إلى معامل الأداء لآلة التبريد بالامتصاص.
أُجريت دراسة مقارنة باستخدام زوجين من السوائل العاملة: الأمونيا–الماء وبروميد الليثيوم–الماء، لتحديد أفضل زوج من حيث الأداء تحت ظروف تشغيل مختلفة.
تم تحليل النتائج الناتجة عن دراسة بارامترية لمتغيرات التشغيل المختلفة ومناقشتها بهدف تحسين الأداء الطاقوي للنظام المركب المقترح.
الكلمات المفتاحية: المحاكاة العددية، آلة التبريد، التوليد المشترك للطاقة، الطاقة الشمسية ، ميكانيكية الاستثارة ، ماتلاب ,

Abstract
This study presents a thermodynamic analysis of a cogeneration cycle incorporating an absorption refrigeration machine, coupled with a parabolic trough solar energy system designed to supply superheated steam to turbines. A computational model was developed using MATLAB to simulate the operation of the proposed cycle. The cycle's performance was evaluated through the calculation of exergy, overall cycle efficiency, and the coefficient of performance (COP) of the absorption refrigeration system. A comparative study was conducted using two working fluid pairs: NH_3 and $LiBr–H_2O$, to determine the most suitable pair under varying operational conditions. The results, obtained from a parametric study of the cycle's operating parameters, are analyzed and discussed to identify optimization strategies and enhance the energy performance of the integrated system.

Keywords: Numerical simulation, Refrigeration machine, Cogeneration, Solar energy , exergy mechanical ,orc ,matlab

Résumé
Cette étude présente une analyse thermodynamique d'un cycle de cogénération intégrant une machine frigorifique à absorption, couplée à un système d'énergie solaire cylindro-parabolique destiné à alimenter des turbines en vapeur surchauffée.
Un code de calcul a été développé sous Matlab afin de simuler le comportement du cycle proposé. L'évaluation de ses performances a été réalisée à travers le calcul de l'exergie**,** du rendement global du cycle**,** ainsi que du coefficient de performance (COP) de la machine frigorifique. Une étude comparative a été menée en utilisant deux couples d'absorption : $NH_3–H_2O$ et $LiBr–H_2O$, dans le but de déterminer le couple le plus performant selon les conditions de fonctionnement. Les résultats, issus d'une étude paramétrique sur les grandeurs influençant le fonctionnement du cycle, ont été analysés et discutés en vue d'optimiser les performances énergétiques du système proposé.
Mots clés : Simulation numérique, Machine frigorifique, Cogénération, Energie solaire , exergie mécanique , orc , matlab

General Introduction

General Introduction

In recent decades, the world has witnessed major transformations in the energy sector, driven by increasing global energy demand, growing concerns about climate change, and declining dependence on fossil fuels. In this context, hybrid energy systems have become a strategic option that combines multiple energy sources (renewable and non-renewable) to improve efficiency, reduce waste, and ensure continuity of energy supply.

Among these systems are those that combine solar thermal energy, fuel cells, and advanced heat conversion cycles, such as the supercritical carbon dioxide (SCO_2) cycle. These systems not only produce electricity but also enable the recovery of waste heat through absorption refrigeration systems, enhancing thermal performance and reducing emissions.

This study focuses on a performance comparison between two types of absorption refrigeration cycles:

NH_3 (ammonia) cycle, which is characterized by its ability to operate at high temperatures.

The LiBr-H_2O (lithium bromide-water) cycle is known for its operational stability and high coefficient of performance at medium temperatures.

This study aims to build a thermal and exergy simulation model using MATLAB and analyze the performance results of each cycle within a hybrid power system containing:

A molten salt solar receiver, an MCFC fuel cell, a supercritical CO_2 cycle, and an additional ORC cycle for heat recycling.

Through this comparative analysis, the study seeks to provide a clear technical insight into the feasibility and energy performance of each cycle, contributing to the development of efficient, flexible, and sustainable multi-purpose generation systems.

Chapter I.

General Information On Cogeneration System

CHAPTER I : General Information on Cogeneration Systems

I-1 :General Introduction

All our daily activities and production processes involve energy in different forms. But in recent decades, the growth of world population, the need to improve living conditions and growth overall economic growth have led to a constant increase, however, they have not never satisfied the energy demand. The response to this growing demand must be approached with great caution. Indeed, the danger represented by emissions of different industrial sectors using fossil fuels is well known [1]

The impact of these emissions manifests itself at several levels, the most important being the climate, environment and human health. At the climatic level, we can cite the effect well-known greenhouse gases (Gas), mainly carbon dioxide. This the latter alone contributes (among other gases) to 60% of global warming[1].

At environmental level, there is acidification of water, soil and corrosion. In terms of human health, these emissions are among the causes of death from diseases cardiovascular and respiratory. For example, the only annual emissions from ships cause the deaths of nearly 60,000 people [1].

This has enabled many possibilities in terms of new technologies energy to find new forms of energy or rather to revise the ancient ways of managing our resources for the world's future generations entire. However, because of our different civilizations, Africa has always been at the forefront. lags behind this technological rush despite being the richest continent in the world in energy resources. Its resources range from oil and gas, large areas sunny, mega tons of biomass coming from agricultural activities, but the production and distribution of thermal energy and electricity leaves much to desire [1].

Cogeneration is the simultaneous production of two forms of energy, usually electrical and thermal, also called heat and electricity combined. Cogeneration productively uses heat normally generated by conventional generators, which results in an overall efficiency higher. In addition, cogeneration facilities are generally located at the point of energy demand, largely avoiding losses associated with transport electricity. As a result, cogeneration plants can achieve a overall energy efficiency of 70 to 90%, compared to an average of only 35% for the supply of conventional electricity from the network [1].



Figure I.1: Installation of a cogeneration engine in Morbihan [35]

I-2 : State of the art :

- MUNIKWA Ropafadzo [1] discusses the need for improved efficiency and performance in heat and power plants to meet the increasing demand for energy while also reducing emissions and investment costs. The proposed cogeneration system is analyzed using the thermodynamic software EES, with data from SONELGAZs COGENcalc modeling tool. Through thermodynamic calculations, the influence of various operating parameters on the cycle and the importance of heat recovery through internal cooling systems are highlighted. The key words for this document include cogeneration, heat recovery, internal cooling circuit, thermal and electrical energy, heat exchanger, and EES [1]. Overall, the document emphasizes the potential benefits of cogeneration in improving energy efficiency and reducing environmental impact. It suggests that investments in such systems should be carefully studied and analyzed through thermodynamic calculations to ensure maximum effectiveness. The audience for this document may include engineers, researchers, and policymakers in the energy industry. It serves to inform and provide recommendations for improving the performance and efficiency of heat and power plants through the implementation of cogeneration systems. The key points of the document include the need for improved efficiency in heat and power plants, the use of thermodynamic software to analyze proposed cogeneration systems, and the importance of heat recovery through internal cooling systems [1] .

- Mohamed Zodi Saddam and all. [26] discusses the analysis of a combined cycle using thermodynamic modeling, with numerical simulation conducted using the software EES. The main focus of the study is improving the performance and efficiency of power plants to meet the increasing demand for energy and reduce emissions and costs. Various optimization studies for combined cycles are available in literature, and this study aims to demonstrate the impact of certain operational parameters, such as heat recovery and pinch point in the recovery boiler. These parameters play a critical role in determining the critical temperature at which the peak efficiency of the combined cycle is observed. The study also highlights the effect of steam saturation pressure on the Rankine cycle power. The target audience for this document is likely researchers and professionals working in the energy industry. Its purpose is to provide insights into optimizing combined cycles for improved efficiency and emission control [26] .

- In summary, ALLAOUI Faiçal and all [27].. presents a thermodynamic study of a gas-steam combined cycle for electricity production using fossil energy. The combined cycle comprises a gas turbine and a steam turbine, with a thermal efficiency of up to 60%, which is close to the efficiency of the ideal CARNOT cycle. Through manual calculations and simulations using ASPEN HYSYS and DWSIM software, the document proposes the majority of fundamental parameters and estimates the overall thermal efficiency of the cycle to be 66%. The document highlights the simplicity and isentropic nature of the combined cycle, making it an attractive option for electricity production. The potential for further improvements in efficiency through optimizing influenceable parameters is also discussed. Overall, this document emphasizes the importance of thermodynamic studies in improving the performance and efficiency of power plants [27].

- Overall,. ALLAOUI Zakarya and all. [8] analyzes the potential of cogeneration for district heating systems and presents a method for designing an optimal piping system. It stresses the importance of sustainable energy solutions and highlights the benefits of cogeneration, particularly in terms of increasing energy efficiency and reducing carbon emissions. The study also emphasizes the significance of considering potential customers and their energy needs in decision-making. The intended audience appears to be stakeholders and decision-makers involved in the implementation of cogeneration for district heating. The document provides recommendations on how to plan and design cogeneration systems, with the goal of promoting sustainable and efficient energy usage [8] .

- Composer BEN ALLA Alaeddine and all [3].focuses on the thermal properties and energy efficiency of the combined cycle power plant at Draouch (SKD) based on principles of thermodynamics and heat transfer. Detailed calculations were performed, taking into account practical data, to determine the actual efficiency of the gas turbine (37.41%), steam turbine (35.47%), and overall combined cycle (57.48%). The use of a combined cycle results in a 53.65% increase in overall efficiency compared to a single gas turbine, meaning a 34.92% reduction in fuel consumption for the same electricity production. The impact of temperature and suction pressure on energy performance was also studied, with results showing higher temperatures lead to a decrease in air flow and lower turbine power, while higher pressure leads to increased air flow and turbine power without affecting efficiency. The document recommends maximizing suction pressure for optimal performance. The intended audience is likely professionals and researchers in the field of power plant design and energy efficiency, and the purpose is to provide factual information and calculations to support the use of combined cycle power plants for increased efficiency [3] .

- Trabelsi Mohammed Nacer-Eddine and all. [4] highlights the significant contribution of fossil fuels to the production of CO2 in the atmosphere and its impact on climate change. It suggests that renewable energy sources offer a solution to this problem but cannot fully replace fossil fuels to meet future energy needs. The document also discusses the discovery of alternative solutions, such as cogeneration, to recover energy losses and increase energy efficiency[4]. Cogeneration is described as a viable tool for sustainable energy management due to its considerable primary energy savings and potential for reducing CO2 emissions in heat and electricity production. The implementation of cogeneration in building sectors shows a significant variation in final energy mix in the medium and long term, indicating its potential in energy and material savings. The integration of cogeneration technologies, particularly fuel cell cogeneration, leads to a considerable reduction in CO2 emissions compared to reference scenarios. The document argues that the adoption of these technologies in the voluntary scenario can play a crucial role in addressing energy, climate, and economic challenges in the long term. The document concludes with a recommendation to promote the use of cogeneration technologies for sustainable energy management and achieving climate goals. The target audience for this document is likely policymakers, energy professionals, and researchers working in the field of energy and environmental sustainability [4] .

- Simon Martinez and all. [7] presents the results of an experimental and numerical study on a prototype solar micro-cogeneration installation. This installation, located on the University of

La Rochelle campus, utilizes a 46.5 m² parabolic trough solar collector field and an oil-free piston steam engine. The tests performed focused on characterizing the solar concentrator, studying steam overheating, and testing operation in winter. Models for the parabolic trough sensor were developed to improve efficiency. The tests also showed the need for an additional charge in order for the installation to function effectively. The second part of the document discusses the modelling of the micro-cogenerator and its integration into a building using thermal simulation software. Different integration options are presented, and it is suggested that positioning the auxiliary on the primary circuit allows for better control of electrical production. However, having a back-up boiler on the distribution prevents control of power generation [7] .

- Chaolei Dang and all. [15] introduces a novel thermal management system based on closed-Brayton-cycle to address the thermal protection and electricity supply challenges for long-endurance hypersonic vehicles. A system model that combines a cycle zero-dimensional model and a cooling channel quasi-one-dimensional model is used to analyze the systems performance. The results indicate that the post-mixing method has higher heat transfer coefficients, and the split ratio of the bottom sub-cycle affects net power and fuel flow rate for cooling. The increase in turbine inlet temperature has a positive impact on net power and fuel mass flow rate, but above 923 K, the difference in net power is minimal. The study also provides optimization results for the system, with a minimum fuel flow rate for cooling of 0.3313 kg/s and a maximum net power of 162.37 kW. The document concludes by stating that the findings can be used to improve thermal protection and electricity supply for long-endurance hypersonic vehicles [15] .

- White and all. 2021 [5] provides an overview of power cycles operating with supercritical carbon dioxide and their potential benefits for future energy applications. It discusses their advantages, current research efforts, and challenges that still need to be addressed for successful implementation at an industrial scale. The audience for this document is likely researchers and industry professionals working in the field of energy generation. The purpose of the document is to inform and provide updates on the current status of sCO2 power cycles and highlight areas for future research and development [5].

- The Li, C and all. [12] focuses on exploring the influence of recompression path selection on the S-CO2 Brayton cycle and proposes two modified layouts to improve cycle performance. Detailed energy and exergy analyses are conducted for both conventional and modified recompression cycles, and optimization is used to determine the optimal recompression path

under different operation conditions. Results show that the modified recompression cycles have higher thermal efficiency compared to the conventional cycle, with further improvements possible through precooling and shifting the recompression path. The document also highlights the importance of considering recompression path selection in off-design operation to mitigate efficiency deterioration [12] .

- Rodríguez and all.2022 [9] evaluates the thermodynamic performance of pure supercritical Carbon Dioxide (CO2) and blended transcritical CO2 power cycles using exergy analysis. The reference power plant is based on a steam Rankine cycle and represents state-of-the-art Concentrated Solar Power (CSP) plants. With two different energy source temperatures (575 ◦C and 725 ◦C) considered, CO2 blends show significant improvement in exergy efficiency compared to SoA Rankine cycles, up to 2.7 percentage points at 575 ◦C and 75.3% at 725 ◦C. This is due to reduced exergy destruction during compression and heat rejection processes. Additionally, internal condensation in the heat recuperator improves exergy efficiency and allows for simpler layouts without split-compression. In addition, CO2 blends have lower exergy efficiency degradation in case of an increase in ambient temperature. These findings support the use of CO2 blends in next generation CSP plants for improved thermodynamic performance [9].

- Li and all.. 2025 [18] discusses the importance of heat exchangers in the efficiency of Brayton cycle-based power and energy storage systems. It highlights the limitations of existing methods for evaluating heat exchanger performance and proposes a new method, the Performance Recovery Coefficient (PRC), which uses component-scale parameters to evaluate the impact of heat exchangers on cycle efficiency. The PRC is validated to be applicable in various cycle configurations and with different parameters and working fluids. The document also demonstrates how the PRC can be used to inform decisions on heat exchanger type and arrangement to improve cycle efficiency. This work has practical applications for designing and optimizing Brayton cycle-based systems for more efficient energy production and storage [18].

- Overall, the Yun Hong and all [13] discusses a novel open-loop air cycle heat pump system that recovers waste energy from compressed gases. It can operate under extreme ambient temperatures and cater to diverse heating needs across a wide temperature range. Experimental results show minimal impact on heating capacity and water temperature difference. The system also has a high efficiency rate. This system offers a sustainable solution for recycling waste energy, making a significant contribution to energy conservation

efforts. The intended audience is likely researchers and professionals in the field of energy conservation [13] .

- This Ramin Ghiami Sardroud and all [20] delves into the advancement and optimization of supercritical CO2 recompression Brayton (SCRB) cycles combined with organic flash cycles (OFC) for sustainable and efficient power generation using renewable resources. The authors utilize various perspectives, such as thermodynamic, techno-economic, environmental, and advanced exergy, to comprehensively investigate the performance and potential improvements of the SCRB/OFC plant. They highlight the need for advanced exergy analysis, as conventional thermodynamic analysis alone cannot provide insight into cause of irreversibilities and performance enhancement opportunities. Multi-objective optimization, based on machine learning, is performed to maximize exergy efficiency, net present value, and net power output. Results show that while the reactor has the worst performance, significant improvements can be made in other components to decrease the total exergy destruction rate and achieve higher exergy efficiency, net present value, and net power output. The authors recommend incorporating advanced exergy analysis and optimization techniques for future SCRB/OFC plants to enhance overall performance and maximize sustainability [20]

- In this Xinyi Wei, and all, [19] the importance of air temperature and humidity control in crop storage is discussed. Current drying methods in agriculture, such as solar heating and air source heat pump, have their limitations. Solar heating can result in low-quality dried products, while air source heat pump may not reach the ideal temperature in harsh environments. To overcome these challenges, a rapid heating drying system based on the reverse Brayton air cycle is proposed. This system can quickly produce high temperature and low humidity air by adjusting the pressure ratio. Additionally, an improved system with a water cooler is suggested to further enhance the drying efficiency. The results show that at a compression ratio of 2.6 and air temperature of 32°C, the improved system can achieve an air temperature of 63°C and humidity content of 0.0098kg/kgDA. This is a significant improvement compared to the system without a water cooler. The total dehumidification rate of the improved system is also higher, reaching 11.51g/s, with a dehumidification energy efficiency of 1.26kg/(kW.h). The authors recommend the use of this improved rapid heating drying system for more efficient crop storage [19].

- Overall, Hao Lia, and all [17] discusses the potential of SCO2 RBC technology for thermal energy generation and addresses the limitations of previous studies that focused on simple models. The development of 1D component models and multi-objective design optimization

have shown promising results in terms of efficiency and cost. The off-design performance analysis and control strategies further enhance the competitiveness and potential of SCO2 RBC cycles. The findings presented in this document have the potential to advance the commercial application of SCO2 cycles in thermal energy generation systems [17].

- Overall, the Chuhua Zhang, and all [13] discusses the potential of Supercritical carbon dioxide (SCO2) recompression Brayton cycle (RBC) for thermal power conversion and heat harvest for a variety of heat sources. The study aims to develop and apply more comprehensive one-dimensional component models for SCO2 compressors, turbines, and heat exchangers to improve the design and off-design performance analysis. Control strategies are also developed to counteract performance degradation due to varying conditions. The multi-objective design optimization demonstrates promising results for a 50MW net power output, with a thermal efficiency of 0.476 and total product unit cost of 11.652 $/GJ. The findings have the potential to advance the commercial application of SCO2 cycles in high-temperature thermal energy systems [13].

- High ambient temperature and heat capacity mismatch in the desert environment are significant factors that hinder the efficiency of the supercritical CO2 Brayton cycle (SCBC). This Xin Wang , and all [11] presents the establishment of the SCBC and its operating parameters for the precooler, low temperature recuperator (LTR), and high-temperature recuperator (HTR). Performance evaluation factors were developed and applied to analyze the effects of different parameters. The findings showed that the precoolers total heat transfer coefficient (HTC) was highest near the pseudo-critical temperature. A smaller hot-side pressure and larger hot-side and cold-side mass flux increased the precoolers heat transfer performance (HTP). Moreover, using CO2-H2S as a fluid in the precooler led to higher HTC and pressure drop (ΔP), while CO2-Propane in the LTR and HTR resulted in higher total HTCs and ΔP at the same critical temperature. This paper also proposes heat transfer correlations for the precooler of pure CO2 and CO2 mixtures. By analyzing the performance evaluation factors, the authors conclude that using CO2-H2S for the precooler and CO2-Propane for the LTR and HTR can achieve better HTP with a smaller ΔP. However, this combination has lower effectiveness under the same ΔP. Overall, the results suggest that CO2-H2S has potential for practical application due to its higher thermal efficiency and tolerance for changes in critical temperature. This paper is relevant for researchers and engineers working on improving the efficiency of supercritical CO2 Brayton cycles [11] .

- The Li, X. L., and all [10] discusses the potential of solar-integrated fuel cell systems in reducing reliance on fossil fuels and decreasing emissions. It highlights the limitations of solar thermal systems, which have intermittent power output, while fuel cell waste heat systems provide continuous energy. To address this issue, the paper proposes a novel solar and molten carbonate fuel cell complementary driven supercritical-CO2 cycle system that operates through a complementary operation mode. The performance and operation modes of the system are investigated, showing that the fuel cell module operates for 23.5% of the time in a year, resulting in a reduction of storage tank volume and heliostat area. The efficiency of the supercritical-CO2 cycle is 43.1%, which increases to 50.89% with the addition of waste heat utilization. The levelized cost of electricity for the proposed system is 0.1861$/kWh. The research results can serve as a valuable reference for designing complementary energy systems. Overall, the proposed system provides a solution for the intermittency of solar thermal systems and the potential for continuous energy output [10] .

- The BEKHEDDA Zeyneb and all [28] explores the need to improve the performance of thermal installations, given the growing demand for energy and increasing costs of resources. It specifically focuses on the use of combined cycle installations for electricity production, which has become popular despite its high costs. The objective of the thesis is to optimize the performance of these installations, with a focus on the first power plant of this kind in the wilaya of Naama. The study conducts a thermodynamic performance analysis of the gas turbine and uses Cycle-Tempo software for simulation of the power station. Through the energy model, sensitivities are made for the optimization of performance. The document ends with a general conclusion that reflects the results obtained and provides recommendations for future improvements. Overall, the study highlights the benefits of investing in these costly systems for improved energy performance [28] .

I-3 :Energy Situation in Africa:

Most sub-Saharan African countries face a major challenge in meeting their social and development obligations due to the inadequacy of modern energy services, despite their vast energy resources. The low rate of access to electricity in Africa reflects this shortcoming: approximately 17% of the region's population and less than 5% of rural areas are electrified . This must change if Africa is to be economically competitive with other developing regions of the world and achieve its sustainable development goals[1]..

Africa's electricity supply sources broadly reflect the energy resources of each subregion. For example, oil and gas reserves are concentrated in North and West Africa. As a result, the

electricity sector in these two subregions is dominated by fossil fuel-based power generation systems. On the other hand, The electricity industries in East and Central Africa are dominated by hydroelectric power plants with limited use of geothermal energy. Hydropower, petroleum products, and coal are the main sources of electricity in most sub-Saharan African countries. In southern Africa, the main sources of electricity are coal (e.g., South Africa and Zimbabwe) and hydropower (e.g., Lesotho, Malawi, and Zambia). Kenya is the only country to commercially exploit geothermal energy for electricity generation. This contrasts with North African countries, which rely on oil-fired electricity generation. In most sub-Saharan African countries, bagasse biomass is used for cogeneration in the sugar industry. The use of wind energy is increasing in North Africa[1]...

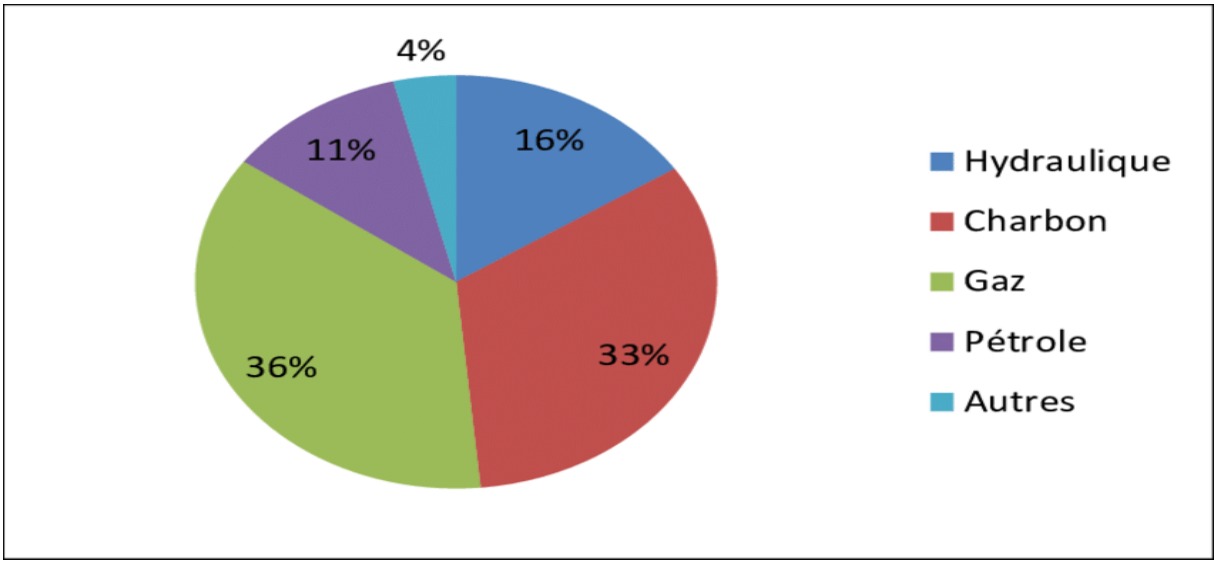


Figure I.2: Distribution of electricity production in Africa in 2015 [41].

selon la source d'énergieMost of the electricity generated in Africa comes from thermal power plants, due to large coal-fired power plants in South Africa and oil-fired power plants in Nigeria and North Africa [41]...

Figure does not include cogeneration, backup power plants, and other off-grid generators, which could make a significant contribution to the economy [41].

Most of the electricity generated in Africa comes from thermal power plants, due to large coal-fired power plants in South Africa and oil-fired power plants in Nigeria and North Africa[29].

Figure does not include cogeneration, backup power plants, and other off-grid generators, which could make a significant contribution to the economy [29].

Most of the electricity generated in Africa comes from thermal power plants, due to large coal-fired power plants in South Africa and oil-fired power plants in Nigeria and North Africa [41].

Figure does not include cogeneration, backup power plants, and other off-grid generators, which could make a significant contribution to the region's electricity supply. Many cogeneration plants, particularly in the agri-food industries, are used for their own consumption (used by the factories/plants producing the electricity) and cannot be recorded in national electricity statistics. For example, in Mauritius, cogeneration accounts for 40% of the country's electricity supply [1].

I-4 :Cogeneration in Sub-Saharan Africa and Algeria:

Combined heat and power (CHP) is an efficient and clean method for generating useful electrical and thermal energy from a single fuel source. It describes a suite of reliable and cost-effective technologies that significantly contribute to meeting global demand for heat and electricity. It is a clean energy solution that directly addresses several national priorities, including improving Africa's competitiveness by reducing energy costs, greenhouse gas emissions, and increasing energy efficiency. The adoption of CHP systems is increasing with energy poverty, reduced carbon emissions, climate change, and energy security. Geographically, Africa (Algeria) enjoys a high availability of natural gas and various renewable energy sources, making their installation relatively easy and cost-effective. The region is one of the potential global markets for cogeneration systems. Electricity is essential both for industrialization and to provide basic energy to the majority of rural residents[1].

Cogeneration offers significant opportunities for generating electricity and/or thermal energy with limited investment, while avoiding the negative environmental impacts of increased fossil fuel combustion. Industries can be located in remote areas not connected to the electricity grid. Additional electricity can be made available to other users through mini-grids. For industries close to the grid, selling surpluses to national utilities would increase their revenues[1] .

The sugar industry is a major user of cogeneration technology, followed by other industries in Africa. Most developments have been recorded in Zimbabwe and Mauritius . Mauritius generates over 40% of its electricity from cogeneration, more than half of which comes from bagasse in the sugar industry. Sugar is a major agricultural export for Ethiopia, Madagascar, Malawi, Mozambique, Swaziland, Zambia, and Zimbabwe. The potential for electricity generation from bagasse is high, as cogeneration equipment is almost always an integral part

of sugar mill designs. Estimates show that up to 16 sub-Saharan African countries could cover a significant portion of their current electricity consumption through bagasse-based cogeneration in the sugar industry[1].

Table I.1: Cogeneration potential (bagasse) for Eastern and Southern Africa[29].

country	2003 (MW)	2003 (GWh)	Quantity (GWh)	% of total generated
Ethiopia	493	1 812	150.3	8.3
Kenya	1143	4 563	530.3	11.6
Malawi	306	1177	250.8	21.3
Mauritius	725	1564	600	38.4
Sudan	1380	3165	643.5	20.3
Tanzania	863	2770	100.8	3.6
Uganda	303	1756	173.4	9.9
Zimbabwe	1961	7906	686.4	8.7
Swaziland	180	395	/	/
Total	7354	25108	3135.5	122.2

At a time when the majority of power plants are equipped with single-cycle gas turbines with an efficiency close to 30%, cogeneration provides a simple way to optimize Algeria's natural gas resources through electricity production[1].

Algeria is moving towards alternative means of production such as solar and wind power; it must preserve its current natural gas resources and not waste them[1].

The cogeneration potential in Algeria exceeds 1,000 MW . In addition to offering unparalleled performance, cogeneration can locally support the national grid by decentralizing electricity production, thus avoiding transmission losses[1] .

In many countries, appropriate pricing systems have enabled the development of this technology. Thanks to its low production cost (cost per kWh, approximately 35% lower than

Sonelgaz's average cost) , it is not necessary to heavily subsidize cogeneration to be profitable and develop massively in Algeria, unlike solar and wind technologies[1]

In the public sector, major projects such as the Grand Mosque showcase this technology. In the private sector, some manufacturers have also chosen to invest because the payback period for cogeneration projects is approximately four years. However, these projects are still too few in number because they are reserved for self-consumption. To move up a gear, the resale of electricity produced from cogeneration systems must become possible at an attractive cost for the producer[1].

I-5 :Cogeneration (Combined Cycles):

Cogeneration or combined cycles (Combined heating and Power) use the power output of the main engine for electricity production, as well as its waste heat for heating. In addition, cogeneration systems compared to conventional energy systems for buildings have several advantages, such as improved overall efficiency, reduced primary energy consumption, and the dispersion of environmental pollutants such as carbon dioxide. [42]

Cogeneration systems comprise a number of other components: engine (thermal), generator, heat recovery and electrical interconnection - configured as an integrated whole. The type of equipment that drives the entire system (i.e. the prime mover) usually identifies the cogeneration system. Cogeneration or combined heat and power systems can use different prime movers, including gas turbines, steam turbines, fuel cells, internal combustion engines and external combustion engines. (Stirling engine) [43]

The aim of this chapter is to have a general description of the overview of the performances of the mainly used first movement technologies consisting of:

1. Reciprocating internal combustion engines
2. Gas turbines
3. Steam turbines

I-5-1 :Advantages and disadvantages:

Table I.2 below summarizes a list of the various advantages and disadvantages of different cogeneration systems.

Table I.2. Advantages and disadvantages of cogeneration technology[1].

Cogeneration system	advantage	Disadvantages	Available sizes
Ignition controlled (SI) reciprocating engine	•High energy efficiency with operational flexibility under partial load. • Fast start-up. • Relatively low investment cost. • Has good load-following ability. • Can be serviced on site with normal operators. • Runs on low-pressure gas.	• High maintenance cost. • Limited cogeneration applications at low temperatures. • Relatively high air emissions. • Must be cooled even if recovered heat is not used. • High levels of low-frequency noise.	1 kW to 10 MW in DG applications
Compression Ignition (CI) Reciprocating Engine			High speed (1,200 rpm) for 4MW
			< 80 MW for low speed (60275 rpm)
Steam Turbine	• High overall efficiency from steam to power. • Can be combined with boilers using a variety of gaseous, liquid or solid fuels. • Ability to meet more than one site heat degree requirement. • Long life and high reliability. • Power to heat ratio can vary.	Slow start-up. • Very low power-to-heat ratio. • Requires a boiler or other steam source.	50 kW to more than 100 MW
Gas turbine	• High reliability. • Low emissions. • High quality heat available. • No cooling required.	• Requires a high-pressure gas compressor. • Low efficiency at low load. • Output decreases as ambient temperature increases.	500 kW to 300 MW

I-5-2 :Types of cogeneration technologies and their assessment:

According to Ref. [44], cogeneration systems can be classified into three categories based on their maximum electrical capacities:

- micro-cogeneration: less than 50 kWh,
- small-scale (or mini) cogeneration: ranging from 50 kWh to 1 MWh

- large-scale cogeneration: greater than 1 MWh.

Sometimes, they can also be classified based on the priority of use of the available energy, i.e. electricity or heat, with a high-cycle (where the priority is to produce electricity) and a base-cycle (where heat takes precedence over electricity).

I-5-3 :Cogeneration system powered by an internal combustion engine (reciprocating motion):

Their long history of technical development and high production levels have contributed to making piston engines a robust, reliable, and economical choice as the primary powerplant for cogeneration applications [45]. Their sizes range from fractional horsepower engines to 5-stage marine propulsion systems weighing over 5 million kilograms and producing over 80 megawatts (MW). The technology has improved significantly over the past three decades, driven by economic and environmental pressures for improvements in power density (more output per unit of engine displacement), increased energy efficiency, and reduced emissions. Electronic power control modules have made more precise control and diagnostic monitoring of the engine process possible. Stationary engine manufacturers and engine research and development companies around the world continue to utilize advanced engine technologies, particularly by accelerating the diffusion of innovative technologies and concepts from the automotive market to the stationary machinery market.

Reciprocating engines have capacities ranging from 10 kW to 10 MW. Multiple engines can be integrated to provide capacities exceeding 10 MW in a single plant. The main applications of cogeneration in the commercial and residential sectors are those with relatively high and consistent electricity and hot water requirements, such as universities, hospitals, water treatment facilities, industrial plants, commercial buildings, and multi-family dwellings.

I-5-3-1: Reciprocating Engine Technology:

There are two main types of reciprocating engines suitable for stationary power generation applications: the spark-ignition Otto cycle engine and the compression-ignition diesel engine. The essential mechanical components of the Otto cycle and the diesel cycle are the same. Both use a cylindrical combustion chamber in which a tightly fitting piston travels the length of the cylinder. The piston connects to a crankshaft, which converts the linear motion of the piston into rotational motion. Most engines have multiple cylinders driving a single crankshaft. The main difference between the two cycles is the fuel ignition method. Spark-ignition (Otto cycle) engines use a spark plug to ignite a premixture of air and fuel introduced

into the cylinder. Compression-ignition engines (diesel cycle) compress the air introduced into the cylinder to high pressure, raising its temperature to the autoignition temperature of the high-pressure fuel [1].



Figure I.3: Cogeneration with modern engine technology[36]

a. Engine System :

The efficiencies of natural gas-fired engines range from approximately 28% (lower heating value) for small engines (< 50 kW) to 46% (lower heating value) for larger, high-performance, lean-burning engines[1] .

Table I. 3 shows some of the attributes of the internal combustion engine used in cogeneration systems.

Table I .3:. The reciprocating motor attribute [1]

Size range	Reciprocating engines for cogeneration are available in sizes ranging from 10 kW to 10 MW. Multiple engines can be combined to provide higher capacities. The majority of cogeneration systems with reciprocating engines have a power output of less than 5 MW.
Exit thermal	Thermal energy can be recovered from engine exhaust gases, cooling water, and lubricating oil, and then used to produce hot water, low-pressure steam, or chilled water (using an absorption chiller).
Partial load operation	Reciprocating engines operate well at part load and are well suited for base load.
Fuel	Reciprocating engines can run on a wide range of gaseous and liquid fuels. For cogeneration, natural gas is the most common fuel.
Reliability	Reciprocating motors are a mature technology with high reliability.
Other things	Reciprocating engines have relatively low installation costs and are widely used in cogeneration applications. Reciprocating engines start quickly and operate at typical natural gas discharge pressures without additional gas compression.

b. Thermal Power Generation:

The profitability of engines in on-site power generation applications often depends on the efficient use of thermal energy contained in the exhaust and cooling systems, which typically accounts for 60 to 70% of the fuel input energy[4].

Approximately 30% of the energy value of these engines is converted into useful mechanical power, with the remainder wasted through heat generated by the cooling system and through exhaust or mechanical losses. Most of the waste heat is available in the engine exhaust gases and the jacket coolant, while smaller amounts can be recovered in the lubricating oil cooler and the turbocharger intercoolers and aftercoolers (if applicable). Forty-five to five percent of the waste heat from engine systems comes from jacket cooling water and lube oil cooling systems at a temperature too low to produce steam. This feature is generally less critical in commercial and institutional applications where hot water heat loads are more common. Steam can be generated from exhaust heat if necessary (maximum pressure of 2756.0 kPa),

but if no hot water is required, the amount of heat recovered by the engine is reduced and the overall efficiency of the cogeneration system decreases accordingly[4].

The heat in the engine jacket coolant accounts for up to 30% of the energy input and can produce hot water between 90 and 120°C. Engines with high-pressure or turbulent cooling systems can operate at temperatures up to 130°C. Engine exhaust heat accounts for 30 to 50% of the available waste heat. The exhaust temperature of systems designed for this purpose ranges from 380 to 530°C. By recovering heat from the cooling and exhaust gas systems, approximately 80% of the fuel's energy can be efficiently used to produce energy and useful heat[4].

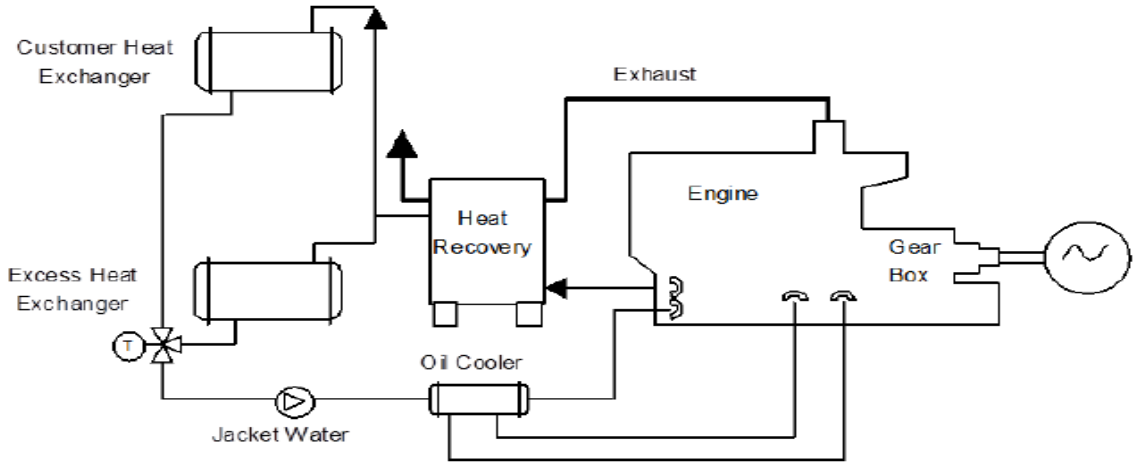


Fig. I.4: Closed-loop heat recovery system[46]

The most common method of engine heat recovery is the closed-loop cooling system, as shown in **Figure I.4**. These systems are designed to cool the engine by forced circulation of coolant through the engine passages and an external heat exchanger. An excess heat exchanger transfers heat from the engine to a cooling tower or radiator in case of excess heat[46].

Closed-loop water cooling systems can operate at coolant temperatures between 90 and 120°C. Depending on the engine and CHP system requirements, post-cooling of the lubricating oil and turbocharger can be an integral part of the jacket cooling system. These cooling systems cool the engine by naturally circulating boiling coolant through the engine. This type of cooling system is typically used with exhaust heat recovery to produce low-pressure steam[46].

The coolant at the engine outlet is maintained in saturated vapor conditions and is generally limited to 120°C and a maximum of 1,034 bar. The uniform temperature throughout the coolant circuit extends engine life and helps improve combustion efficiency[46]

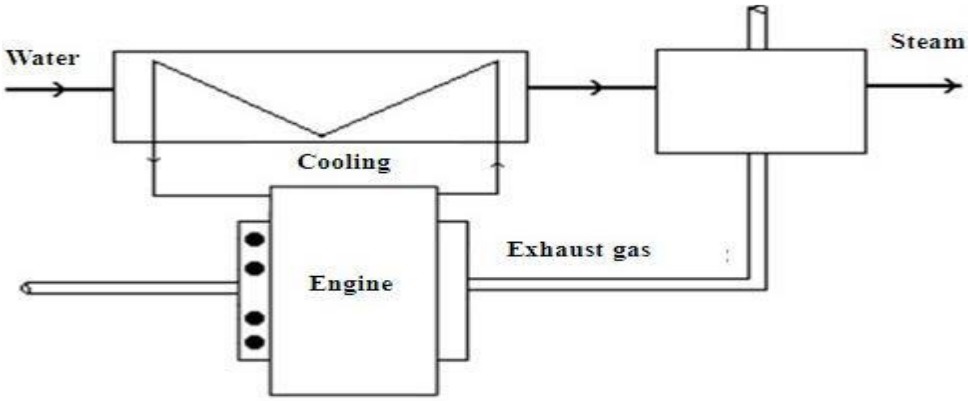


Fig. I.5. Internal combustion engine cogeneration unit[47].

Exhaust heat recovery can be independent of the engine cooling system or coupled to it. In a typical district heating system, jacket cooling, lubricating oil cooling, single-stage cooling, and exhaust heat recovery are all integrated for steam production[46].



Fig. I.6 : Cogeneration installations Principle[38]

c. Performance:

The table I .4 summarizes the performance characteristics of cogeneration systems using a natural gas spark-ignition engine and is commercially available in a range of sizes from 100 kW to 9 MW. This size range covers the majority of market applications for engine-driven cogeneration.

Cogeneration heat recovery estimates are based on hot water production for process or space heating purposes.

Table I.4. Typical performance parameters of the cogeneration engine for spark-ignition engines[1]

Performance Characteristics	System				
	1	2	3	4	5
Basic electrical capacity(kW)	105	635	1120	3329	9345
Engine speed (rpm)	2500	1800	1800	1500	720
CHP Features					
Exhaust temperature (°C)	655	505	425	382	354
Total Heat Recovered (kW)	199	812	1260	3127	7852
Form of recovered heat	H20	H20	H20	H20	H20, steam
Total effectiveness	80.0 %	78.9 %	78.4 %	78.3 %	76.5 %
Thermal power / fuel input	53.0 %	44.4 %	41.6 %	37.9 %	35.0 %
Power/heat ratio	0..51	0.78	0.89	1.06	1.19

d. Engine Speed Classification:

Reciprocating engines are classified as high, medium, or low speed. The **table I.5.** shows the standard speed ranges for each class, as well as the engine types and sizes available.

Table I.5. Types of reciprocating motors by speed (Values available in MW) [48]

Classification by speed Speed of the	Engine speed (rpm)	Stoic / Rich Burn, Spark Ignition (MW)	Lean Burn, spark ignition (MW)	Dual-fuel (MW)	Diesel (MW)
High speed	1000-3600 rpm	0.01 – 1.5	0.15 - 3.0	1.0 - 3.5	0.01 – 3.5
Average speed	275-1000 rpm	None	1.0 – 18	1.0 – 17	0.5 – 18
Low speed	58-275 rpm	None	None	2.0 – 65	2 – 84

e. Installation:

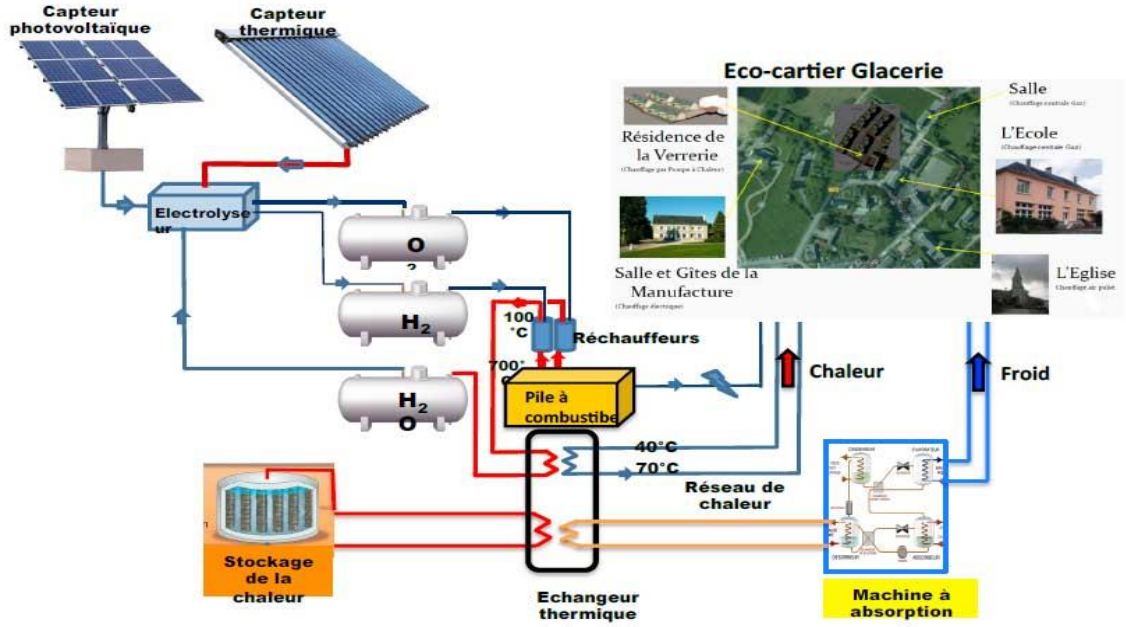


Fig. I.7 : Fuel cell micro-tri-generation[49]

Internal combustion engines are the main drivers of cogeneration systems and offer many advantages, such as simple setup and low maintenance costs. As presented in the study by Harrord et al., there are few disadvantages, such as low thermal efficiency, high fuel consumption, high noise generation, and significant pollutant production. Since the exhaust gases from a combustion engine have high temperatures and this potential heat will always be wasted into the environment, the idea of using an internal combustion engine to recover this waste heat can be beneficial in cogeneration systems [50].

Meybodi and Behnia presented a comprehensive sensitivity analysis to estimate the influence of certain economic parameters, such as taxes on activated carbon, on the size of a cogeneration system with an internal combustion engine as the prime mover [51].

Asaee et al. evaluated the technical and economic performance of a cogeneration system with a thermal engine under five different meteorological conditions in Canada [52]. Arbabi et al. conducted a technical and economic study of a cogeneration system with an integrated circuit engine for the critical loads of a rudimentary building in Iran. They also proposed different scenarios for this system [53].

I-5-3-2 : Gas Turbine Cogeneration System with Heat Recovery:

Introduction:

Gas turbines generally exhibit favorable economics for sizes greater than five MW. Gas turbines are well-suited for industrial and institutional cogeneration applications because high-temperature gas turbine exhaust gases can be used to generate high-pressure steam or directly for heating or drying.

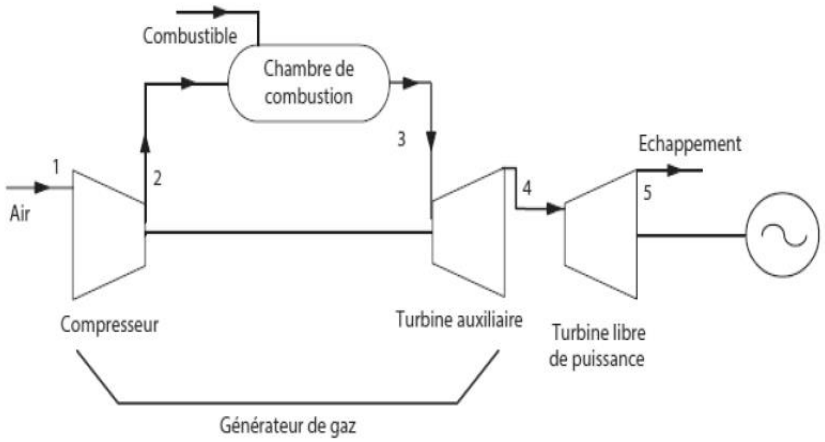


Fig. I..8: Single-cycle gas turbine cogeneration systems (Brayton cycle) integrated into a waste heat steam boiler [54].

Gas turbines produce high-temperature exhaust heat that can be recovered in a cogeneration configuration to produce steam for processing. Such cogeneration configurations can achieve an overall system efficiency (electricity and useful thermal energy) of 70 to 80%. The efficiency and reliability of small gas turbines (1 to 40 MW) have increased sufficiently to make them an attractive choice for industrial users and large Institutional users for cogeneration applications. Gas turbine emissions are very low compared to other fossil fuel generation technologies. Gas turbines emit significantly less carbon dioxide (CO2) per kilowatt hour (kWh) than other fossil fuel technologies used commercially [55].

Gas turbines are ideally suited for cogeneration applications because their high-temperature exhaust gases can be used to generate process steam at temperatures as high as 83.7 bar (62 bar) and 482°C (880°F) or directly in industrial heating or drying processes. A typical commercial/institutional cogeneration application for gas turbines on a college or university campus features a 5 MW single-cycle gas turbine. Approximately 8 MWth of steam (or hot water) is generated in an unheated heat recovery steam generator (HRSG) and sent to a central heating loop for winter campus heating [56].

Table I.6. Summary of gas turbine attributes [1]

Size range	Simple cycle turbines are available in sizes ranging from 30 kW (known as microturbines) to 300 MW (some products exceed 300 MW).
Thermal output	Gas turbines produce high-temperature exhaust gases, and the thermal energy can be recovered to produce steam, hot water, or cold water (using an absorption chiller). The exhaust gases can also be used directly for drying or heating industrial processes.
Partial loading operation	The electrical production efficiency of gas turbines decreases significantly as the load decreases. Therefore, gas turbines offer the best economic performance in base-load applications where the system operates at or near full load.
Fuel	Gas turbines can operate on a wide range of gaseous and liquid fuels. For cogeneration, natural gas is the most common fuel.
Reliability	Gas turbines are a mature technology with high reliability.
Others	Gas turbines have relatively low emissions and require no cooling. Gas turbines are widely used in cogeneration applications and have relatively low installation costs.

I-5-3-2-1 :Gas turbine system technology:

Gas turbine systems operate according to the thermodynamic Brayton cycle, which is an open-cycle heat engine at constant pressure. The Brayton cycle consists of a compressor, a combustion chamber, and a turbine. The compressor heats and compresses the incoming air, which is then heated by adding fuel to the combustion chamber. The mixture of hot air and combustion gases drives the expansion turbine, producing enough energy to power the generator or mechanical process and also drive the compressor. The power produced by the turbine and consumed by a compressor is proportional to the absolute temperature of the gas passing through the device. Fuel consumption can be reduced by preheating the compressed air with heat from the exhaust gases using a recuperator or regenerator. Compressor work can also be reduced and net power increased by using intercooling or precooling techniques. In a

combined cycle, exhaust gases can be used to increase steam in a boiler and generate additional energy[1].

A gas turbine system is considered a combined heat and power (CHP) configuration if the waste heat (i.e., thermal energy) generated by the turbine is applied to the end use. For example, a single-cycle gas turbine using exhaust gases in a direct heating process is a cogeneration system. A gas turbine that uses exhaust gases from a heat generator and then uses the steam from that generator to generate electricity in a steam turbine is a combined-cycle unit and is not considered a cogeneration plant (no thermal end use). The latter configuration is a waste heat to power (WHP) system[1].

I-5-3-2-2: Types of Gas Turbines:

a. Aeroderivative Gas Turbines:

Aeroderivative gas turbines for stationary power are adapted from their counterparts in jet engines and turbines. Although these turbines are lightweight and thermally efficient, they are generally more expensive than products designed and built exclusively for stationary applications. The largest aeroderivative gas turbines available have a capacity of 40 to 50 MW. Many aeroderivative gas turbines for stationary use operate at compression ratios of around 30:1, requiring an external high-pressure fuel gas compressor[1].

b. Industrial gas turbines:

Industrial gas turbines, or frame gas turbines, are exclusively designed for stationary power generation and are available in capacities ranging from 1 to over 300 MW. They are generally less expensive, more robust, can operate longer between overhauls, and are better suited to continuous base-load operation with longer inspection and maintenance intervals than flight turbines. However, they are less efficient and much heavier. Industrial gas turbines generally have lower compression ratios (up to 16:1) and often do not require an external fuel gas compressor[1].

c. Performance Characteristics:

The efficiency of the Brayton cycle is a function of the pressure ratio, ambient air temperature, turbine inlet air temperature, compressor and turbine component efficiency, turbine blade cooling requirements, and any additional air cooling, reheating, steam injection, or combined cycle[1].

Table I .7 summarizes the performance characteristics of cogeneration systems using commercially available gas turbine cogeneration plants, ranging in size from 3 to 45 MW.

The data in the table shows that electrical efficiency generally increases with the size of combustion turbines. As electrical efficiency increases, the absolute amount of thermal energy available to produce steam decreases per unit of power, and the heating power ratio of the cogeneration system increases. Changing the electricity-to-heat ratio impacts the project's economics and can affect customer decisions regarding cogeneration acceptance, sizing, and energy sales opportunities. It is generally recommended to size a cogeneration system based on the site's heat load demand. Therefore, such heating power ratios are important characteristics to consider.

Table I. 7. Summary of performance characteristics of cogeneration systems using gas turbine cogeneration plants [57].

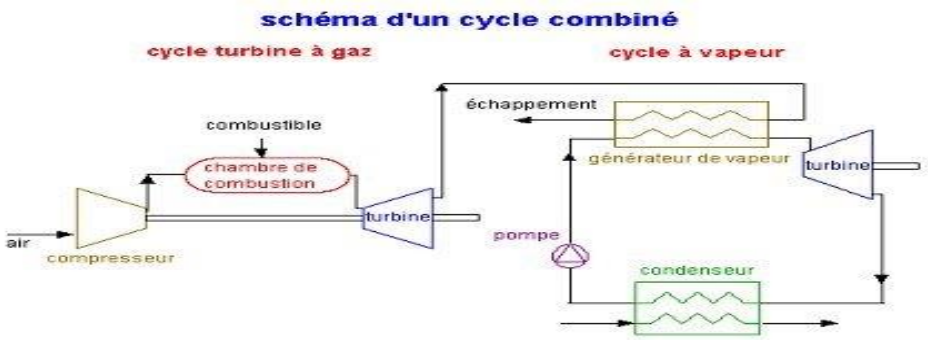
Cost and performance characteristics	System				
	1	2	3	4	5
Characteristics of cogeneration					
GT exhaust temperature (°C)	449	490	488	465.2	461.4
Exhaust temperature HRSG (°C)	172	153	165	167	154
Steam power (equivalent kW)	5762	10093	15342	22806	40646
Total cogeneration efficiency (%)	65.6	70.3	69.6	70.6	68.9
Power / heat ratio	0.56	0.69	066	0.88	1.08
Net heat rate (Kj / kWh)	7,186	6004	6233	5782	5898
Effective electrical efficiency (%)	50	62	59	61	63

d. Heat Recovery:

A significant amount of heat is lost through the flue gases because not all of the heat produced by the gas turbine combustion process can be transferred to the water or steam in the steam boiler. Therefore, recovering heat from the exhaust gases can help improve the overall efficiency of the cogeneration system. Heat can be recovered from the flue gases by passing

them through a heat exchanger or by using an Organic Rankine Cycle (ORC) machine to generate electricity from the low-quality waste heat.

Fig. I.9. Centrale de cogénération à turbine à gaz[60]



The economics of gas turbines as CHPs in process applications depend heavily on the efficient use of the thermal energy contained in the exhaust gas. The figure I.9 provides a schematic representation of a gas turbine generator with exhaust heat recovery transferring energy to a heat recovery steam generator (HRSG) that can provide steam for the process or drive a steam turbine generator. Thermal energy typically accounts for 60–70% of the fuel input. The most common use of this energy is steam production in unstretched or supplemental combustion heat recovery steam generators. However, gas turbine exhaust can also be used as a direct energy source for fired or unfired process fluid heaters, or as preheated combustion air for electric boilers. A recycled heat generator is the simplest steam cogeneration configuration and can generate steam up to approximately 83 bar.

I-5-3-3. Steam Turbine

Introduction

Its capacity can range from 50 kW to several hundred MW for large power plants. Steam turbines are widely used for cogeneration (combined cycle and combined heat and power applications worldwide) [1].

Unlike gas turbines and other engines in cogeneration systems, steam turbines normally produce electricity as a by-product of heat (steam) production. A steam turbine is captive to a separate heat source and does not directly convert fuel into electrical energy. Energy is transferred from the boiler to the turbine by high-pressure steam, which powers the turbine and generator. This separation of functions allows steam turbines to operate on a wide variety of fuels, from clean natural gas to solid waste[1].

In cogeneration applications, low-pressure steam is extracted from the steam turbine and used directly in a process, for district heating, or to be converted into other forms of thermal energy, including steam, hot water, or chilled water[1].

Table I. 8: Summary of steam turbine attributes described in detail in this chapter[1]

Size range	Steam turbines are available in sizes ranging from less than 100 kW to over 250 MW. In the multi-megawatt size range, the industrial and utility steam turbine designations merge, with the same turbine (high-pressure section) being suitable for both industrial and small utility applications.
Custom design	Steam turbines can be designed to meet cogeneration pressure and temperature requirements. The steam turbine can be designed to maximize electrical efficiency while providing the desired thermal efficiency.
Thermal output	Steam turbines are capable of operating over a very wide range of steam pressures. Utility steam turbines operate with inlet steam pressures up to 241.3 bar and exhaust gases under vacuum conditions as low as 0.14 bar. Steam turbines can be custom-designed to meet the thermal requirements of cogeneration applications through the use of backpressure or extraction steam at appropriate pressures and temperatures.
Fuel flexibility	Steam turbines offer a wide variety of fuels, using different fuel sources in the associated boiler or another heat source, including coal, oil, natural gas, wood, and waste, in addition to waste heat recovered in a heat recovery steam generator.
Reliability and longevity	The service life of steam turbine equipment is extremely long. Some steam turbines have been in service for over 50 years. When properly operated and maintained (including proper monitoring of boiler water chemistry and ensuring dry steam), steam turbines are extremely reliable, with overhaul intervals measured in years. Larger turbines require controlled thermal transients because the massive casing heats up slowly and differential expansion of parts must be minimized. Small wind turbines are generally not subject to start-up restrictions.

I-5-3-3-1 : Steam Turbine Cogeneration System Technology

The thermodynamic cycle of the steam turbine is called the Rankine cycle. This cycle forms the basis of conventional power plants and consists of a heat source (boiler) that converts water into high-pressure steam. In the steam cycle, the water is first pumped at medium or high pressure, depending on the size of the unit and the temperature to which the steam is ultimately heated. It is then heated to the boiling point corresponding to the pressure, boiled (from liquid to steam), and then, most often, superheated (heated to a temperature above boiling). The pressurized steam is expanded to reduce the pressure in a turbine and then discharged to a vacuum condenser or an intermediate-temperature steam distribution system, providing steam for industrial or commercial applications. Condensate from the condenser or industrial steam system is returned to the feed pump to continue the cycle[1].

I-5-3-3- 2:Cogeneration System Components:

The figure shows a schematic representation of a steam turbine power system.

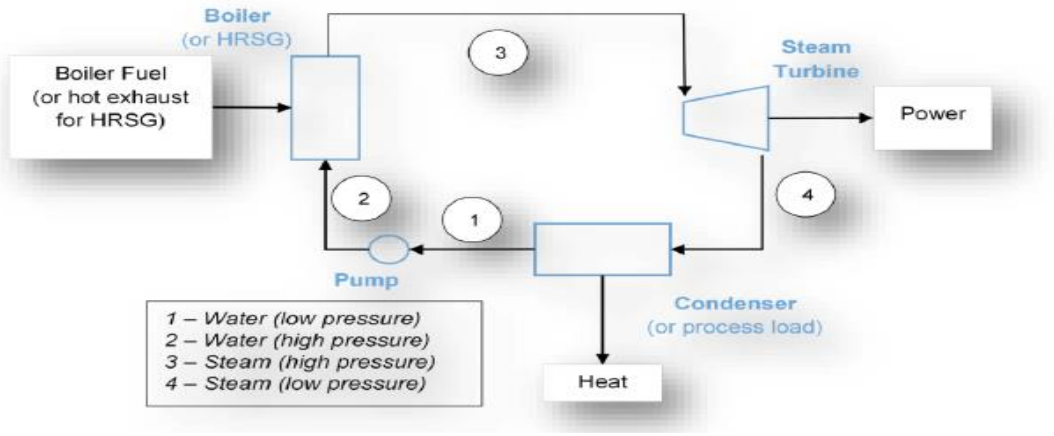


Fig I.10: Boiler/steam turbine system [59]

A fuel-fired boiler produces steam, which is expanded in the steam turbine to generate power. When the system is designed solely for electricity generation, such as in a large distribution network, the steam is extracted from the turbine at the minimum usable pressure, using a water-cooled condenser to extract maximum energy from the steam turbine[59].

In cogeneration plants, the steam is extracted from the steam turbine at a pressure sufficient for use by the heating system. There is no condenser in the cogeneration configuration; the steam and condensate, after leaving the process, are returned to the boiler[59].

Steam systems range from low-pressure pipelines used primarily for space heating and food preparation, to medium-pressure and temperature applications used in industrial processes and cogeneration, to high-pressure and high-temperature applications for electricity generation. Generally, as the system grows, economics favor higher pressures and temperatures, along with their heavier-walled boiler tubes and more expensive alloys[59].

a. Boilers :

Steam turbines differ from other engines and gas turbines because the fuel is burned in the boiler, which is separate from the power-generating equipment. The energy is transferred from the boiler to the steam turbine generator, usually via pressurized steam. Some of the most commonly used boilers are:

*Large, shop-assembled boilers, usually capable of burning only gas or oil.

*Large, locally built industrial boilers using solid and residual fuels are similar to utility boilers, except for the solid fuel injection.

*Large boilers typically use pulverized coal. However,

intermediate boilers and small coal- or solid-fuel-fired boilers use different types of solid feed systems [2].

b. Steam Turbine :

In a steam turbine, steam is expanded to a lower pressure, providing shaft power to drive a generator or perform a mechanical process. There are two distinct designs for steam turbines: impulse turbines and jet turbines. The difference between these two designs is illustrated in **Figure I.10.**

In impulse turbines, steam jets are directed toward the bucket-shaped rotor blades, where the pressure exerted by the jets causes the rotor to rotate and reduces the steam's velocity as its kinetic energy is transferred to the blades. The series of blades reverse the direction of the steam before it passes into the second row of blades. In reaction turbines, the rotor blades of the reaction turbine have a shape more similar to that of aerodynamic blades, arranged so that the cross-section of the chambers formed between the fixed blades decreases from the inlet side to the exhaust side. The chambers between the rotor blades are essentially formed as nozzles, so that as the steam moves through the chambers, its speed increases while its pressure decreases, as in the nozzles formed by the fixed blades. [59]

Fixed nozzles accelerate steam to high speeds by expanding it at a lower pressure. A rotating bladed disc changes the direction of the steam flow, creating a force on the blades which, due to the geometry of the impeller, translates into a torque on the shaft on which the impeller is mounted. The combination of torque and speed corresponds to the turbine's power output. A reduction gear can be used to reduce the turbine speed to the required generator output speed. Compared to steam engines of comparable size, steam turbines operate at much higher rotational speeds, which reduces their cost per unit of power. In addition, the intake and

exhaust valves of reciprocating steam engines cause steam pressure losses that do not contribute to power. Such losses do not occur in steam turbines. Due to these design differences, steam turbines are more efficient than other steam engines operating under the same intake and exhaust conditions[59].Steam turbines used for cogeneration can be classified into two main types: non-condensing systems and extraction systems.

I-5-3-3-3 Performance Characteristics

Steam boilers and turbines used for power generation in large power plants can achieve energy efficiencies exceeding 45%, although the average efficiency of all units in the field is around 33%. Backpressure steam turbines used in cogeneration applications only extract a portion of the steam's energy to generate electricity, with the remainder being used for processing. As a result, the electricity generation efficiencies for the examples presented are all less than 10% of the HHV[1].

Table I. 9: Summary of performance characteristics of commercially available boosted steam turbines used in cogeneration applications from 500 kW to 15 MW [1]

Steam Turbine Parameters 67	System		
	1	2	3
Nominal electricity capacity (kW)	500	3000	15000
Typical application	Industrial, PRV applications	Industrial, academic, hospital	Industrial, academic, hospital
Isentropic turbine efficiency (%)	52.6	61.3	78.1
Inlet pressure (bars)	34.6	41.4	48.2
Inlet Temperature (°C)	289	303	345
Outlet Pressure (bar)	3.5	10.4	10.4
Outlet Temperature (°C)	152	189	196
Cogeneration System Parameters	1	2	3
Boiler Efficiency (%)	80	80	80
Electrical Efficiency (%)	6.28	4.93	7.32
Steam to be Processed (kW)	5845	45625	148485
Total Cogeneration Efficiency (%)	79.58	79.66	79.70

The efficiency of an isentropic steam turbine refers to the ratio of the power actually generated by the turbine to that generated by a perfect turbine with no internal flow path losses using steam under the same inlet conditions and discharging at the same downstream pressure. Turbine efficiency should not be confused with electrical production efficiency, which is the ratio of the net power generated to the total fuel input in the cycle. Steam turbine efficiency measures how effectively the turbine extracts energy from the steam itself. It is useful for identifying the conditions of the steam as it exits the turbine and for comparing the performance of various steam turbines. [1]

Heat recovery methods in steam turbines use backpressure or exhaust steam. However, in the case of steam turbines, it is the steam turbine that can be defined as a heat recovery device. Steam turbine cogeneration systems are typically characterized by very low power-to-heat ratios, typically between 0.05 and 0.2. This is because electricity is a by-product of heat production, as the system is optimized for steam production. Therefore, while the electrical efficiency of steam turbine cogeneration systems may seem very low, it is because the primary objective is to produce large quantities of steam. However, the actual electrical efficiency of steam turbine systems is typically very high because almost the entire energy difference between the high-pressure boiler and low-pressure turbine power is converted into electricity. This means that the total efficiency of the cogeneration system is typically very high and close to the boiler efficiency level. Steam boiler efficiency ranges from 70% to 85% of the HHV, depending on the type and age of the boiler, fuel, duty cycle, application, and steam. [1]

Table I. 10: Performance Characteristics of Backpressure Steam Turbine[1]

Steam turbine parameters	System		
	1	2	3
Power/heat ratio	0.088	0.065	0.102
Net heat rate (kJ/kWh)	4.542	4.541	4.444
Effective electrical efficiency (%),	75.16%	75.19%	76.85%
Heat/fuel ratio	0.734	0.749	0.725

Table I. 11: Performance characteristics of a steam turbine of a natural gas boiler [1]

Description	System		
	1	2	3
Net electrical power (kW)	500	3000	15000
Steam inlet pressure (bar)	34.6	41.3	48.5
Steam inlet temperature (°C)	288.1	301.8	343.5
Steam outlet pressure (bar)	3.6	10.5	10.5
Steam outlet temperature (°C)	147.9	189.5	193.2
Power to heat ratio	0.086	0.066	0.102
Electrical efficiency (%)	6.4	5.1	7.4
Thermal efficiency (%)	73.4	74.9	72.5
Overall efficiency (%)	79.5	79.8	79.6

CHAPTER II:

Theoretical and Numerical Study

CHAPTER II: Theoretical and Numerical study

II.1. Introduction

To address the growing need for high-efficiency and sustainable energy systems, this study proposes a hybrid multi-generation configuration that integrates multiple energy conversion technologies. The system is designed to recover and utilize thermal energy at various temperature levels, aiming to optimize overall energy and exergy performance. It combines a solar thermal subsystem using molten salt as a heat transfer and storage medium, a molten carbonate fuel cell (MCFC) for clean and efficient electricity production, and a supercritical CO_2 Brayton cycle for high-efficiency power generation.

In addition, the system incorporates absorption refrigeration cycles using two different working fluid pairs: ammonia (NH_3) and lithium bromide–water ($LiBr–H_2O$), each suited for different temperature recovery levels. A bottoming Organic Rankine Cycle (ORC) is also included to capture remaining low-grade heat. This configuration allows for comprehensive thermal cascade utilization, making it ideal for solar-rich and energy-diverse environments.

The following section provides a detailed description of the system's components and their interactions, supported by a schematic diagram that illustrates the flow of energy through the system.

II-1 : System Description

Depending on the form of concentrated light, concentrating solar power systems include parabolic trough sensor . The parabolic trough sensor-type collector system has a high energy conversion efficiency and a wide range of applications . Taking into account the instability of solar thermal systems, a molten salt storage system is added. The two-tank molten salt storage system is more reliable and widely used than single-tank heat storage . The parameters of the Heliostat field and thermal storage system are designed and the design parameters of the solar collector system and the molten salt thermal storage system are shown in Table 2.

Molten salts are used as heat transfer fluid (HTF) in concentrated solar power plants. Considering the chemical and thermodynamic properties of molten salt ,

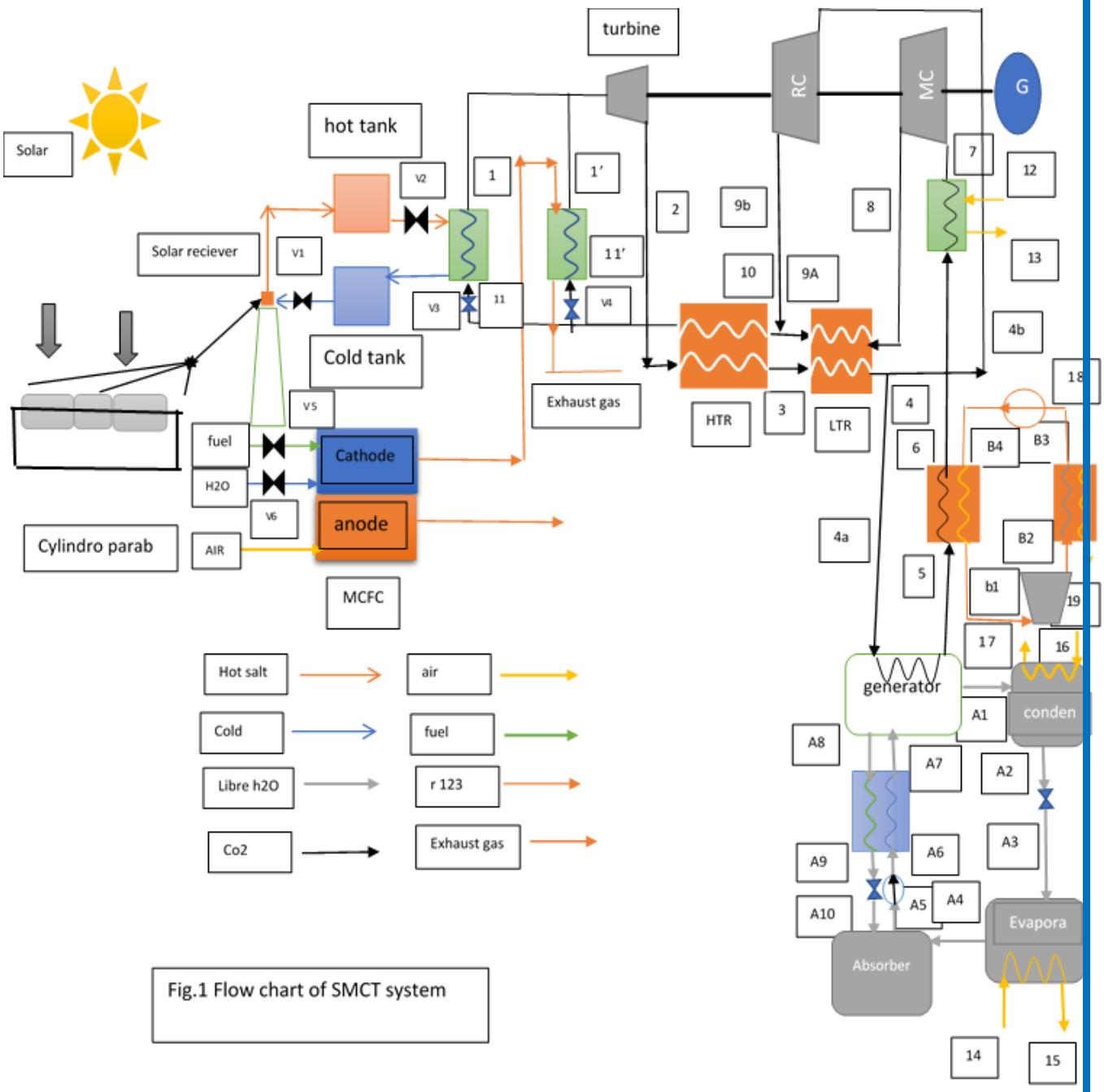


Fig II.1:flow chart of SMCT system.

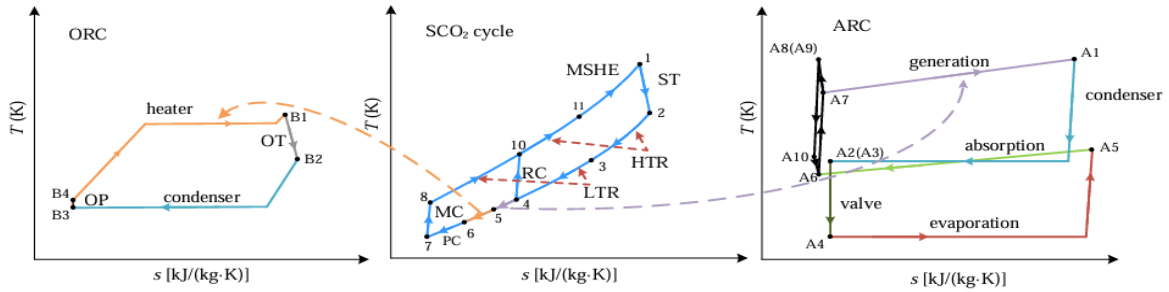


Fig II.2: T-s diagram of SCO2 cycle, ORC, and ARC

the heat storage medium used in this study is a mixture of 60% NaNO3 and 40% KNO3 with the physical parameters :

$$\rho = 2090 - 0.636 \cdot T \quad \text{(II. 1)}$$

$$C_p = 1443 + 0.172 \cdot T \quad \text{(II. 2)}$$

$$\lambda = 0.443 + 1.9 \cdot 10^{-4} \cdot T \quad \text{(II. 3)}$$

Table II.1 Input parameters of SMCT system [14]

Parameters	**Symbol**	**Value**
Total area of heliostat field (m2)	A hel	532396
Direct Normal Irradiance (W/m2)	δ DNI	850
Efficiency of the solar receiver (%)	η rec	91
Volume of hot tank (m3)	V hot	10227
Hot tank inlet temperature (K)	T hot,in	853.15
Cold tank outlet temperature (K)	T cold,out	663.15
MCFC operating temperature (K)	T MCFC	927.15
Fuel utilization ratio (%)	U f	85
The mass flow rate of the fuel (kg/s)	m fuel	6.4
The inlet temperature of ST (K)	T ST,in	823.15
Inlet pressure of ST (MPa)	P ST,in	20
Efficiency of ST (%)	η ST	90
Inlet temperature of MC (K)	T MC,in	305.15
Inlet pressure of MC (MPa)	P MC,in	7.4
Efficiency of MC (%)	η MC	85
Efficiency of RC (%)	η RC	85
Ambient temperature (K)	T0	298.15
Ambient pressure (MPa)	P0	0.1
Electricity price ($/kWh)	**Z** ele	0.1066
Natural gas price ($/GJ)	Z fuel	3.3
Life time (year)	n	20
Annual operating hours (h)	τ	8000
Interest rate	ir	0.12
Maintenance factor	γ k	0.06

To ensure the electrical power output of the SCO2 Brayton cycle and the continuous operation of the refrigeration and power generation bottom cycle, the input parameters of the MCFC module are
set according to the heat demand of the Brayton cycle. Figure 3 shows the flow chart of the integrated system of MCFC and SCO2 Brayton cycle.

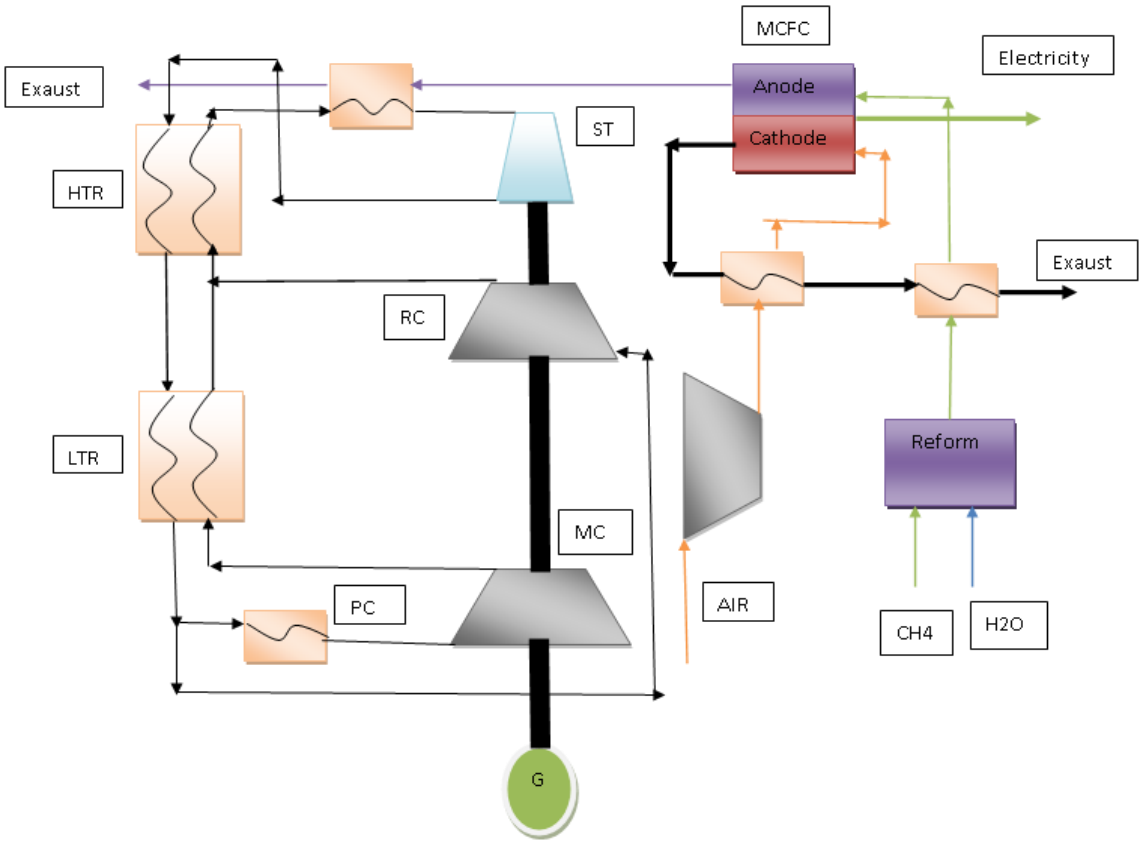


Fig.II .3 : Flow Chart of MCFC-SCO2 Brayton Cycle System.

In the MCFC system, fuel and steam are mixed into the reformer to produce CO and H2, and the reaction equation is as in Eq. (4). Hydrogen-rich fuel enters the fuel cell from the anode, and air is pressurized in the compressor before entering the cathode for reaction. MCFC converts the chemical energy of the fuel into electrical energy through electrochemical 1 reactions. The cathode electrochemical reactions are shown in Eq. (5) and Eq. (6).

$$H_2O + CH_4 \rightarrow CO + 3H_2 \qquad \text{(II. 4)}$$

$$3H_2 + 3CO_3^{2-} \rightarrow 3CO_2 + 3H_2O + 6e^- \qquad \text{(II. 5)}$$

$$4CO_2 + 2O_2 + 8e^- \rightarrow 4CO_3^{2-} \qquad \text{(II. 6)}$$

In this study, a closed recompression SCO2 Brayton cycle is used, where CO2 is heated in a molten salt heat exchanger and then high-temperature and high-pressure CO2 enters the turbine. After doing work, the CO2 passes through HTR and LTR. The CO2 is then split into two parts, one passing through the pre-cooler into the MC and the other directly into the RC. The mass from MC enters the low temperature recuperator and merges with the mass from RC back to the molten salt heater to complete a cycle.

II-2 : Principle of the absorption machine:

The principle consists of spraying water in fine droplets into a vacuum container. Due to the low pressure, the water evaporates. To do this, it requires a certain amount of heat, which is extracted from the water to be cooled, circulating in a circuit through the container. But this system cannot function for very long time, the vacuum container will quickly become saturated with water vapor, and the dispersed water will no longer evaporate. Therefore, a means is needed to maintain or recreate the vacuum in the container! [22]

This is where the sorbent comes in. It is either a liquid, in which case it is called an absorbent, or a porous solid, in which case it is called an adsorbent. It "drinks" the water vapor contained in the environment and retains it. As it absorbs/adsorbs water vapor, its ab/adsorption capacity decreases until it reaches zero, at saturation. The sorbent is then heated to a certain temperature and “gives back” the water vapor. It then recovers all of its ab/adsorption properties. [22]

How the absorption machine works :

The absorption refrigeration machine is divided into four main components:

1) the evaporator.
2) the absorber.
3) the concentrator.
4) the condenser.

In the evaporator, the refrigerant (in this case, water) is sprayed into a very low-pressure environment. A water circuit runs through the evaporator. As it evaporates, the refrigerant removes its heat from the water, which is then cooled. Some of the sprayed refrigerant does not evaporate and falls to the bottom of the evaporator, where it is pumped back to be sprayed again[22]

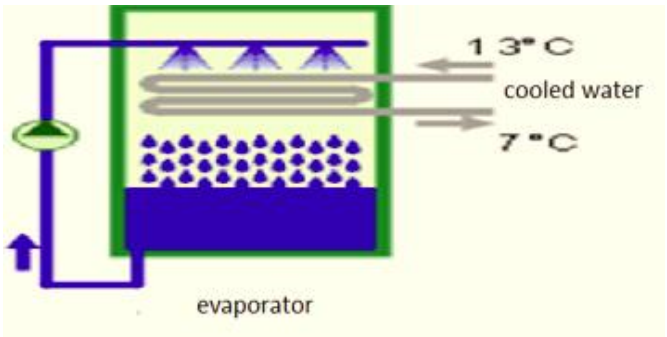


Fig.II .4 : the evaporator in the absorption machine[22]

1) The water vapor created in the evaporator is fed to the absorber. It contains the absorbent solution (LiBr), which is continuously pumped into the bottom of the container for spraying. The LiBr absorbs the water vapor from the evaporator, maintaining the low pressure necessary for vaporizing the refrigerant. As it absorbs water vapor, the absorbent solution becomes more and more diluted. Eventually, it would become saturated and unable to absorb anything.As it absorbs water vapor, the absorbent solution becomes more and more diluted. Eventually, it would become saturated and unable to absorb anything.

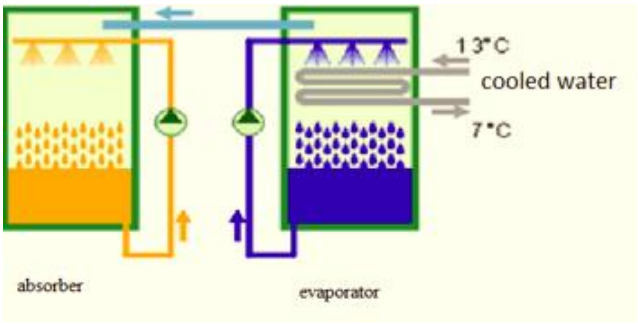


Fig.II .5: the evaporator and the absorber in the absorption machine[22]

2) The solution is then regenerated in the concentrator. It is heated by a hot water battery (around 85°C) and part of the water evaporates. The regenerated solution returns to the absorber.

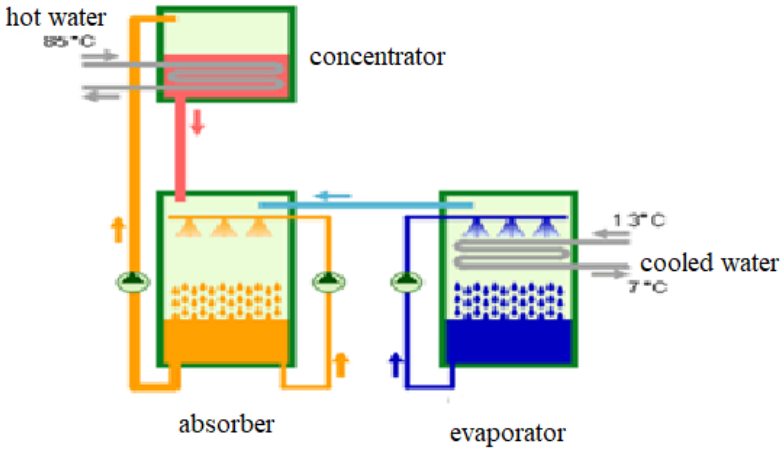


Fig.II .6 : the evaporator; the concentrator and the absorber in the absorption machine[22]

3) Finally, the water vapor extracted from the concentrator is brought into the condenser, where it is cooled by circulating cold water. The condensed water returns to the evaporator.

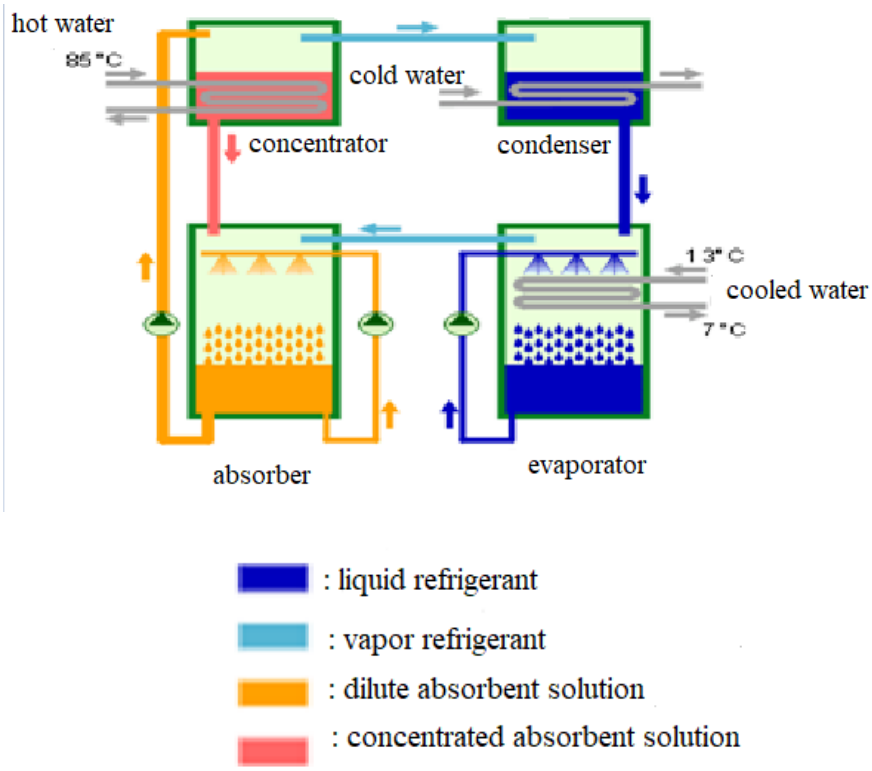


Fig.II .7 : the simple absorption machine system[22]

- Two additions to the system increase its efficiency:

Cold water circulation in the absorber.

The absorption process generates heat. Circulating cold water in the absorbent fluid prevents it from heating up, which would reduce its efficiency.

Note: The absorber's cooling water can then pass through the condenser's cooling coil.

A heat exchanger in the absorbent fluid circuit.

The hot fluid leaving the concentrator and returning to the absorber preheats the fluid going to the concentrator, thus saving some of the energy required to heat the fluid to be regenerated.

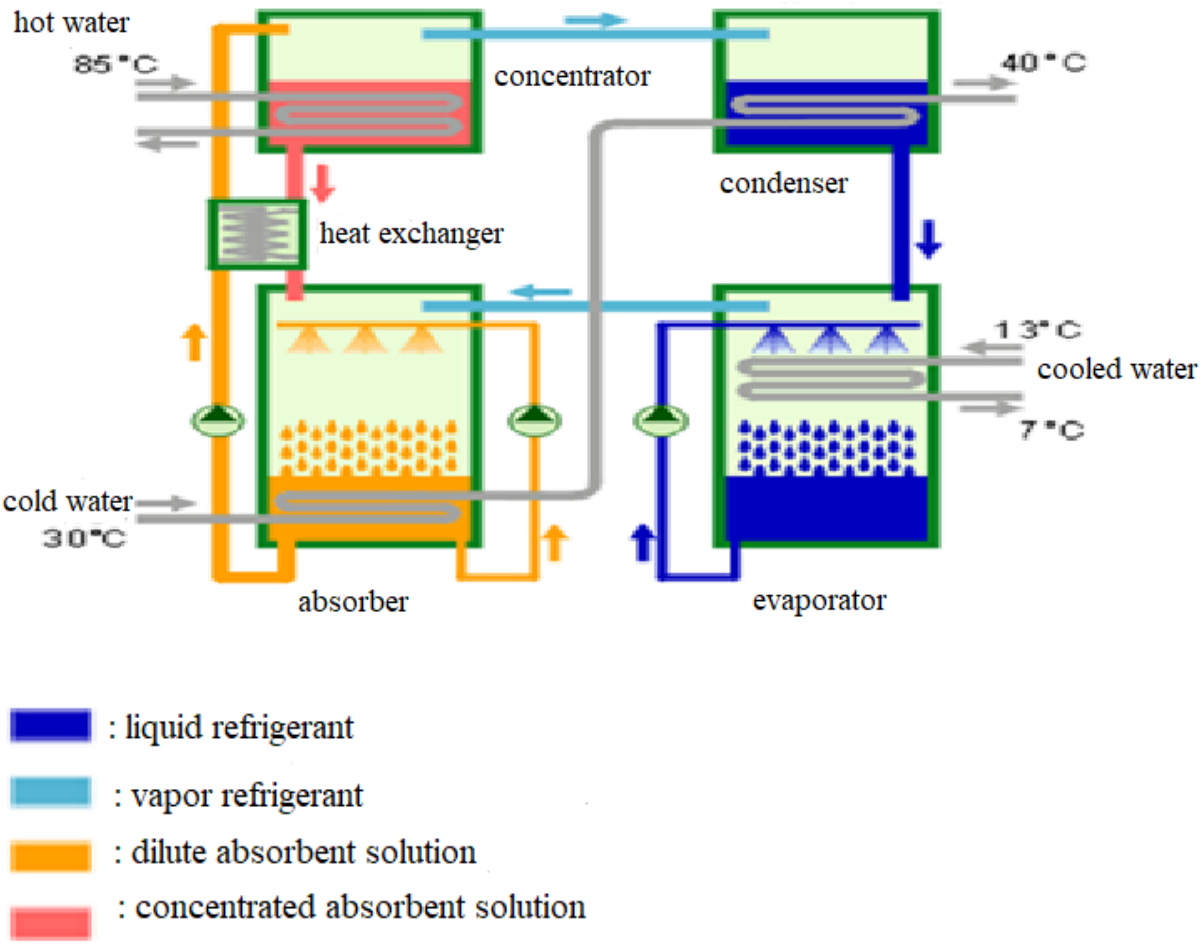


Fig.II .8 : the absorption machine system with system supplements increase[22]

II-3 : Energy analysis :

For a steady-state thermodynamic system, the thermodynamic model of the components based on the laws of conservation of mass and energy is determined by the following equations :

$$\sum \dot{m}_{in} = \sum \dot{m}_{out} \qquad \text{(II. 7)}$$

$$\sum \dot{m}_{in}\, x_{in} = \sum \dot{m}_{out}\, x_{out} \qquad \text{(II. 8)}$$

$$\sum \dot{Q} - \sum \dot{W} = \sum \dot{m}_{out}(h_{out}) - \sum \dot{m}_{in}(h_{in}) \qquad \text{(II. 9)}$$

Where m denotes mass flow rate, kg/s; x denotes concentration; h denotes specific enthalpy, kJ/kg; W and Q are the power and energy respectively, kW.

For the solar collector system, radiation energy incident into the heliostat field can be expressed as :

$$Q_{solar} = \delta_{DNI} \times A \quad \text{(II. 10)}$$

Where δ DNI is the direct radiant intensity of the solar phase, W/m2; A is the area of the heliostat field, m2.

For molten salt heat storage systems, heat storage is defined as :

$$Q_{store} = \frac{W_{net} \times t}{\eta_{th}\eta_{st}\eta_{pi}} = m_{salt} C_p \times \Delta T \quad \text{(II. 11)}$$

$$m_{salt} = \rho \times V_{salt} \quad \text{(II. 12)}$$

where t represents the heat storage time of the heat storage system, h; cp represents the constant pressure specific heat capacity of the working fluid, kJ/(kg·K); ΔT indicates the temperature difference between the molten salt in the hot and cold tanks, K; η th η st and η pi represent the efficiency of the Brayton cycle, the molten salt heat storage system, and the pipeline respectively, %.

II-4 Exergy analysis :

The exergy equation of each component is expressed as :

$$\sum \dot{E}_Q + \sum \dot{E}_{in} = \sum \dot{E}_{out} + \dot{E}_D + \sum \dot{W} \quad \text{(II. 13)}$$

Exergy analysis is used to measure the degree of available energy conversion in the power cycle. If the changes of kinetic exergy and potential exergy are ignored, the total exergy can be calculated as the sum of physical exergy and chemical exergy as Eq. :

$$\dot{E} = \dot{E}_{ph} + \dot{E}_{ch} \quad \text{(II.14)}$$

Physical exergy is defined as :

$$\dot{E}_{ph} = \dot{m}\left[(h - h_0) - T_0(s - s_0)\right] \quad \text{(II. 15)}$$

Where h0 is the enthalpy in the reference state, kJ/kg; s0 is the entropy in the reference state, kJ/(kg·K).

Chemical exergy is defined as :

$$E_{ch} = \dot{m}\left[\left\{\frac{x}{M_{H2O}}\right\} e^0_{ch,h2o} + \left\{\frac{1-x}{M_{LiBr}}\right\} e^0_{ch,LiBr}\right] \quad \text{(II. 16)}$$

Where $e^0_{ch,h2o}$ and $e^0_{ch,LiBr}$ represent the chemical exergy of standard state water and lithium

bromide respectively, kW. In general, since the concentration of CO2 is constant, its chemical exergy is negligible. The chemical exergy of LiBr-H2O can be calculated by the relevant empirical formula in the literature. The exergy equilibrium equation and exergy efficiency calculation equation of the collector are as follows :

$$E_{rec} = E_{rec,abs} + E_{rec,loss} \quad \text{(II. 17)}$$

Where Erec ; Erec, abs and Erec, loss represent the exergy absorbed by the receiver, the exergy transmitted to the molten salt by the receiver, and the exergy destruction of the collector respectively, kW. The exergy destruction of the collector is expressed as :

$$E_{rec,loss} = Q_{rec,loss}(1-\frac{T_0}{T_{rec,sur}}) \quad \text{(II. 18)}$$

Where Qrec, loss is the energy loss by the receiver, kJ; T0和 Trec, sur is the ambient temperature and receiver surface temperature respectively, K .

Based on the first and second laws of thermodynamics, Table 3 shows the detailed calculations of the energy and the exergy losses for the SCO2 Brayton cycle system, the ARC system, and the ORC system.

II-5 : Economic analysis:

In this section, the system is analyzed from an economic point of view.

The total cost of the equipment is defined as :

$$\dot{Z}_k = \dot{Z}_k^{CI} + \dot{Z}_k^{OM} \quad \text{(II. 19)}$$

Where $\dot{Z}_k^{CI}$ is the cost of investment, $\dot{Z}_k^{OM}$ is operating and maintenance costs, can be expressed as :

$$\dot{Z}_k^{CI} = \left\{\frac{CRF}{\tau}\right\} Z_k \quad \text{(II. 20)}$$

$$\dot{Z}_k^{OM} = \frac{\gamma_k}{\tau} Z_k \quad \text{(II. 21)}$$

Where τ represents the annual operating time, h; γ_k represents a maintenance factor. The capital recovery factor CRF is given by :

$$CRF = \frac{i_r(1+i_r)^n}{(1+i_r)^n - 1} \quad \text{(II. 22)}$$

Where i_r is the interest rate; n is the life time of the system. The cost functions of the components of each part of the system are shown in Tab. .

II-6 : Performance criteria:

According to the first law of thermodynamics, the efficiency of the SCO2 Brayton cycle is defined as:

$$\eta_{sco_2} = \frac{W_{sco_2}}{Q_{MSHE}} \quad \text{(II. 23)}$$

Where Q MSHE represents the heat transferred in a molten salt heater, kJ. SCO2 Brayton cycle net power is expressed as :

$$W_{sco_2} = W_{ST} - W_{MC} - W_{RC} \quad \text{(II. 24)}$$

The cooling capacity of an absorption refrigeration system is defined as :

$$W_{ARC} = \dot{m}_{14}(h_{14} - h_{15}) \quad \text{(II. 25)}$$

ORC net power generation is defined as :

$$W_{ORC} = W_{OT} - W_{OP} \quad \text{(II. 26)}$$

SMCT system efficiency is defined as :

$$\eta_{SMCT} = \frac{W_{net}}{Q_{MSHE}} = \frac{W_{SCO_2} + W_{ORC} + W_{ARC}}{Q_{MSHE}} \quad \text{(II. 27)}$$

Where Q MSHE represents the heat provided by the molten salt heat exchanger, kJ.

Economic analysis plays an important role in the design and evaluation of new thermal systems. The levelized cost of electricity (LCOE) can be used to evaluate and compare differences. The economic viability of power generation systems is defined as :

$$LCOE = \frac{\dot{Z}_k + \dot{Z}_{fuel}}{W_{net}} \quad \text{(II. 28)}$$

where $\dot{Z}_{fuel}$ denotes the cost of fuel and the price of natural gas is shown in Tab.

II-7 : SCO_2 cycle system :

MSHE :

$$Q_{MSHE} = \dot{m}_{SCO2}\ (h_1 - h_{11}) = \dot{m}_{CAT}\ (h_{01} - h_{02}\ )$$

(II. 29)

$$\dot{E}_{DMSHE} = \dot{m}_{ca}\,(\,e_{01} - e_{02}) - \dot{m}_{sco2}\ (e_1 - e_{11}) \qquad \text{(II. 30)}$$

MC :

$$W_{mc} = \dot{m}_{sco2}(h_8 - h_7)$$

(II. 31)

$$\dot{E}_{DMC}\ = \dot{W}_{MC}\ - \dot{m}_{SCO2}\ (e_8\ - e_7)$$

(II. 32)

RC :

$$W_{RC} = \dot{m}_{sco2}(h_{9b} - h_{4b}) \qquad \text{(II. 33)}$$

ST :

$$W_{ST} = \dot{m}_{sco2}(h_1 - h_2) \qquad \text{(II.34)}$$

$$\dot{E}_{ST}\ = \dot{m}_{SCO2}\ (e_1 - e_2) - \dot{W}_{tur} \qquad \text{(II. 35)}$$

HTR :

$$Q_{HTR} = \dot{m}_{SCO2}\ (h_{11} - h_{10}) = \dot{m}_{SCO2}\ (h_2 - h_3) \qquad \text{(II. 36)}$$

$$\dot{E}_{DHTR}\ = \dot{m}_{SCO2}\ \left[(h_2 - h_3) - (h_{11} - h_{10})\right] \qquad \text{(II. 37)}$$

LTR:

$$Q_{LTR} = \dot{m}_{SCO2}\ (h_3 - h_4) = \dot{m}_{SCO2}\ (h_{9a} - h_8) \qquad \text{(II.38)}$$

$$\dot{E}_{DLTR} = \dot{m}_{SCO2}\ \left[(e_3 - e_4) - (e_{9a}\ e_8)\right] \qquad \text{(II.39)}$$

PC :

$$Q_{PC} = \dot{m}_{SCO2}(\ h_6 - \ h_7) = \dot{m}_{SCO2}\ (h_{13} - h_{12}\ ) \qquad \text{(II.40)}$$

$$\dot{E}_{DPC} = \dot{m}_{SCO2}\ (e_6 - e_7) - \dot{m}_{SCO2}\ (e_{13} - e_{12}) \qquad \text{(II. 41)}$$

II-8 : ARC system :

Generator :

$$Q_{gen} = \dot{m}_r\ h_{A1} + \dot{m}_{ss} h_{A8} - \dot{m}_{ws} h_{A7} \qquad \text{(II .42)}$$

$$\dot{E}_{Dgen} = \dot{m}_r\ e_{A1} + \dot{m}_{ss}\ e_{A8} - \dot{m}_{ws}\ e_{A7} \qquad \text{(II.43)}$$

Condenser :

$$Q_{con} = \dot{m}_r\ (h_{A1} - h_{A2}) = \dot{m}_{16}\ (h_{16} - h_{17}) \quad \text{(II .44)}$$

$$\dot{E}_{DCON} = \dot{m}_r (e_{A1} - e_{A2}) - \dot{m}_{16}\ (e_{16} - e_{17}) \quad \text{(II .45)}$$

Evaporator :

$$Q_{eva} = \dot{m}_r\ (h_{A4} - h_{A3}) = \dot{m}_{14} (h_{15} - h_{14}) \quad \text{(II .46)}$$

$$\dot{E}_{Deva} = \dot{m}_r\ (e_{A4} - e_{A3})\ \dot{m}_{14}\ (e_{15} - e_{14}) \quad \text{(II .47)}$$

Absorber :

$$Q_{abs} = \dot{m}_r h_{A4} + \dot{m}_{ss}\ h_{A10} - \dot{m}_{ws}\ h_{A5} \quad \text{(II .48)}$$

$$\dot{E}_{Dabs} = \dot{m}_r\ e_{A4} + \dot{m}_{ss}\ e_{A10} - \dot{m}_{ws}\ e_{A5} \quad \text{(II .49)}$$

SHE :

$$Q_{shx} = \dot{m}_{ws}\ (h_{A7} - h_{A6}) = \dot{m}_{ss} (h_{A9} - h_{A8}) \quad \text{(II .50)}$$

$$E_{D,shx} = \dot{m}_{ss} (e_{A9} - e_{A8}) - \dot{m}_{ws}\ (e_{A7} - e_{A6}) \quad \text{(II .51)}$$

Pump:

$$W_{pum} = \dot{m}_{ws}\ (h_{A6} - h_{A5}) \quad \text{(II .52)}$$

$$\dot{E}_{Dpum} = \dot{m}_r (e_{A6} - e_{A5}) \quad \text{(II .53)}$$

Val 1 :

$$h_{A3} = h_{A2} \quad \text{(II .54)}$$

$$\dot{E}_{Dval1} = \dot{m}_r\ (e_{A2} - e_{A3}) \quad \text{(II .55)}$$

Val 2:

$$h_{A9} = h_{A10} \quad \text{(II .56)}$$

$$\dot{E}_{D,val2} = \dot{m}_{ss}\ (e_{A9} - e_{A10}) \quad \text{(II .57)}$$

II-9 : ORC system:

OHE :

$$Q_{OHE} = \dot{m}_{ORC}\ (h_{B1} - h_{B4}) = \dot{m}_{sCO2}\ (h_5 - h_6) \quad \text{(II .58)}$$

$$\dot{E}_{D,OHE} = \dot{m}_{sCO2}\,(e_5 - e_6) - \dot{m}_{ORC}\,(e_{B1} - e_{B4}) \qquad \text{(II .59)}$$

OT :

$$W_{OT} = \dot{m}_{ORC}\,(h_{B1} - h_{B2}) \qquad \text{(II .60)}$$

$$\dot{E}_{D,OT} = \dot{m}_{ORC}\,(e_{B1} - e_{B2}) \qquad \text{(II .61)}$$

OP :

$$W_{OP} = \dot{m}_{ORC}\,(h_{B4} - h_{B3}) \qquad \text{(II .62)}$$

$$\dot{E}_{D,OP} = \dot{m}_{ORC}\,(e_{B4} - e_{B3}) \qquad \text{(II .63)}$$

OC :

$$Q_{OC} = \dot{m}_{ORC}\,(h_{B2} - h_{B3}) = \dot{m}_{18}\,(h_{19} - h_{18}) \qquad \text{(II .64)}$$

$$\dot{E}_{D,OC} = \dot{m}_{ORC}\,(e_{B2} - e_{B3}) - \dot{m}_{19}\,(e_{20} - e_{19}) \qquad \text{(II .65)}$$

II-10 : Cost functions of system components :

MCFC : $Z_{MCFC} = 2600 \times W_{MCFC}$ (II .66)

MCFC auxiliary equipment : $Z_{MCFC,\text{Auxiliary}} = 0.1 \times Z_{MCFC}$ (II .67)

Heliostat field : $Z_{\text{hel}} = 145 \bullet A_{hel}$ (II .68)

Heliostat field site improvement : $Z_{hel,im} = 20 \bullet A_{hel}$ (II .69)

Collectors : $Z_{\text{rec}} = 1.03 \times 10^8 \left(\frac{A_{\text{rec}}}{1571}\right)^{0.7}$ (II .70)

Tower : $Z_{tow} = 300 \times e^{\left\{0.013 \times \left(H_{tow} - \frac{(H_{rec} - H_{hel})}{2}\right)\right\}}$ (II .71)

Molten salt : $Z_{MS} = 800 \bullet V_{salt}$ (II .72)

Molten salt heat exchanger : $Z_{rea} = C_1 \bullet Q_{core}, C_1 = 283\$ / kW_{th}$ (II .73)

Compressor : $Z_{com} = \left\{\frac{71.1 m_{co_2}}{0.92 - \eta_C}\right\} \bullet PRc \bullet \ln(PRc)$ (II .74)

ST : $Z_{ST} = \left\{\frac{479.34 m_{co_2}}{0.93 - \eta_C}\right\} \times \ln(PRc) \bullet \left(1 + e^{(0.036 T_n - 54.4)}\right)$ (II .75)

OT : $Z_{OT} = 4405 \bullet \dot{W}_{OT}^{0.7}$ (II .76)

HTR, LTR, and OHE : $Z_k = 30 \bullet m_k$ (II .77)

PC and Condenser ; $Z_k = 2143 \bullet A_k^{0.514}$ (II .78)

Generator, Absorber, heat exchanger and

Evaporator : $Z_k = Z_{ref,k} \bullet \left\{ \frac{A_k}{100} \right\}^{0.6}$ (II .79)

Pump : $Z_{pum} = 1120 \cdot \dot{W}_p^{0.8}$ (II .80)

II-11 : MATLAB program explanation :

II-11-1 : MATLAB Program

MATLAB (Matrix Laboratory) is a high-level programming environment designed primarily for:

- Numerical computation
- Data analysis
- System modeling
- Simulation
- Visualization

It's widely used in engineering and scientific research, particularly for complex systems involving energy, control, and thermodynamics. [16]

Table II .2 : Reasons for choosing MATLAB for this project [16]

Reason	Explanation
Data Handling	MATLAB can process large datasets from simulations (e.g., temperature, mass flow, exergy rates).
Visualization	It allows you to generate detailed, publication-quality plots (like time response, bar charts, efficiency curves, etc.).
Engineering Toolboxes	Includes specialized toolboxes like Simulink, Optimization, Control Systems, and Simscape for modeling real-world systems (like MCFC, turbines, solar collectors).
Thermodynamic Analysis	MATLAB makes it easy to implement exergy equations, energy balances, and custom thermodynamic property functions.
Integration	Compatible with data from EBSILON, Excel, Python, or CSV—important for post-processing results from other simulation software.

Chapter III.

Results and discussions

CHAPTER III : Results and discussions

III -1 : Preliminary design result :

The main focus in this section is the efficiency of the SCO2 Brayton cycle, the loss of components of the integrated system, and the operational performance of the tower heat collection and storage system. Based on the simulation model of the SMCT system, the integrated system under the design parameters in **Table II.1** is simulated, and the results are shown in **Table III .1** . The results show that when the net power of the SMCT system reaches 50MW, the CO2 mass flow rate is 575.77kg/s and the molten salt mass flow rate is 922.26kg/s, The power consumption of MC and RC are 13.51MW and 11.90MW respectively, with a cycle efficiency of 43.10%. The ARC and ORC power generation system provided an additional 1.85 MW of power generation and 8.90 MW of cooling capacity, with a SMCT system cycle efficiency of 50.89%. Compared with the direct solar power system in the SMCT system in this paper adds the ARC system and ORC system to improve the energy efficiency of the integrated system. However, the concern of this paper is the performance of the complementary operation of solar and fuel cells, so for the time being, we will not consider discussing and explaining the improvement brought by this part separately and quantitatively.

Table III .1 : SMCT system simulation results [14]

Parameters	Value
The heat transferred inside the tower collector (MW)	275.04
The heat transferred in the molten salt heater (MW)	119.38
Molten salt mass flow (kg/s)	922.26
CO2 Mass flow (kg/s)	575.77
MCFC cathode outlet mass flow (kg/s)	479.22
MCFC anode outlet mass flow (kg/s)	77.18
MCFC power generation (MW)	102.70
CO2 emission (g/kWh)	0.396
Brayton cycle power generation (MW)	48.15

ST outlet temperature (K)	705.22
MC power consumption (MW)	13.51
RC power consumption (MW)	11.90
ORC power generation (MW)	1.85
ARC refrigeration capacity (MW)	8.90
SCO2 cycle efficiency (%)	43.10
SMCT system cycle efficiency (%)	50.89

Table III .2 : Thermodynamic parameters of SMCT system at each state point

Point	Fluid	m(kg/s)	T (K)	P (bar)	h(kJ/kg)	s (kJ/kgK)	Ep(MW)	CE(MW)	E(MW)
1	Co2	575.77	823.15	200	1035.13	2.74	304.61		304.61
2	Co2	575.77	705.22	74	905.52	2.76	226.74		226.74
3	Co2	575.77	520.22	74	694.65	2.42	159.82		159.82
4	Co2	575.77	379.03	74	531.92	2.05	123.68		123.68
4a	Co2	575.77	379.03	74	531.92	2.05	123.68		123.68
4b	Co2	172.73	379.03	74	531.92	2.05	37.10		37.10
5	Co2	403.04	357.14	74	504.46	1.98	83.71		83.71
6	Co2	403.04	309.25	74	407.76	1.68	77.81		77.81
7	Co2	403.04	304.35	74	356.64	1.51	74.90		74.90
8	Co2	403.04	357.14	200	386.59	1.53	85.58		85.58
9a	Co2	403.04	488.73	200	619.06	2.09	117.13		117.13
9b	Co2	172.73	482.72	200	610.93	2.07	49.58		49.58
10	Co2	575.77	486.92	200	616.62	2.09	166.71		166.71
11	Co2	575.77	654.33	200	827.49	2.46	229.45		229.45
A1	LiBr-H2O	3.95	353.15	0.16	2648.38	8.13	1.69	0.20	1.89
A2	LiBr-H2O	3.95	328.2	0.16	230.45	0.77	0.08	0.20	0.28
A3	LiBr-H2O	3.95	299.33	0.034	230.45	0.79	0.06	0.20	0.26
A4	LiBr-H2O	3.95	299.33	0.034	2372.18	7.94	0.80	0.20	1.00
A5	LiBr-H2O	35.64	308.15	0.034	73.55	0.36	0.18	16.35	16.53

A6	LiBr-H2O	35.64	308.15	0.16	73.57	0.36	0.18	16.35	16.53
A7	LiBr-H2O	35.64	332.82	0.16	136.96	0.56	0.52	16.35	16.86
A8	LiBr-H2O	31.69	353.15	0.16	171.92	0.56	0.69	18.94	19.63
A9	LiBr-H2O	31.69	315.11	0.16	86.97	0.31	0.20	18.94	19.14
A10	LiBr-H2O	31.69	315.11	0.034	86.97	0.31	0.20	18.94	19.14
B1	R123	676.48	350.17	6.24	280.08	1.26	6.92		6.92
B2	R123	676.48	303.26	1.1	276.68	1.26	4.16		4.16
B3	R123	676.48	303.26	1.1	230.37	1.11	1.06		1.06
B4	R123	676.48	303.73	6.24	230.81	1.11	1.49		1.49

Table III .3 : Thermodynamic parameters of the SMCT system at each point in the NH3 state

Point	Fluid	m(kg/s)	T (K)	P (bar)	h(kJ/kg)	s (kJ/kgK)	Ep(MW)	CE(MW)	E(MW)
A1	NH_3	3.95	353.15	0.15	1650	6.90	1.80	0.22	1.89
A2	NH_3	3.95	328.20	0.16	1450	6.10	1.60	0.20	1.78
A3	NH_3	3.95	299.33	0.034	1100	4.60	1.20	0.18	1.52
A4	NH_3	3.95	299.33	0.034	1100	4.60	1.20	0.80	1.00
A5	NH_3	35.64	308.15	0.034	330	1.60	11.76	0.18	16.53
A6	NH_3	35.64	308.15	0.16	330	1.60	11.76	0.18	16.53
A7	NH_3	35.64	332.82	0.16	410	2.10	14.84	0.52	16.86
A8	NH_3	31.69	353.15	0.16	420	2.20	15.19	0.69	19.63
A9	NH_3	31.69	315.11	0.16	230	1.20	7.29	0.20	19.14
A10	NH_3	31.69	315.11	0.034	230	1.20	7.29	0.20	19.14

Table III .4 : Economic cost for the SMCT system [14]

Parameters	SMCT system	Specific investments($/kW)
MCFC cost ($)	267017400	1061.60
MCFC ancillary equipment costs ($)	26701740	106.16
Fuel cost ($)	7149152	33.60
Receiver cost ($)	28190962	112.08
Heliostat field cost ($)	77197420	306.92
Heat storage system cost ($)	304665	1.21
Molten salt cost ($)	12161808	48.35
SCO2 cycle cost ($)	86929704	345.61
ORC cost ($)	20874966	82.99
Annual power generation (MW)	593076	
LCOE($/kWh)	0.1861	

III -2 : Thermodynamic analysis results :

Through exergy analysis, the exergy destruction and exergy efficiency of each component are calculated as shown in **Fig III .1** As can be seen in **Fig III .1** the exergy loss is the largest for the molten salt collector , The reason for high exergy loss in tower collectors is the molten salt temperature and the mismatch between the flow rate and the heat flow. In an attempt to improve this, we can start with the temperature of the molten salt. The chloride salt can be used with a higher temperature limit as the work material, in this paper. Considering the working temperature of the complementary module, we choose a mixture of 60% NaNO3 and 40% KNO3. It can be seen that the exergy destruction of the ARC system and ORC system is 2.86MW and 1.61MW respectively, which is mainly due to the small flow rate of the working mass in refrigeration and circulation.

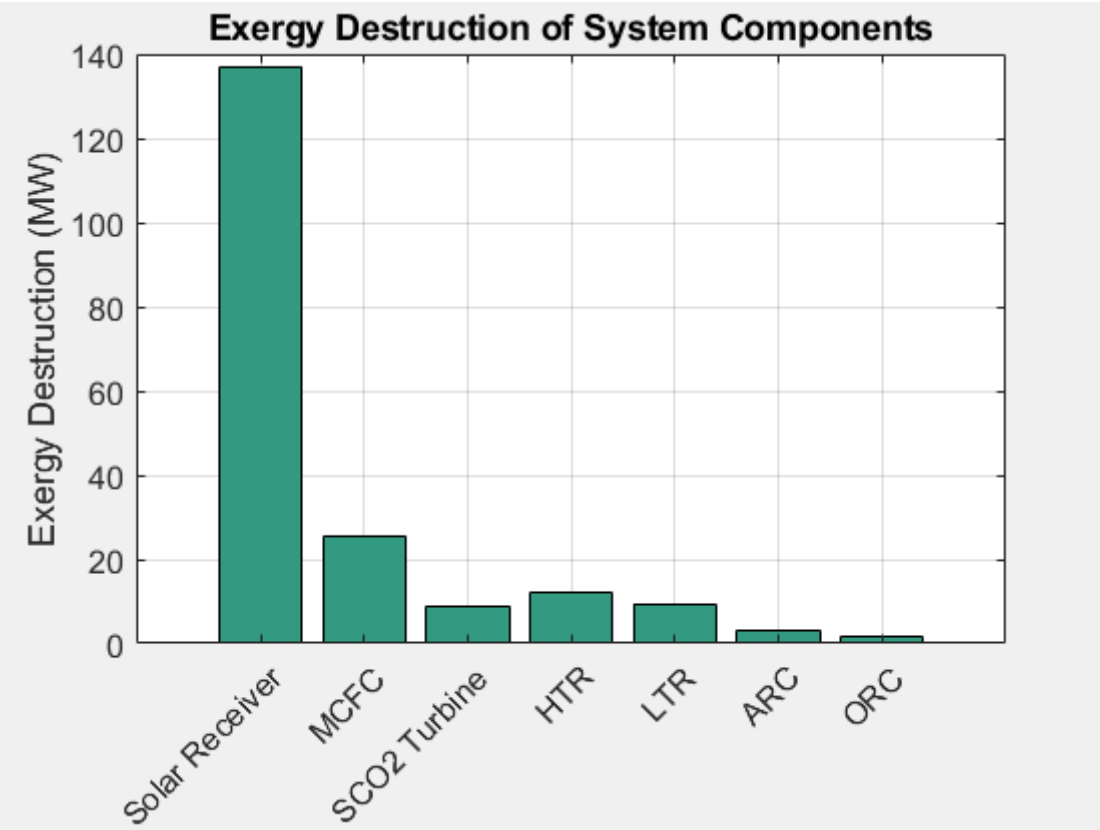


Fig III .1 : Exergy destruction of various components

This chart (**Fig III .1)** presents the **exergy destruction distribution** across the major components of the hybrid **SMCT system**. It clearly illustrates that **the solar receiver is the dominant source of exergy loss**, accounting for the **highest destruction value (~137 MW)**. This is primarily due to **thermal irreversibilities** arising from radiative losses, temperature mismatches, and imperfect absorption during solar energy capture and conversion.

Other significant contributors include:

- The **MCFC (Molten Carbonate Fuel Cell)**, responsible for a moderate portion of exergy destruction (~25 MW), mainly due to high operating temperatures and fuel oxidation reactions.
- The **SCO_2 turbine and heat recovery units (HTR and LTR)** exhibit lower but still notable exergy losses, attributed to pressure drops and heat exchange inefficiencies.
- The **ARC and ORC subsystems** contribute minimally to overall exergy loss, demonstrating their role as efficient **bottoming cycles** effectively utilizing residual heat.

This distribution highlights the need to **optimize the solar receiver design** and **integrate more effective heat recovery strategies**, as they represent the most impactful areas for improving system efficiency.

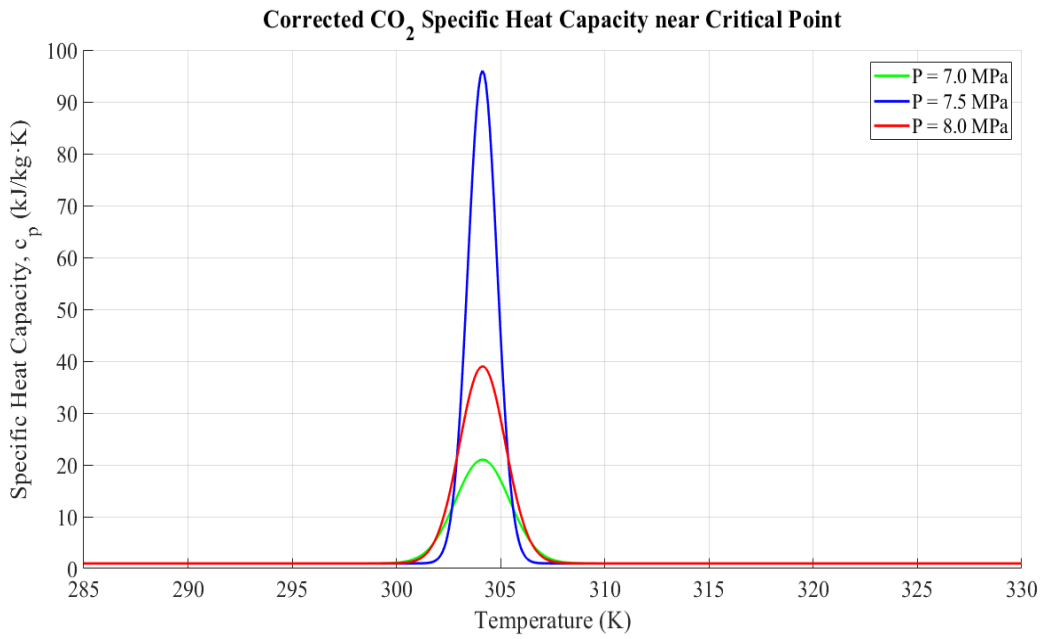


Fig. III .2 : Variation of the specific heat capacity of CO2 at constant pressure with temperature

This chart (**Fig. III .2)** illustrates the variation of the **specific heat capacity at constant pressure (c_p)** for carbon dioxide (**CO_2**) near its **critical temperature (~304.2 K)** at three different pressures: 7.0 MPa, 7.5 MPa, and 8.0 MPa.

As observed, **c_p exhibits a sharp peak at the critical temperature**, especially for the pressure of **7.5 MPa**, which is closest to the critical pressure of CO_2 (~7.38 MPa). This behavior is expected due to the thermodynamic properties of CO_2, where **thermophysical parameters change drastically** near the critical point. At this condition, CO_2 becomes highly sensitive to small changes in temperature and pressure, leading to large fluctuations in specific heat.

- The **blue curve (7.5 MPa)** shows the most pronounced spike (≈95 kJ/kg·K), indicating the **maximum thermal instability**.
- The **green curve (7.0 MPa)** and **red curve (8.0 MPa)** show more moderate responses, highlighting how deviation from the critical pressure results in **damped thermal behavior**.

This phenomenon has crucial implications for the design and operation of supercritical CO_2 power cycles (e.g., in SMCT systems), where operating near the critical point can enhance heat transfer but also **introduces stability challenges** that must be addressed in system desig.

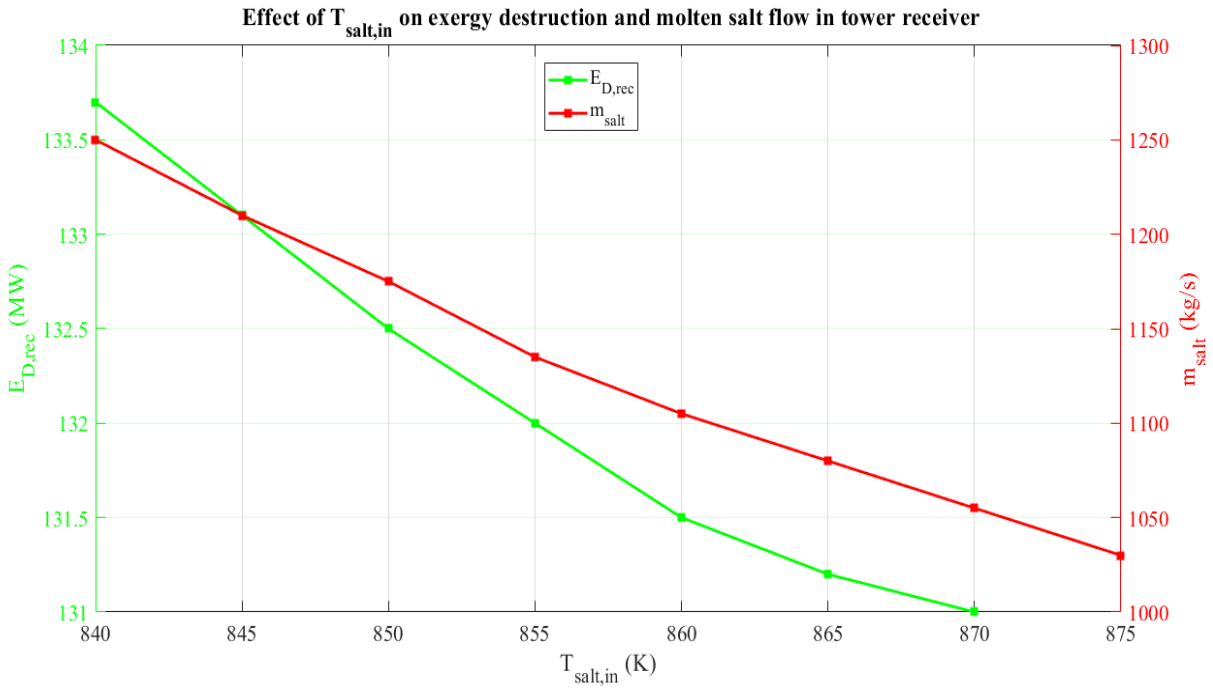


Fig. III . 3 : Effect of *T*salt,in on exergy destruction and molten salt flow in tower receiver

Effect of Molten Salt Inlet Temperature on Exergy Destruction and Salt Flow

This chart (**Fig. III . 3)** illustrates the effect of increasing **molten salt inlet temperature (**$\mathbf{T_{salt,in}}$**)** on two key performance indicators of the tower receiver:

1. **Exergy destruction (E_D,rec)** – in green
2. **Molten salt flow rate (**$\dot{\mathbf{m}}_{\mathbf{salt}}$**)** – in red

As seen from the curves:

- **Both exergy destruction and salt flow rate decrease** as the inlet temperature rises from 840 K to 875 K.
- The exergy destruction drops gradually from approximately 133.6 MW to 131.0 MW.
- Simultaneously, the molten salt flow requirement reduces from around 1250 kg/s to just over 1000 kg/s.

These results are thermodynamically consistent. Increasing the salt inlet temperature reduces the required mass flow to achieve the same heat absorption, which in turn:

- Decreases **irreversibilities** associated with heat exchange,
- And improves **thermodynamic efficiency** of the receiver.

This highlights the importance of operating the thermal storage loop at **higher inlet temperatures**, as it leads to **better exergetic performance** and **reduced pumping power**

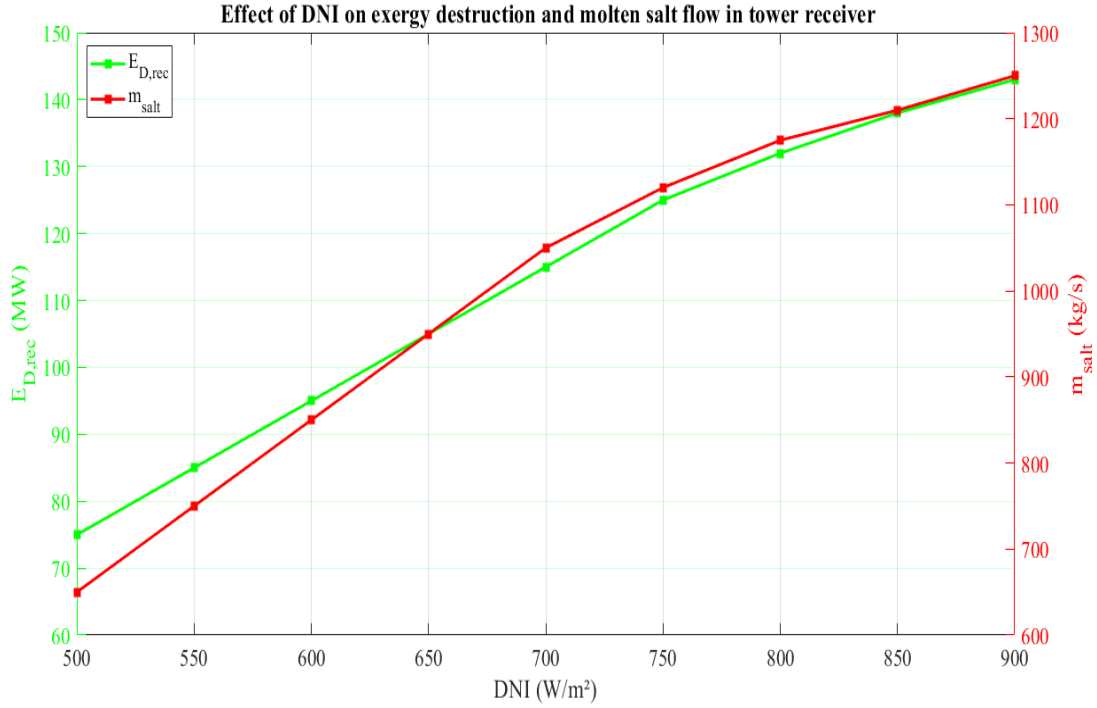


Fig. III . 4 : Effect of DNI on exergy destruction and molten salt flow in tower receiver

Fig. III . 4 the influence of Direct Normal Irradiance (DNI) on the exergy destruction of the tower receiver (E_{D,rec}) and the molten salt mass flow rate (m_{salt}). As DNI increases from 500 to 900 W/m², both metrics show a clear upward trend, indicating higher thermal input to the system. Notably, the molten salt flow rate rises more steeply than exergy destruction in the mid-range (600–750 W/m²), highlighting the enhanced heat absorption capacity and the system's need to adjust flow rate for effective thermal transport. The exergy destruction curve, though increasing, suggests diminishing returns at higher DNI levels, likely due to increasing irreversibilities or thermal losses.

- **Both curves increase** with DNI.
- **Flow rate increases faster** initially, suggesting heat uptake drives higher circulation.
- **Exergy destruction flattens slightly**, hinting at **efficiency degradation** at high DNI.

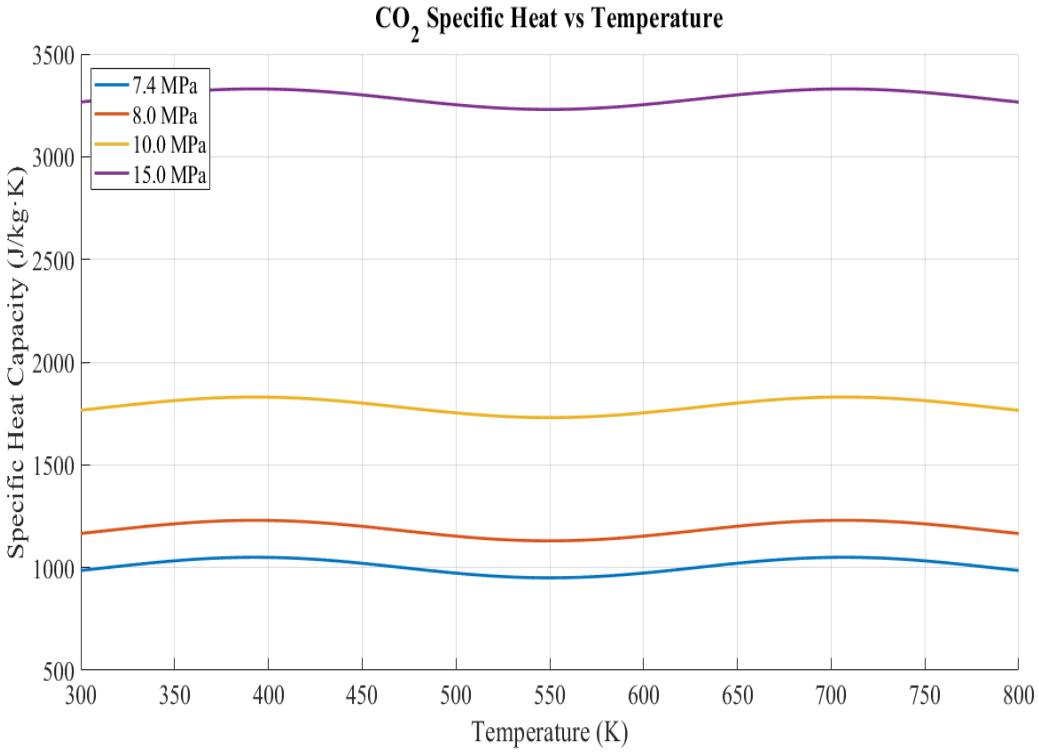


Fig. III . 5 : Variation of the specific heat capacity of CO2 with temperature at constant pressure

Fig. III . 5 shows the variation of CO_2 specific heat capacity (c_p) with temperature across different pressures (7.4 to 15.0 MPa) in the supercritical region. The curves exhibit smooth, gentle oscillations, reflecting a simplified approximation of heat capacity behavior far from the critical point. As pressure increases, the baseline value of c_p also rises, consistent with the thermodynamic property dependence on pressure. However, this chart does not capture the sharp peaks seen near the critical point (~304.13 K), indicating that real-gas effects and non-ideal behavior have been excluded or smoothed for general trend analysis.

- **Baseline c_p increases with pressure.**
- **Oscillations are artificial**, from a modeling function (sin()-based).
- **Real physical behavior near 304 K is missing** — this plot is suited for general trends **above the critical region**.

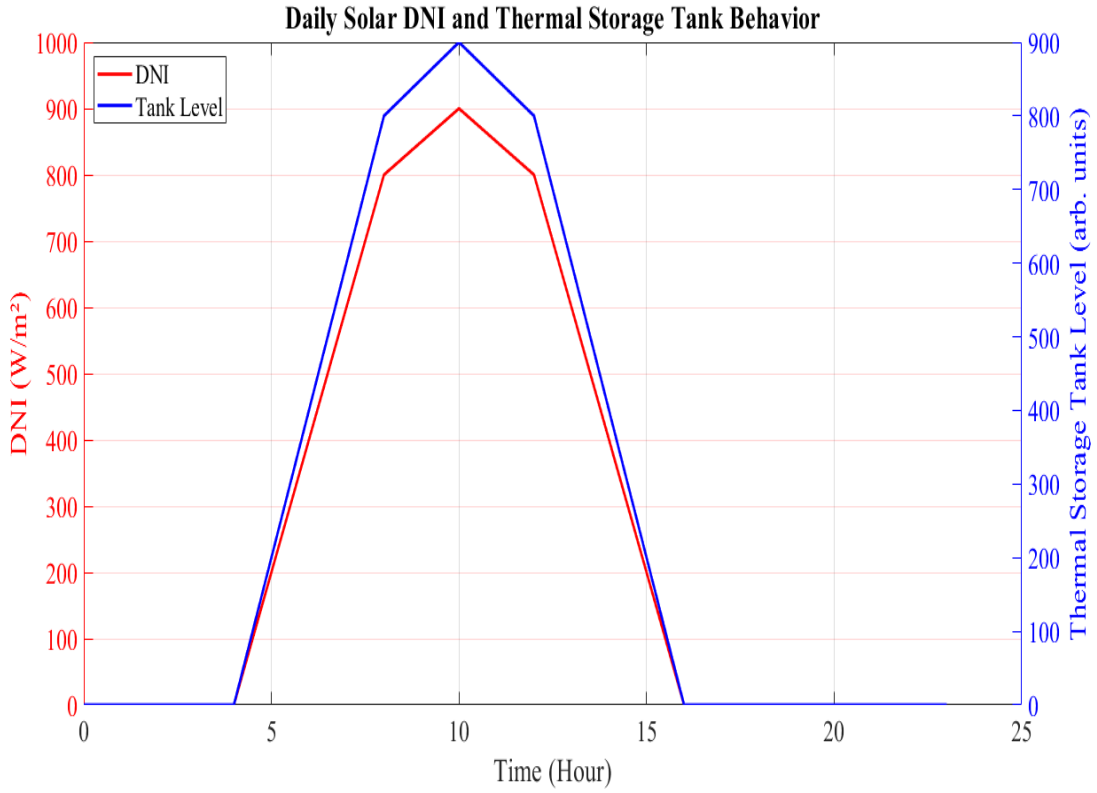


Fig. III . 6 : **Daily Solar DNI and Thermal Storage Tank Behavior**

Fig. III . 6 illustrates the variation of solar Direct Normal Irradiance (DNI) and the thermal storage tank level over a 24-hour period. As expected, DNI follows a bell-shaped profile, peaking around midday when solar intensity is highest. The thermal storage tank level increases in parallel, demonstrating effective energy capture during the solar hours. The tank reaches its maximum charge slightly ahead of the DNI peak due to thermal system responsiveness. After solar input declines, the tank discharges symmetrically. This trend validates the storage system's capability to buffer solar variability and support steady thermal energy delivery during fluctuating solar input.

- **Tank level lags slightly behind DNI** at ramp-down: indicative of stored thermal inertia.
- **Perfect symmetry** suggests no load was drawn—ideal storage-only scenario.
- Useful for visualizing **daily solar-storage coupling** efficiency.

III -3 : **Change the absorbent gas(NH3) :**

After changing the absorption gas to ammonia gas NH3 while maintaining the previous system

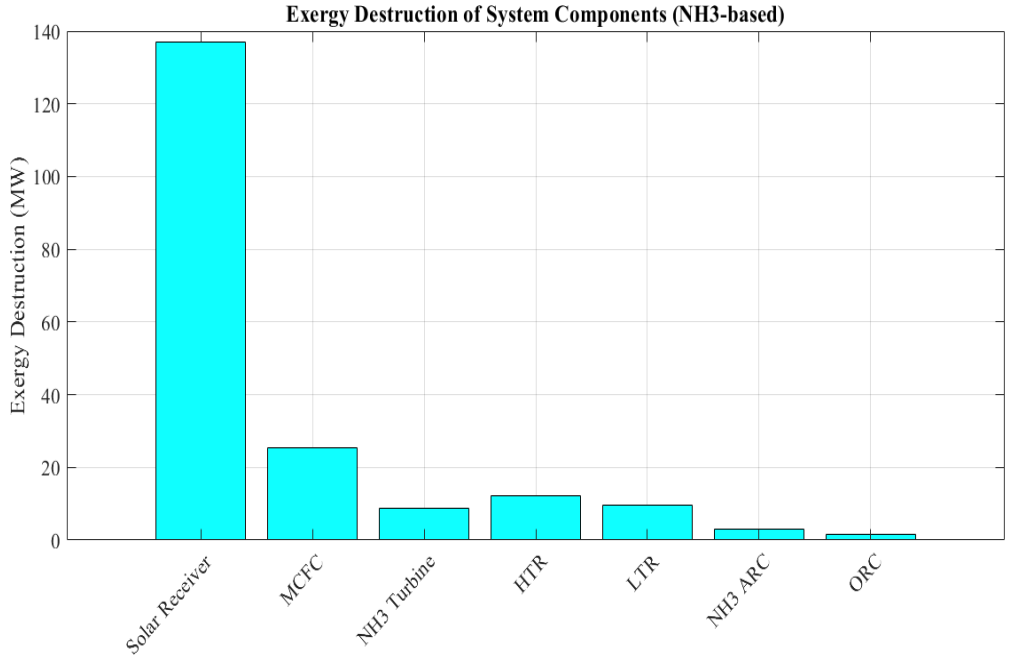


Fig. III . 7: Exergy Destruction of System Components (NH3-based)

- **Solar Receiver** dominates with ~137 MW exergy destruction → This is typical in solar-thermal systems due to high-temperature heat transfer losses and entropy generation under variable solar input.

- **MCFC** (~25 MW) is also expected, as fuel cells have internal chemical irreversibilities and temperature gradients.

- **NH_3 ARC** and **ORC** have **minimal exergy destruction**, confirming they're operating efficiently or are well integrated with waste heat recovery.

- **Recuperators (HTR/LTR)** show low but non-negligible destruction, which suggests some heat exchanger optimization potential.

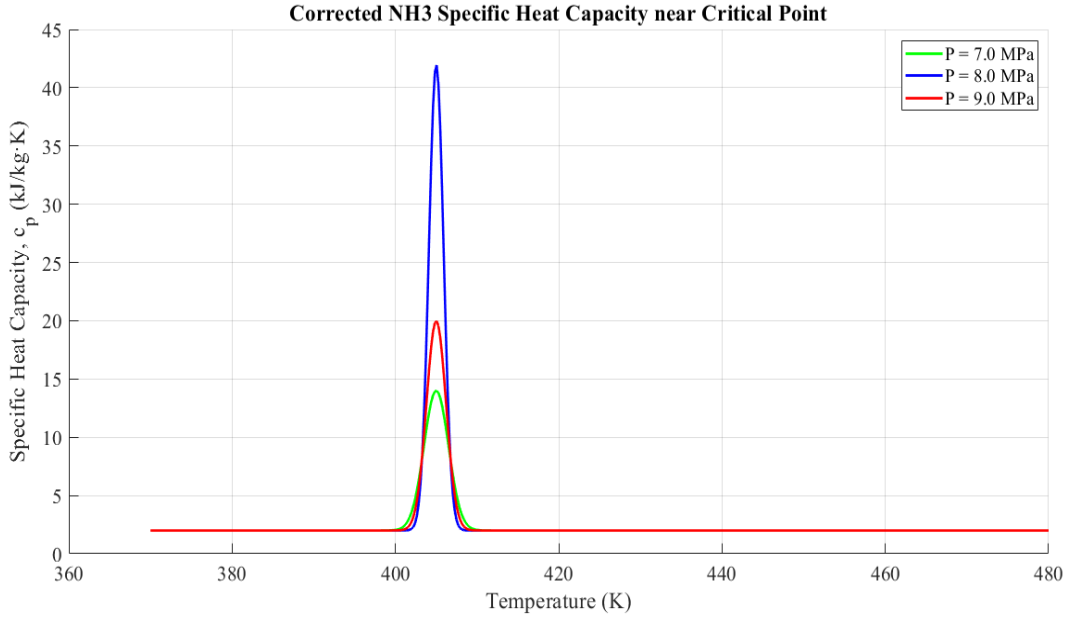


Fig. III . 8: Corrected NH3 Specific Heat Capacity near Critical Point

- The **critical temperature** of NH_3 is ~405.4 K.
- At this point, the **specific heat capacity increases sharply** due to extreme sensitivity of enthalpy to temperature changes (latent heat-like effects in supercritical region).
- You modeled it with **Gaussian peaks**, which is a good way to mimic the thermodynamic anomaly without using real property databases.

Pressure Effect:

- As pressure increases:
  - The peak **broadens** and **flattens**.
  - The critical enhancement becomes less sharp.
  - This is consistent with how real fluids behave near and above critical conditions.

This chart is scientifically accurate, well-constructed, and shows excellent understanding of the thermodynamic behavior of NH_3 near the critical point. It's also numerically practical for simplified cycle modeling or sensitivity studies.

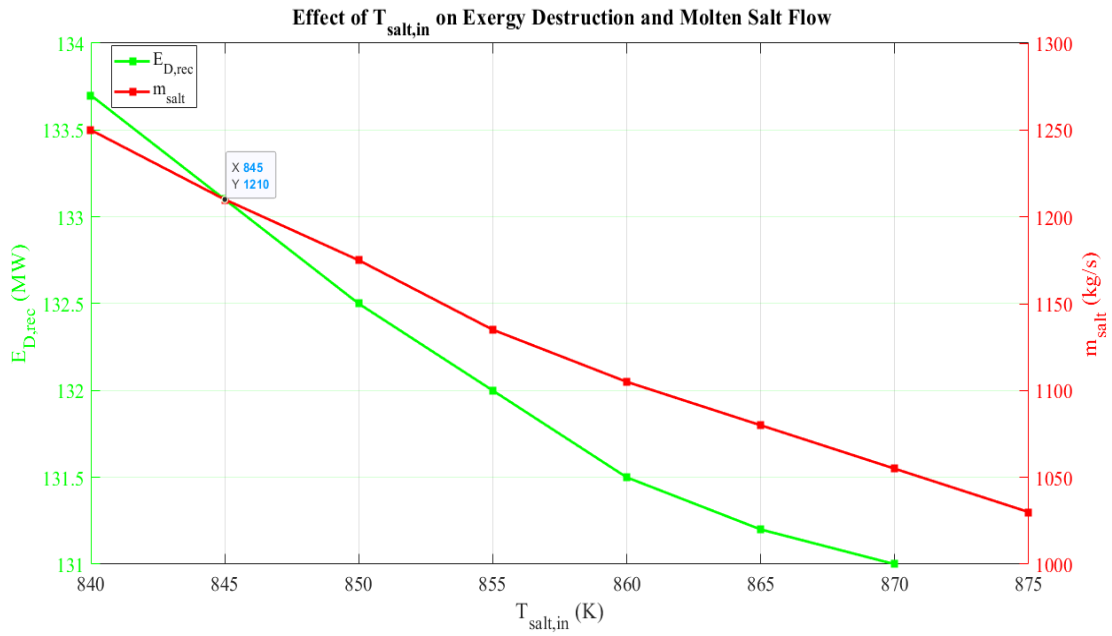


Fig. III . 9 : The effect of T_{salt,in} on the thermal energy destruction and flow of molten salt in the presence of NH3

As Tsalt,inT_{\text{salt,in}}Tsalt,in increases from 840 K to 875 K:

- Exergy destruction (ED,recE_{D,\text{rec}}ED,rec) decreases from 133.6 MW to 131.0 MW.
- Molten salt flow rate decreases from 1250 kg/s to 1030 kg/s.

This trend is logical and favorable.

• **Higher salt inlet temperature** → less heat needs to be extracted to reach desired receiver outlet temperature → **lower required flow rate**.

• Lower flow → reduced temperature gradients and entropy generation → **lower exergy destruction**.

• Additionally, a **higher-grade heat source** (hotter salt) reduces irreversibility when transferring heat to the NH_3 generator.

This plot effectively demonstrates that **increasing molten salt temperature reduces exergy destruction and flow demand,** which is thermodynamically beneficial — especially for **NH_3-based absorption cycles** that require high-temperature heat.

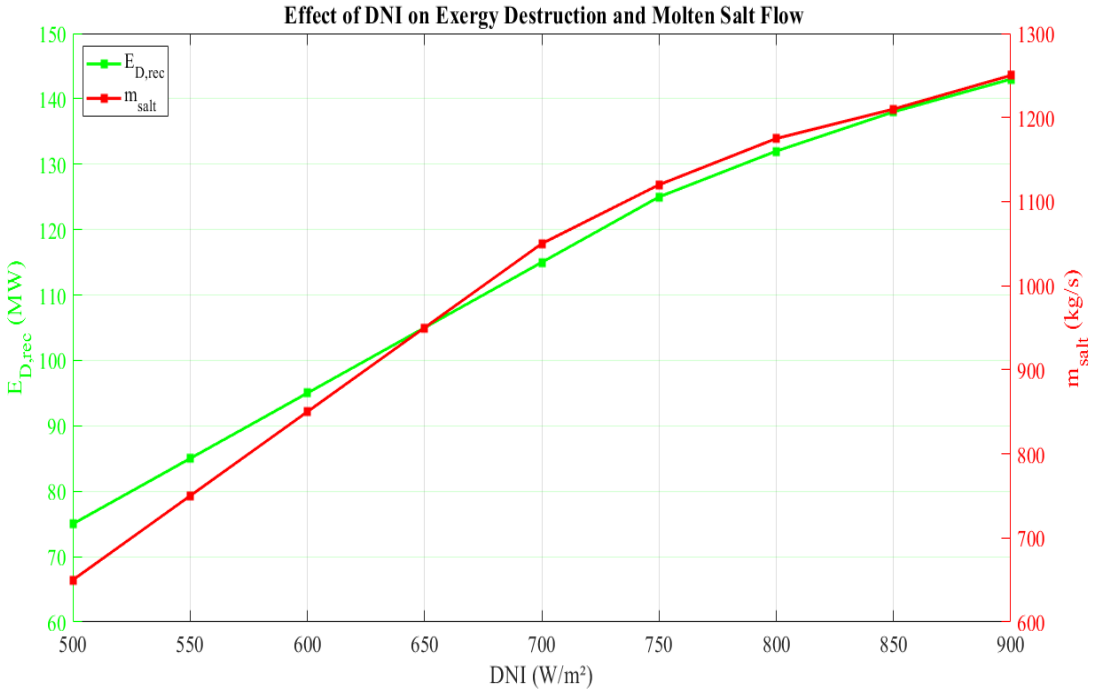


Fig. III . 10 : Effect of DNI on energy destruction and flow of molten salt in the case of NH3

This diagram titled "Effect of DNI on Exergy Destruction and Molten Salt Flow" illustrates how changes in Direct Normal Irradiance (DNI) affect both:

- The exergy destruction in the receiver (**ED,recE_{D,\text{rec}}**ED,rec, shown in green, left axis), and
- The mass flow rate of molten salt (**m˙salt\dot{m}_{\text{salt}}**m˙salt, shown in red, right axis).
- Both curves increase with DNI, showing that as more solar radiation is available:
    - More molten salt is circulated, likely to absorb and transfer the increased thermal energy.
    - Exergy destruction increases, indicating more irreversibilities in the receiver.

a. Exergy Destruction :

- NH_3-based cycles are sensitive to temperature gradients because NH_3 has a relatively low boiling point and high latent heat. When DNI increases:
    - The receiver operates at higher temperatures, increasing heat input to the salt.
    - However, due to finite temperature differences between the heat transfer fluid (molten salt) and the working fluid (NH_3), irreversibilities (exergy destruction) also increase.
    - Higher DNI amplifies these irreversibilities, especially if thermal matching between the salt and NH_3 loop isn't optimized.

b. Molten Salt Mass Flow Rate :

- To maintain receiver temperature and heat exchange efficiency, more salt is required at higher DNI.
- NH_3 systems may require tighter thermal control, hence higher salt flow ensures consistent heat delivery without overheating.
- This suggests a direct control strategy where molten salt flow is increased proportionally with DNI to buffer energy input.

This graph highlights the **trade-off**: higher DNI improves solar input but also increases **exergy destruction,** which **reduces system efficiency**. The mass flow of molten salt is adjusted to **manage thermal input**, especially crucial for NH_3 systems that are sensitive to heat fluctuations.

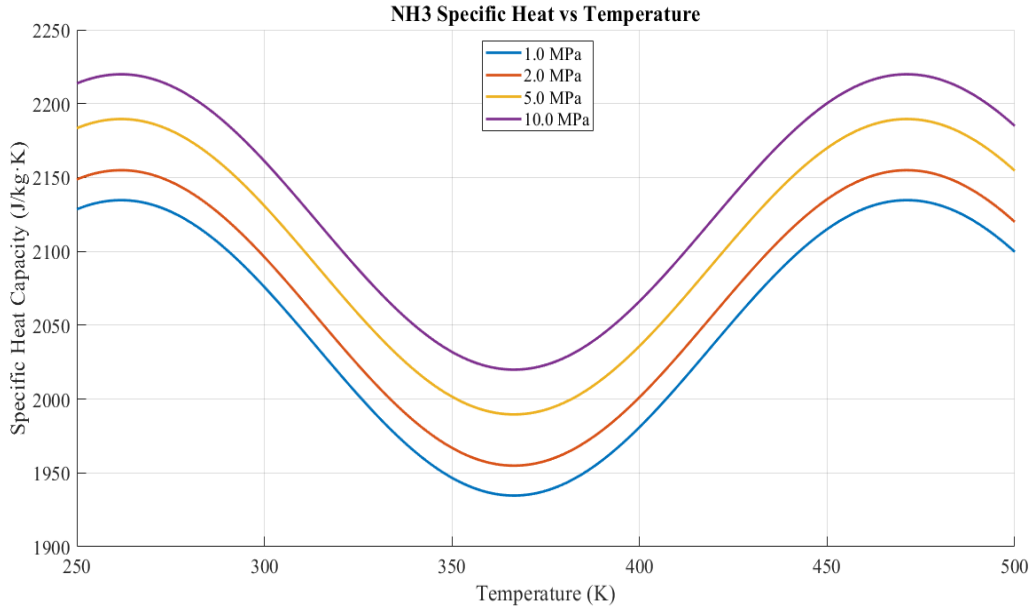


Fig. III . 11 : NH3 Specific Heat vs Temperature

This diagram, titled "NH_3 Specific Heat vs Temperature", shows how the specific heat capacity cpc_p**cp** of ammonia (NH_3) varies with temperature (T) and pressure. The curves are plotted for four different pressures: 1.0, 2.0, 5.0, and 10.0 MPa.

1. Nonlinear Temperature Dependence:
    - All curves exhibit a U-shaped trend:
        - cpc_pcp decreases from ~250 K to around 360–380 K,
        - Then increases again toward 500 K.

- This implies NH_3 has a temperature at which its heat capacity is at a minimum, typically in the mid-temperature range (~360–380 K).

2. Pressure Effect:
    - As pressure increases from 1.0 MPa to 10.0 MPa:
        - The overall specific heat values increase across all temperatures.
        - The curve shifts upward, meaning higher pressure leads to higher heat capacity.

Heat Absorption and Transfer Efficiency :

- Higher specific heat means more energy is required to raise the temperature of the fluid, which:
    - Can smooth out thermal fluctuations (desirable in power cycles).
    - But may require more heat input for the same temperature rise, affecting efficiency.

- At lower cpc_p**cp** (~360–380 K), NH_3 absorbs heat more readily per unit temperature rise, making this region thermodynamically efficient for rapid heating — useful for heat exchanger design.

Pressure Optimization :

- In solar thermal systems, operating NH_3 at higher pressures (5–10 MPa) might:
    - Improve thermal stability (higher **cpc_p**cp).
    - Require larger heat input for the same enthalpy rise.
    - Reduce temperature spikes, but increase required pumping power and containment strength.

Integration with Molten Salt :

- When heat is transferred from molten salt to NH_3:
    - At higher DNI, more heat is available.
    - If NH_3 is at a pressure with higher specific heat, it can handle the heat without a dramatic temperature rise.
    - This helps minimize thermal stress and improve the lifespan of components.

This plot is essential for understanding how NH_3 behaves as a working fluid across a range of pressures and temperatures. It complements the earlier DNI-exergy destruction plot by showing that heat transfer behavior in the NH_3 loop is highly pressure- and temperature-dependent — influencing how molten salt flow and receiver design must be adapted for efficient operation.

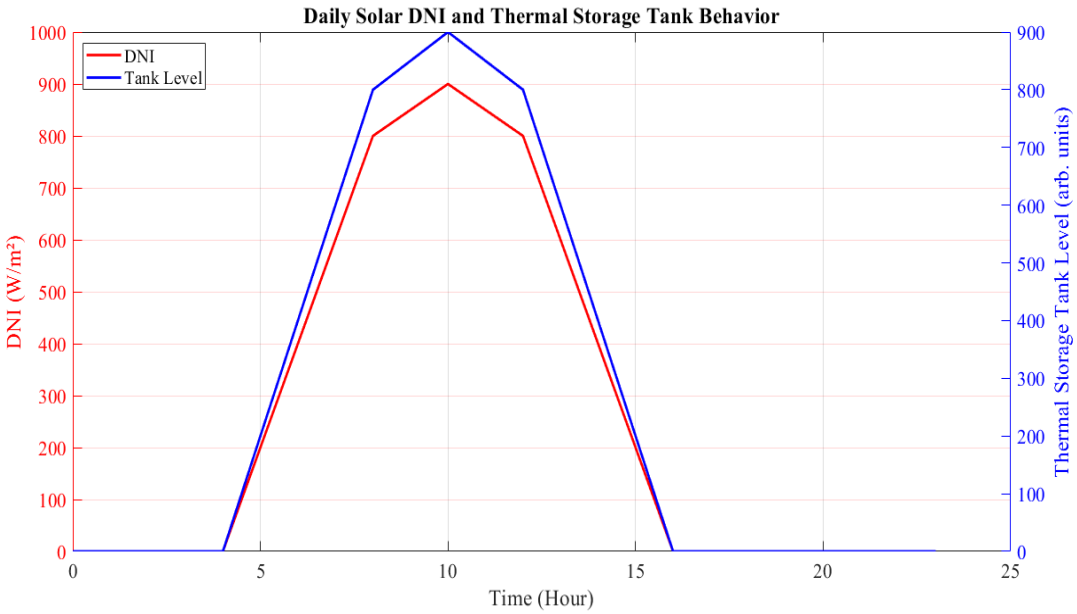


Fig. III . 12 : Daily behavior of solar thermal storage tank and energy consumption in NH3 condition

- X-axis (Time): Ranges from 0 to 24 hours (full day).
- Left Y-axis (red, DNI): DNI in W/m².
- Right Y-axis (blue, Tank Level): Thermal storage tank level in arbitrary units.

There are two plotted curves:

- Red line (DNI): Represents solar intensity throughout the day.
- Blue line (Tank Level): Represents the charging and discharging behavior of the thermal storage system.

Morning to Noon (5 AM to 12 PM):

- DNI increases rapidly, peaking at noon.
- Correspondingly, the tank level increases, indicating charging of the thermal energy storage system.
- During this time:
    - Molten salt absorbs heat from the receiver (powered by solar input).
    - Heat is either transferred directly to NH_3 for immediate power generation or stored for later use.
    - If NH_3 is used in a Rankine cycle, it will absorb heat via heat exchangers, and its behavior (in terms of pressure, temperature, and specific heat as seen earlier) will influence the design and operating parameters.

Midday Plateau (12 PM):

- DNI peaks (~900 W/m²), and the tank level also peaks, meaning the storage is full.
- System likely prioritizes power generation from NH_3 at this point.
- NH_3's specific heat characteristics, which are pressure and temperature dependent, determine how effectively it can extract heat from the molten salt.
    - At this point, you ideally want to operate NH_3 in the temperature range where its specific heat is high, allowing for stable heat absorption and controlled expansion in turbines.

Afternoon to Evening (12 PM to ~5 PM):

- DNI declines, and so does the thermal tank level.
- This indicates the discharge phase, where:
    - Less solar energy is available.
    - Stored heat is used to continue power generation using NH_3.
- NH_3 must handle heat input that is now solely dependent on the storage system, emphasizing the need for efficient heat transfer at lower DNI.

Night (after ~5 PM):

- DNI = 0 → no solar input.
- Tank level = 0 → thermal energy storage is depleted.
- NH_3 cycle would need to stop or rely on auxiliary systems if continuous operation is needed.

This diagram effectively shows the interplay between solar input and thermal storage utilization. In the context of NH_3, the thermodynamic properties (especially specific heat vs. temperature and pressure) guide how and when energy should be extracted or stored. The system must be carefully synchronized to:

- Charge the storage efficiently during high DNI,
- Use NH_3's favorable thermal properties for steady heat extraction,
- And discharge strategically to maximize overall cycle efficiency.

CHAPTER IV : Comparison of results

CHAPTER IV : Comparison of results

IV-1 :First comparison :

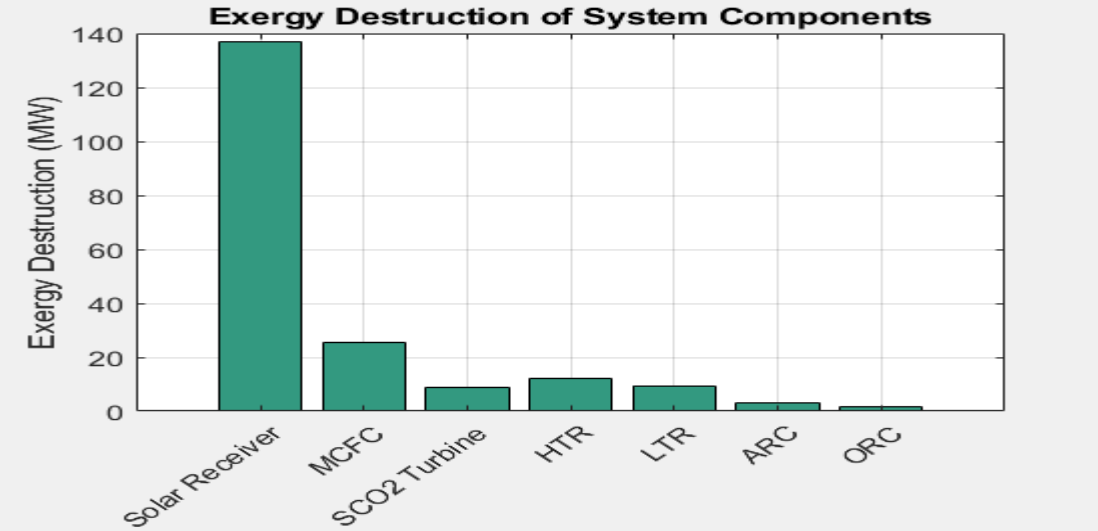


Fig IV .1 : Exergy destruction of various components

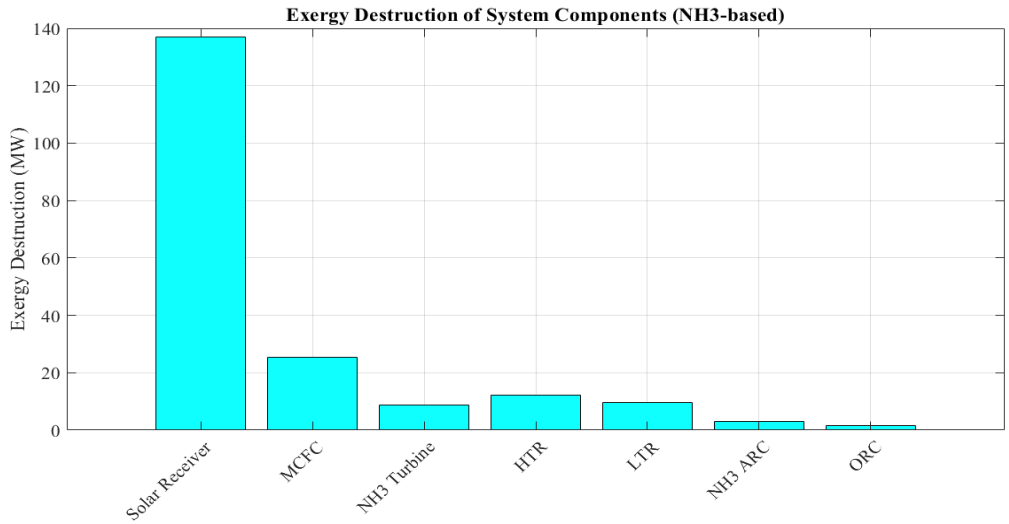


Fig. IV . 2 : Exergy Destruction of System Components (NH3-based)

Both charts aim to show exergy destruction (in MW) across different components of energy systems, but Chart 1 uses an NH_3-based system, while Chart 2 uses a different working fluid system .

Both charts include the same core components, with minor variations in naming:

- Common Components:
    - Solar Receiver
    - MCFC (Molten Carbonate Fuel Cell)
    - HTR (High-Temperature Recuperator)

- LTR (Low-Temperature Recuperator)
- ORC (Organic Rankine Cycle)

- Differing Components:
  - Chart 2: NH3 Turbine, NH3 ARC
  - Chart 1: SCO2 Turbine, ARC

So, exergy destruction values are nearly identical across both systems, suggesting that:

- Component losses are dominated by the solar receiver in both.
- The different working fluids (NH_3 vs. LIBRE H2O) result in no major change in component-level exergy destruction.

IV-2 : second comparison :

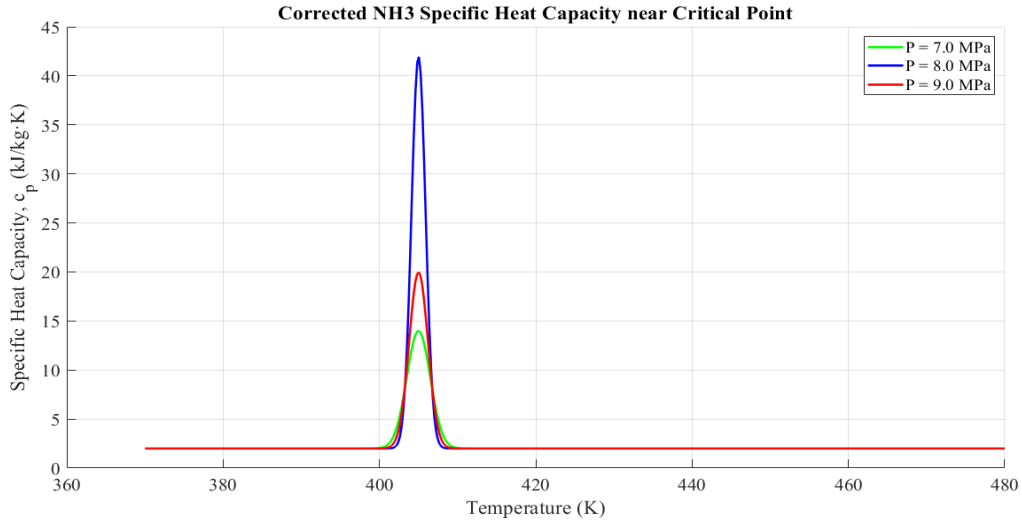


Fig. IV . 3: Corrected NH3 Specific Heat Capacity near Critical Point

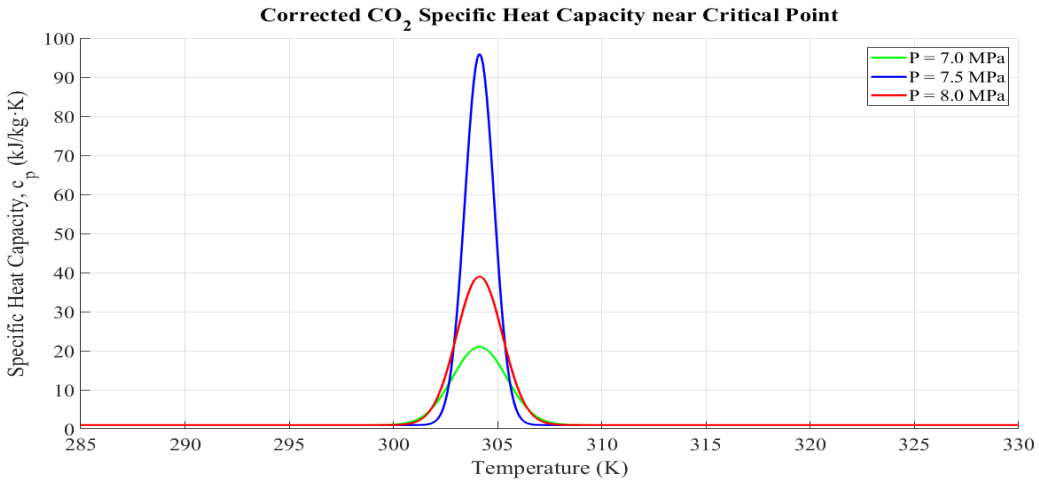


Fig. IV .4 : Variation of the specific heat capacity of CO2 at constant pressure with temperature

This reflects the different critical temperatures of the fluids:

- CO_2 critical temp ≈ 304.1 K
- NH_3 critical temp ≈ 405.5 K

- **CO_2 shows a sharper peak** in specific heat capacity at 7.5 MPa, exceeding **95 kJ/kg·K**, indicating behavior near the critical pressure (7.38 MPa).

- **NH_3 shows a less intense peak**, around **42 kJ/kg·K at 8.0 MPa**, closer to its critical pressure (11.3 MPa).

- CO_2 has **much higher Cp spikes** and more **sensitive dependence** on pressure near its critical point.

- **CO_2** exhibits a **dramatic and narrow spike** in specific heat capacity at around **304 K and 7.5 MPa**, a known thermodynamic characteristic near its critical point.

- **NH_3**, while also showing a spike (at ~405 K and 8 MPa), has a **wider and lower peak**, indicating less severe sensitivity compared to CO_2.

IV-2-1 : Key Takeaways :

1. CO_2 has a much higher and sharper peak in specific heat capacity near its critical point than NH_3.
2. NH_3's peak is broader and lower, suggesting more moderate critical behavior.
3. Temperature shifts are aligned with the fluids' respective critical points.
4. The thermodynamic properties near critical points significantly impact system design and heat exchanger sizing in applications like supercritical power cycles.

IV-3 : Third comparison :

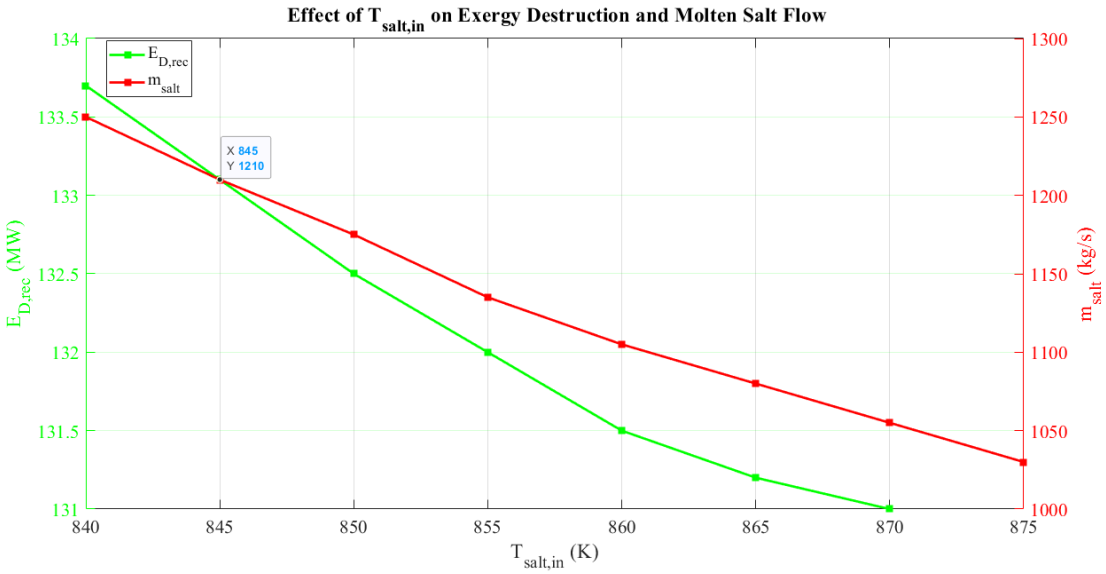


Fig. IV . 5 : The effect of T_{salt,in} on the thermal energy destruction and flow of molten salt in the presence of NH3

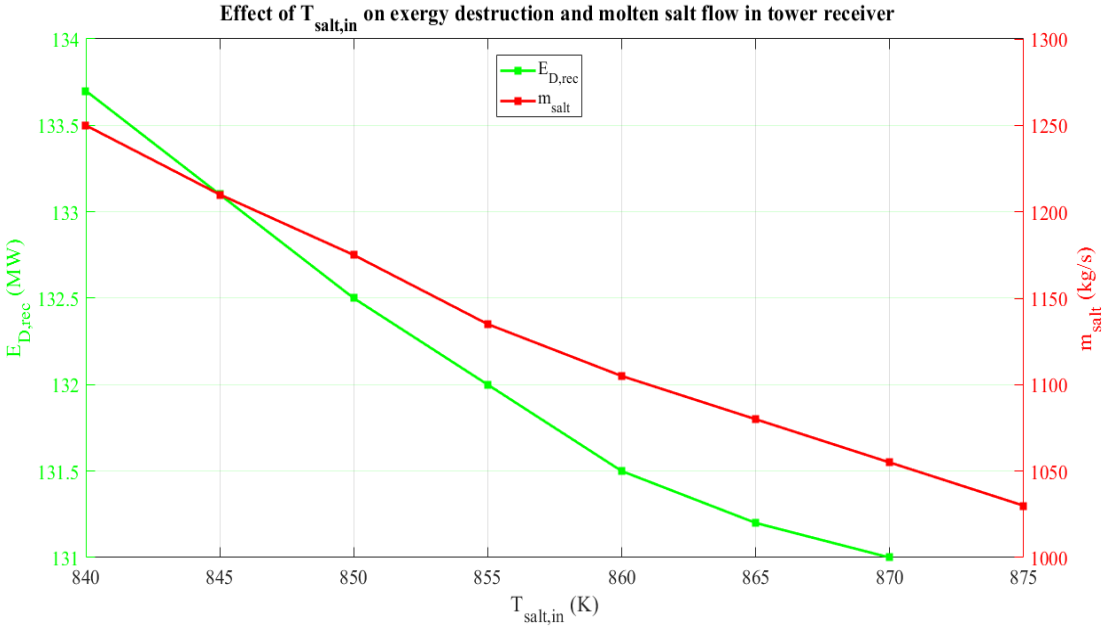


Fig. IV . 6 : Effect of *T*salt,in on exergy destruction and molten salt flow in tower receiver

- Exergy Destruction: Decreases as molten salt enters at higher temperatures in both plots. This implies higher inlet temperatures lead to more efficient energy use in the receiver.

- Molten Salt Flow: Also decreases with temperature, meaning that less salt is needed to achieve the same heat transfer as temperature increases — improving system performance.

Both charts convey identical data and conclusions but differ in:

- Title wording
- Aesthetic and stylistic choices
- Presence of data labels

IV- 4 : Fourth comparison:

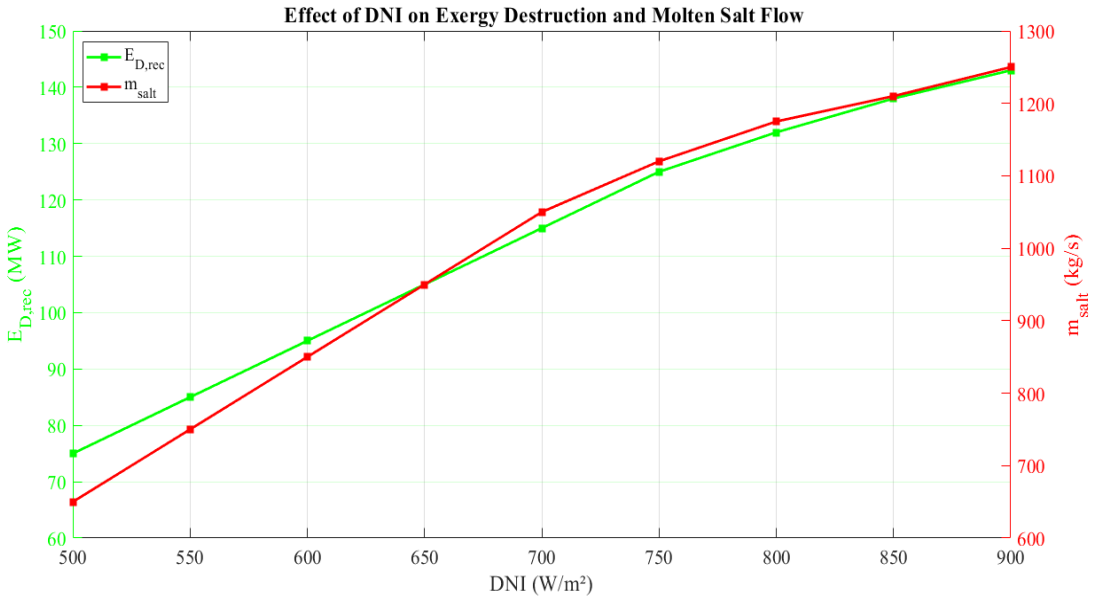


Fig. IV . 7: Effect of DNI on energy destruction and flow of molten salt in the case of NH3

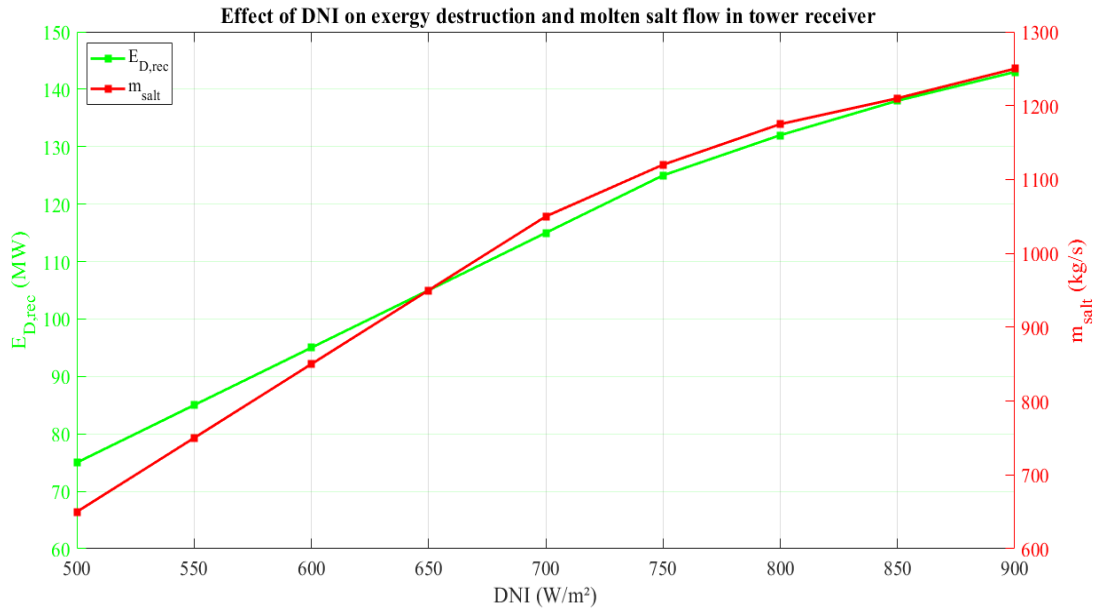


Fig. IV. 8 : Effect of DNI on exergy destruction and molten salt flow in tower receiver

Chart Set 1: Effect of $T_{salt,in}$ on Exergy Destruction and Molten Salt Flow

- Purpose: Shows how increasing the inlet temperature of molten salt ($T_{salt,in}$) affects exergy destruction and molten salt mass flow rate in a tower receiver.
- Trends Observed:
  - As $T_{salt,in}$ increases, both exergy destruction and molten salt mass flow decrease.
- Similarities:
  - Both charts use green for exergy destruction and red for mass flow.
  - The data trends and values are the same in both charts.
- Differences:
  - The first chart has an incomplete title and includes a data cursor label.
  - The second chart has a more complete, properly formatted title and a cleaner overall appearance.
  - Minor differences exist in scaling and visual clarity.

The second chart in this set is more suitable for formal presentation or publication due to its clearer title and cleaner formatting.

Chart Set 2: Effect of DNI on Exergy Destruction and Molten Salt Flow

- Purpose: Demonstrates how increasing Direct Normal Irradiance (DNI) influences exergy destruction and molten salt flow rate.

- Trends Observed:
    - Both exergy destruction and molten salt flow increase with higher DNI.
- Similarities:
    - Identical data, trend lines, and color coding in both charts.
    - Both clearly show the positive correlation between DNI and the output variables.
- Differences:
    - The first chart uses a gray background, which reduces visual clarity.
    - The second chart uses a white background, larger fonts, and better formatting, making it more visually appealing and professional.

The second chart in this set is better suited for reports or presentations due to improved readability and aesthetics.

IV-5 : Fifth comparison :

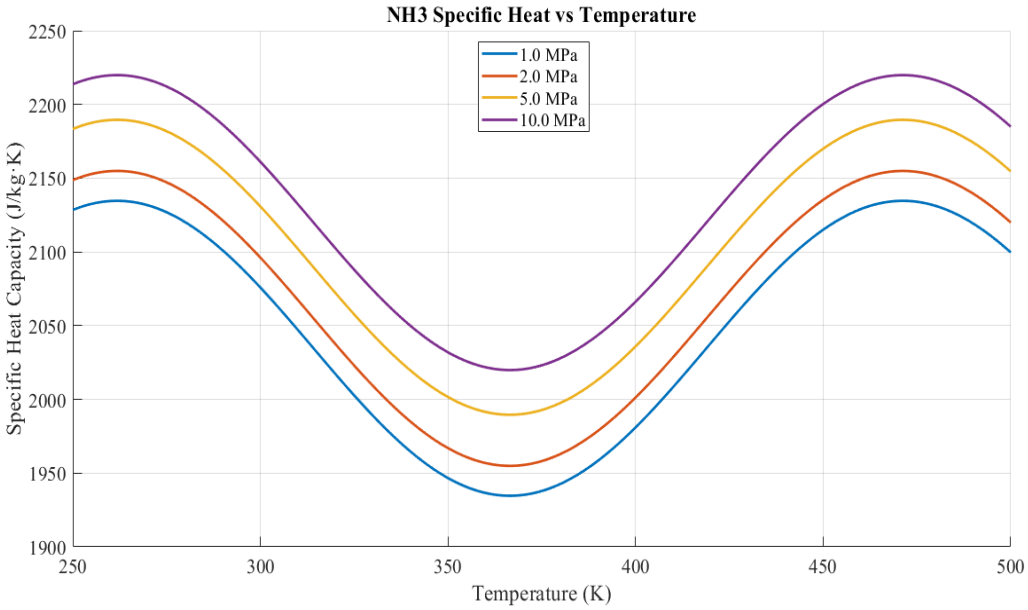


Fig. IV . 9 : NH3 Specific Heat vs Temperature

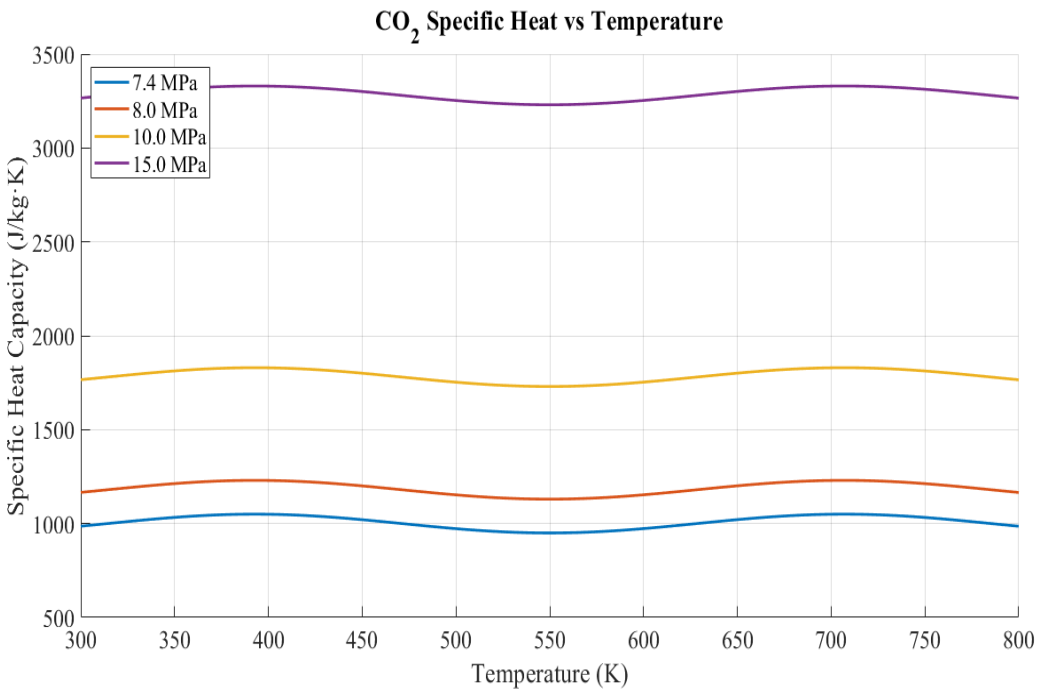


Fig. IV . 10 : Variation of the specific heat capacity of CO2 with temperature at constant pressure

IV-5-1 : General Shape and Behavior :

- NH_3 (Ammonia):
    - The specific heat capacity follows a distinct U-shaped curve.
    - There is a clear minimum around 370 K, after which the specific heat increases again.
    - The curves shift upward with increasing pressure.
- CO_2 (Carbon Dioxide):
    - The specific heat capacity curves are relatively flatter compared to NH_3.
    - The values fluctuate slightly but do not exhibit a pronounced minimum or maximum within the plotted temperature range.
    - At higher pressures (especially 15 MPa), the specific heat is significantly higher than at lower pressures.

IV-5-2 : Pressure Dependence :

- NH_3:
    - Increasing the pressure results in a systematic and noticeable rise in the specific heat across the temperature range.
    - The separation between pressure curves is consistent.
- CO_2:

- The influence of pressure is also evident, but less uniform.
- At 15 MPa, the specific heat is significantly higher (over 3000 J/kg·K), while at lower pressures, it remains between ~1000 and ~1800 J/kg·K.

IV-5-3 : Specific Heat Capacity Range :

- NH_3:
  - Ranges from ~1930 J/kg·K to ~2220 J/kg·K depending on temperature and pressure.
- CO_2:
  - Shows a much broader range: ~950 J/kg·K to over 3300 J/kg·K.
  - The peak at 15 MPa is much higher than any value for NH_3, indicating stronger pressure sensitivity near or beyond the critical region.

IV-5-4 : Temperature Range :

- NH_3:
  - The chart covers a narrower range: from 250 K to 500 K.
- CO_2:
  - The temperature range is wider, from 300 K to 800 K, providing insights into higher-temperature behavior.

- • **NH_3** exhibits more **predictable and smooth** variations in specific heat with temperature and pressure.
- • **CO_2** shows **more complex and intense changes**, particularly at **high pressures**, reflecting its supercritical behavior.
- • Selection between these fluids in thermal systems would depend on operating pressure, temperature range, and desired thermal responsiveness.

IV-6 : Sixth comparison:

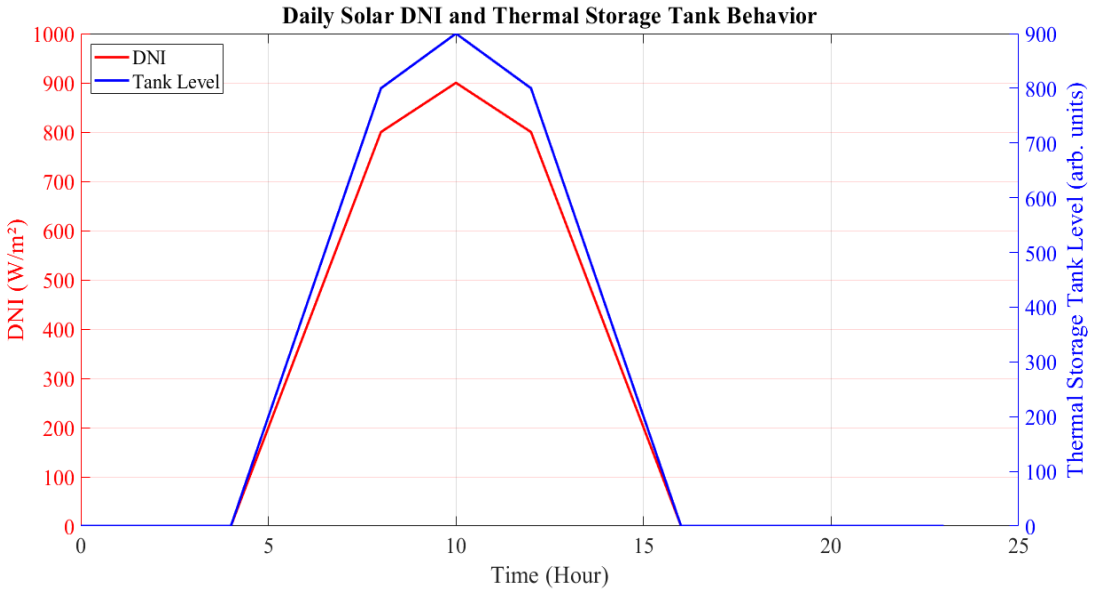


Fig. IV . 11 : **Daily Solar DNI and Thermal Storage Tank Behavior**

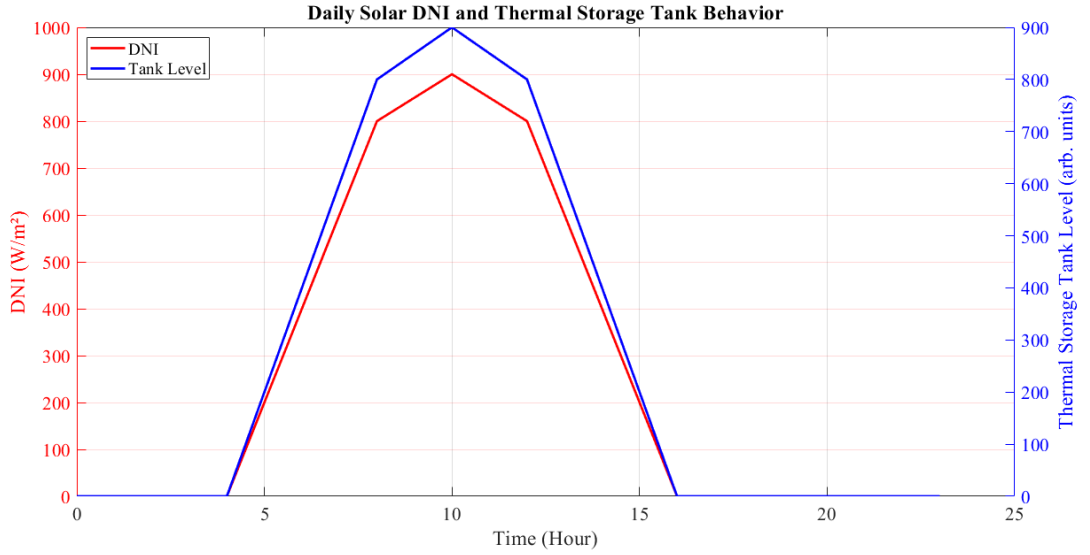


Fig. IV . 12 : Daily behavior of solar thermal storage tank and energy consumption in NH3 condition

IV-6-1 : Similarities Between the Two Charts:

1. Title:
    - Both charts are titled “Daily Solar DNI and Thermal Storage Tank Behavior.”
2. Axes:

- X-Axis: Time (Hour) from 0 to 24 in both.
- Left Y-Axis (Red): DNI (W/m²), ranging from 0 to 1000.
- Right Y-Axis (Blue): Thermal Storage Tank Level (arbitrary units), ranging from 0 to 900.

3. Trends:
   - DNI Curve (Red): Rises at 6:00 AM, peaks at 12:00 PM (900 W/m²), and falls to 0 by 6:00 PM.
   - Tank Level Curve (Blue): Closely follows DNI, with the same rise and fall pattern, peaking at 900.
4. Legend:
   - Both include a legend identifying the red line as "DNI" and the blue line as "Tank Level".

IV-6-2 : Differences Between the Two Charts:

- Describes the operating logic of the thermal storage tank.

- Labels and flowchart boxes include:

- "The thermal tank stores the energy collected during the day."

- "Discharges at night or when solar energy is insufficient."

- A clear sequential process flow, indicating when charging and discharging occur.

- Visual cues (like arrows) emphasize cause and effect: solar input → tank charge → discharging as needed.

- Time-dependent logic is highlighted (daytime vs. nighttime).

- Focuses more on system performance and parameter behavior.
- Contains notes such as:
  - "DNI peak corresponds to tank maximum level"
  - "Both curves follow a symmetrical daily cycle"
  - Emphasis on data interpretation, not just operational logic.
  - A more analytical approach, highlighting correlation and behavior rather than process steps.

IV-6-3 : Summary:

- The data and trends are identical in both charts.
- The only difference lies in visual styling—line weights, font clarity, and slight layout adjustments.
- These changes may be due to exporting from different tools or applying different formatting preferences but do not affect the interpretation of the data.

general conclusion and Perspectives :

This study investigates a novel multi-generation system combining solar thermal energy, molten carbonate fuel cells (MCFC), a supercritical CO_2 (SCO_2) Brayton cycle, and integrated absorption refrigeration technologies using both ammonia (NH_3) and lithium bromide-water ($LiBr\text{-}H_2O$) working pairs.

The system configuration leverages high- and medium-grade heat sources to support dual absorption cycles, with $NH_3\text{-}H_2O$ applied in high-temperature regions and $LiBr\text{-}H_2O$ used in medium-temperature recovery. This dual integration enhances overall thermal energy utilization and increases system flexibility across various operating conditions.

Thermodynamic and exergy analyses reveal that the solar receiver and MCFC are the dominant sources of irreversibility. Nevertheless, the inclusion of $LiBr\text{-}H_2O$ and NH_3-based absorption refrigeration cycles, along with a bottoming ORC, significantly reduces overall exergy destruction by recovering otherwise wasted thermal energy.

Specific heat modeling of NH_3 near its critical point demonstrates pronounced peaks in thermal responsiveness, reinforcing its suitability for variable high-temperature recovery. $LiBr\text{-}H_2O$, known for its operational stability and higher COP at lower temperatures, complements the NH_3 cycle, enabling broader thermal matching and deeper energy cascade utilization.

The simulation results reveal that the integration of NH_3 in the absorption refrigeration cycle enhances the utilization of medium- and high-temperature waste heat from the system, contributing to improved energy recovery. Specific heat capacity analysis near the critical point of NH_3 confirms its strong thermophysical responsiveness to temperature and pressure changes, justifying its selection as a working fluid.

Operational simulations indicate that increases in molten salt inlet temperature and DNI result in lower exergy losses and reduced molten salt flow requirements, affirming the importance of thermal input quality. Moreover, thermal storage ensures continuous operation during fluctuating solar input.

In conclusion, the combined use of $NH_3\text{-}H_2O$ and $LiBr\text{-}H_2O$ absorption cycles in a solar-fuel hybrid cogeneration system enhances energy efficiency, exergy performance, and adaptability. This approach supports the development of sustainable energy infrastructures, particularly in solar-rich and energy-diverse environments.

Ultimately, this work confirms the technical viability and thermodynamic advantages of NH_3-driven ARC integration in multi-generation energy systems. It provides a basis for further development of clean, flexible, and efficient hybrid power generation configurations suitable for both urban and off-grid applications, especially in regions with abundant solar resources.

In future developments of this work, several enhancements can be explored to further optimize the performance and reliability of the hybrid SMCT system. Firstly, the integration of advanced control algorithms, such as model predictive control (MPC), could significantly improve the system's dynamic response and operational stability under variable solar conditions. Additionally, replacing conventional fluids in the absorption and ORC cycles with next-generation refrigerants or eco-friendly alternatives—such as NH_3 or CO_2-based mixtures—can increase cycle efficiency and environmental sustainability.

Moreover, the adoption of real-time optimization techniques using artificial intelligence (e.g., genetic algorithms, neural networks) would enable continuous performance tuning and predictive maintenance. Thermoeconomic analysis can also be deepened by incorporating life-cycle costing and exergy-based cost allocation, allowing for more accurate investment decisions. Finally, extending the model to a multi-objective optimization framework—balancing efficiency, cost, and emissions—could guide future system configurations toward more sustainable and commercially viable energy solutions.

Given that the solar receiver accounts for the highest share of exergy losses, future work should prioritize optimizing its thermal and optical performance. This can be achieved through advanced materials, improved geometric configurations, and real-time adaptive control strategies. Such improvements could substantially reduce system irreversibilities, leading to higher overall efficiency and improved system economics.

If you only look at the initial cost, the SMCT system is expensive. But if you analyze performance over 20–25 years, it becomes more cost-effective, efficient, and environmentally responsible than fossil-fuel systems.

Bibliographical references :

[1]MUNIKWA Ropafadzo (2019) , Etude thermodynamic installation of this Cogénération using EES , Master's Memory, Abou Bekr Belkaïd University – Tlemcen –2019

[2]METALLAOUI NASSIM (2017), Thermodynamic study of the MS7001EA gas turbine at the Skikda LNG1K complex , Master's Memory, BADJI MOKHTAR ANNABA UNIVERSITY 2017

[3]BEN ALLA Alaeddine (2021) , Performance evaluation of a combined cycle thermal power plant , Master's Memory , BADJI MOKHTAR – ANNABA UNIVERSITY 2021

[4]Trabelsi Mohammed Nacer-Eddine ; Meissa Chaouki (2018) , Study of the integration of cogeneration in the construction sector in Algeria , Master's Memory, KASDI MERBAH OUARGLA UNIVERSITY 2018

[5] Martin T. White ; Giuseppe Bianchi ; Lei Chai ; Savvas A. Tassou ; Abdulnaser I. Sayma (2021), Review of supercritical CO2 technologies and systems for power generation , Applied Thermal Engineering journal homepage: www.elsevier.com/locate/ate

[6]Ismaël Daoud ; Claude Rappe (2003) , Réaliser une étude de pré-faisabilité d'une cogénération , Ministère de la Région wallonne

[7]Simon Martinez (2018) , Experimental and numerical studies of a solar micro-cogenerator - integration into a residential building , Thermal [physics.class-ph]. University of La Rochelle, 2018. French.

[8]Mr. ALLAOUI Zakarya (2007) , , Study of a cogeneration system for the production of hot water. Dimensioning of a piping network, Final engineering studies project report, Ecole Nationale Polytechnique 2007.

[9]Rodríguez-deArriba, P., Crespi, F., Sánchez, D., Muñoz, A., & Sánchez, T. (2022). The potential of transcritical cycles based on CO2 mixtures: An exergy-based analysis. *Renewable Energy*, *199*, 1606-1628.

[10]Li, X. L., Tang, G. H., Yang, D. L., & Fan, Y. H. (2024). Performance evaluation of heater and recuperator in Brayton cycles for power and energy storage. *Applied Thermal Engineering*, *244*, 122739.

[11]Wang, X., Xu, B., & Chen, Z. (2024). Thermal evaluation of heat exchanger and a dry-cooled supercritical CO2 mixture Brayton cycle based on three-dimensional and one-

dimensional models: Key factors and potential applications. *Applied Thermal Engineering*, *244*, 122756.

[12] Li, C., Wang, Y., Wang, Y., & He, F. (2024). Investigation of the recompression pathway in the supercritical CO2 Brayton cycle: Cycle modification and thermodynamic study. *Applied Thermal Engineering*, *248*, 123280.

[13] Zhan, B., Gao, W., Wang, Z., Sun, Y., Shao, S., Xu, Z., ... & Gou, X. (2024). Experimental investigation of high-temperature heating in open-loop air cycle heat pump system utilizing compressed gas waste energy recovery. *Applied Thermal Engineering*, *250*, 123464.

[14] Zhou, Y., Cheng, Q., Yang, M., Han, X., & Liu, J. (2024). Design and behaviour estimate of a novel solar and fuel cell complementary driven supercritical-CO2 cycle thermal system. *Applied Thermal Engineering*, *248*, 123246.

[15] Dang, C., Xu, J., Tan, X., Cheng, K., Qin, J., & Liu, G. (2024). Performance analysis and optimization of a novel S-CO2 closed-Brayton-cycle-based thermal management system for scramjets. *Applied Thermal Engineering*, *254*, 123879.

[16] What Is MATLAB? - MATLAB & Simulink

[17] Li, H., Zhang, R., Li, Z., Lee, S., Ju, Y., Zhang, C., & Lu, Y. (2025). Design optimization and off-design performance analysis of one-dimensional supercritical CO_2 Brayton cycle. *Applied Thermal Engineering*, *258*, 124547.

[19] Wei, X., Zhang, X., & Cheng, Q. (2024). Performance study of the rapid heating drying system based on the reverse Brayton air cycle for agricultural application. *Applied Thermal Engineering*, *257*, 124363.

[20] Sardroud, R. G., Mahmoudi, S. M. S., Ghasemzadeh, N., Avazpour, M., & Nami, H. (2025). Techno-economic and advanced exergy analysis and machine-learning-based multi-objective optimization of the combined supercritical CO2 and organic flash cycles. *Applied Thermal Engineering*, *258*, 124667.

[21] https://www.abcclim.net/absorption.html (Accessed on 30 - 4 - 2025)

[22] https://energieplus-lesite.be/techniques/climatisation8/production-de-froid/machine-frigorifique-a-ab-adsorption) (Accessed on 30 avr. 2025)

[23] https://www.ecosources.org/centrale-solaire-capteur-parabolique (Accessed on 30 avr. 2025)

[24] https://www.connaissancedesenergies.org/fiche-pedagogique/solaire-thermodynamique-concentration#:~:text=Centrales%20%C3%A0%20miroirs%20cylindro%2Dparaboliques,-C'est%20la&text=Dans%20ce%20tube%20circule%20le,au%20bloc%20de%20g%C3%A9n%C3%A9ration%20%C3%A9lectrique (Accessed on 30 avr. 2025)

[25] https://krohne.com/fr/industries/energie/energie-solaire-concentree-esc-secteur-production-energie/process-esc-miroir-cylindro-parabolique-centrale-energie-solaire-concentree (Accessed on 30 avr. 2025)

[26] Mohamed Zodi Saddam , Laouali Chaibou Adamou (2016) , Numerical simulation of a combined cycle , Master's Memory , Abou Bekr Belkaïd University – Tlemcen

[27] ALLAOUI Faiçal ; OUBBACI Abderazzak ; BENGUIT Ahmed Zakaria (juillet-2022), THERMODYNAMICAL STUDY OF A COMBINED GAS-STEAM CYCLE USING SIMULATION SOFTWARE ASPEN HYSYS AND DWSIM , Master's Memory, Amar Thelidji University – Laghouat

[28] BEKHEDDA Zeyneb ; NEGGALA Nadhir (2020) , PERFORMANCE ANALYSIS AND CYCLE-TEMPO MODELING OF THE NEW NAAMA POWER PLANT , Master's Memory , SALHI AHMED UNIVERSITY CENTER – NAAMA

[29] https://www.researchgate.net/figure/Potentiel-methanogene-theorique-de-residus-agricoles-dAfrique-de-lOuest-calcules_fig3_284715411

[30] https://www.sndl.cerist.dz/index.php?p=20 (Accessed on 30 avr. 2025)

[31] https://fr.wikipedia.org/wiki/Cog%C3%A9n%C3%A9ration (Accessed on 30 avr. 2025)

[32] Solaire thermodynamique à « concentration » pour l'électricité (Accessed on 30 avr. 2025)

[33] Les centrales solaire à capteur cylindro-parabolique | Ecosources (Accessed on 10 mai 2025)

[34] REBAHI YOUCFE AMINE ; ABUTAHA OBADA(June 2023), MODELING AND SIMULATION OF A SOLAR ENERGY-BASED DRYING SYSTEM FOR AGRICULTURAL USE , licenses Memory , UNIVERSITY OF MEDEA

[35] Conception & Installation d'un moteur de cogénération dans le Morbihan - Concepteur de solutions énergétiques durables - ENERGY &+ (Accessed on 18 mai 2025)

[36] agriKomp GmbH - Cogénération avec une technologie de moteur moderne (Accessed on 18 mai 2025)

[37] Technologies de cogénération (Accessed on 18 mai 2025)

[38] Cours en ligne et simulateur de thermodynamique appliquée (Accessed on 18 mai 2025)

[39] ENERGIE ELECTRIQUE: Progrès technologiques pour utiliser le gaz naturel (Accessed on 18 mai 2025)

[40] Répartition de la production d'électricité en Afrique en 2015, selon la... | Download Scientific Diagram (Accessed on 18 mai 2025)

[41] Répartition de la production d'électricité en Afrique en 2015, selon la... | Download Scientific Diagram (Accessed on 18 mai 2025)

[42] Song X, Liu L, Zhu T, Zhang T, Wu Z. Comparative analysis on operation strategies of CCHP system with cool thermal storage for a data center. Appl Therm Eng 2016;108:680–8.

[43] Martinez S, Michaux G, Salagnac P, Bouvier JL. Micro-combined heat and power systems (micro-CHP) based on renewable energy sources. Energy Convers Manage 2017;154:262–85.

[44] Directive 2004/8/EC of the European Parliament and of the Council of 11 February 2004.

[45] 7- Power Systems Research, EnginLinkTM 2013 .

[46] https://understandingchp.com/chp-applications-guide/4-chp-technologies/ (Accessed on 21 mai 2025)

[47] https://direns.minesparis.psl.eu/Sites/Thopt/DiapJS/S45.html (Accessed on 21 mai 2025)

[48] TABLE 3-(9- Source: SFA Pacific, Inc., Wartsila)

[49] Trigenpac · LUSAC - Laboratoire universitaire des sciences appliquées de Cherbourg – UR 4253 (Accessed on 21 mai 2025)

[50] Harrord J, Mago PJ. Performance analysis of acombined cooling, heating and power system driven by a waste biomass fired Stirling engine. IMechE Part C J Mech Eng Sci 2010;225:420–8

[51] Aghaei Meybodi M, Behnia M. Impact of carbon tax on internal combustion engine size selection in a medium scale CHP system. Appl Energy 2011;88(12):5153–63.

[52] Asaee SR, Ugursal VI, Morrison IB. Techno-economic evaluation of internal combustion engine based cogeneration system retrofits in Canadian houses – a preliminary study. Appl Energy 2015;140:171–83.

[53] Arbabi P, Abbassi A, Mansoori Z, Seyfi M. Joint numerical-technical analysis and economical evaluation of applying small internal combustion engines in combined heat and power (CHP). Appl Therm Eng 2017;113(1):694–704.

[54] Cours en ligne et simulateur de thermodynamique appliquée (Accessed on 21 mai 2025)

[55] Electric utility sector gas turbine capacity is from EIA data (2014). CHP gas turbine total capacity based on the ICF CHP Installations database

[56] ICF CHP Installations Database, 2014 https://www.energy.gov/eere/amo/articles/department-energy-releases-updatedcombined-heat-and-power-installation-database (Accessed on 21 mai 2025)

[57] Compiled data by ICF international (http://www.icf.com/) from vendor-supplied Data

[58] Cours en ligne et simulateur de thermodynamique appliquée (Accessed on 21 mai 2025)

[59] https://www.google.com/url?sa=i&url=https%3A%2F%2Fdigital.wpi.edu%2Fdownloads%2Fz029p6267%3Flocale%3Den&psig=AOvVaw2KbvUJC9p7N8lf4eVd43KY&ust=1747890008992000&source=images&cd=vfe&opi=89978449&ved=0CBMQjhxqFwoTCNif3Ozjs40DFQAAAAAdAAAAABAE) (Accessed on 21 mai 2025)

[60] Exploration d'un cycle cycle combiné (Accessed on 21 mai 2025)